LAPPEENRANTA UNIVERSITY OF TECHNOLOGY
Department of Mechanical Engineering
Packaging Technology

Matti Väkeväinen

ALTERNATIVE FILLER FOR CALCINED KAOLIN IN PACKAGING BOARD SOLUTIONS

Examiners: Prof. Kaj Backfolk
Prof. Juha Varis

Supervisor: Isto Heiskanen

ABSTRACT

LAPPEENRANTA UNIVERSITY OF TECHNOLOGY

Department of Mechanical Engineering

Packaging Technology

Matti Väkeväinen

Alternative filler for calcined kaolin in packaging board solutions

Master's Thesis 2017

109 pages, 48 figures, 12 diagrams, 41 tables, 10 appendices.

Examiners: Prof. Kaj Backfolk, Prof. Juha Varis

Keywords: Filler, Precipitated calcium carbonate, packaging board

The purpose of this work was to study and test inline-precipitated calcium carbonate as alternative filler in paperboard for packaging solutions. Whether it offers any advantages compared to the traditional precipitated calcium carbonate (PCC) application method was also studied. The idea was to develop a method for applying precipitated calcium carbonate using reactor technology. Another objective was to study the effects on the optical and mechanical properties of the paperboard. Previous studies in the field, patents and competitive filler application technologies were examined and conclusions of the pros and cons drawn. The experimental work was carried out by installing inline-PCC equipment for pilot scale paper machine and performing a number of trial runs. The properties of the manufactured paperboard and the effects of various parameters were tested in laboratory and different trial points were compared with calcined kaolin which acted as a reference point.

TIIVISTELMÄ

LAPPEENRANNAN TEKNILLINEN YLIOPISTO
Konetekniikan osasto
Pakkaustekniikka

Matti Väkeväinen

Vaihtoehtoinen täyteaine kalsinoidulle kaoliinille pakkauskartonki sovelluksissa

Diplomityö 2017
109 sivua, 48 kuvaa, 12 diagrammia, 41 taulukkoa, 10 liitettä
Tarkastajat: Prof. Kaj Backfolk, Prof. Juha Varis
Hakusanat: Täyteaine, Saostettu kalsiumkarbonaatti, Pakkauskartonki

Työn tarkoitus oli tutkia ja testata kartonkikoneen lyhyeen kiertoon reaktoritekniikalla saostetun kalsiumkarbonaatin käyttöä vaihtoehtoisena täyteaineena pakkaus-kartonkisovelluksissa. Työ koostui teoriaan sekä aiheeseen liittyviin aiempiin tutkimuksiin ja patentteihin tutustumisesta, laitteiston asennuksesta, menetelmän kehittämisestä, sekä paperikoneella suoritetuista koeajoista. Koeajoissa valmistetun kartongin optisia ja mekaanisia ominaisuuksia sekä eri muuttujien vaikutuksia analysoitiin laboratoriossa käyttäen vertausarvona kalsinoitua kaoliinia täyteaineena sisältävä kartonki. Tutkimuksessa otettiin myös huomioon mahdolliset edut joita reaktoritekniikalla saostettu kalsiumkarbonaatti toisi perinteiseen kalsiumkarbonaatin valmistukseen ja annosteluun verrattuna.

TABLE OF CONTENT

APPENDICES

ABBREVIATIONS

AKD = Alkyl ketene dimmer, sizing agent

ASA = Alkenyl succinic anhydride, sizing agent

CMC = Carboxymethyl cellulose

FTIR = Fourier transform infrared spectroscopy

GCC = Ground calcium carbonate

MBF = Moving belt former

MFC = Micro fibrillated cellulose

Milk of lime, Slaked lime = Calcium hydroxide

PCC = Precipitated calcium carbonate

RO-Water = Reverse osmosis purified water

SBS = Solid bleached sulfate cellulose

SEM = Scanning electron microscope

XRD = X-ray diffraction

1 INTRODUCTION

In the past decades, the paperboard manufacturing business has not had many dramatic innovations in improving profitability. In the same time overall costs and current demands of paperboard properties have risen considerably. If some of the ingredients of paper are replaced by less expensive ones, manufacturing costs can be reduced. In short, by replacing the most expensive part of the paper, fibers, by something less expensive, direct savings in the overall costs of manufacturing are achieved. Nowadays, fillers are not widely employed in many packaging board applications, as their use may result in inadequate bulk and strength properties. In certain packaging board applications where fillers are essentially needed for improving the optical properties, highly expensive specialty pigments such as calcined kaolin or titanium dioxide are used. With current technology, utilizing inexpensive calcium carbonate is usually not an option due to the aforementioned disadvantages.

The purpose of this study was to examine whether calcium carbonate precipitated inline onto fibers in short circulation could be used as replacement filler for currently used calcined kaolin in paperboard manufacturing. This study explored whether the optical and mechanical properties of the top ply in packaging board could be improved while less expensive precipitated calcium carbonate was applied using inline technology. The target was to find an optimal filler content level in contrast to 5% calcined kaolin. The optimal result would be to maintain or even improve the properties of the board while replacing a part of the fibers with filler. A number of studies in the field of filler application have been made and various other technologies have been tested earlier with varying results. An innovative method for producing filler-fiber composite by precipitating the calcium carbonate directly to the process at short circulation has been developed. (Imppola,WO Pat.2009/083633)

The method has many advantages compared to the traditional filler application methods: good strength properties, increased surface properties, good retention, and improved runnability of the machine due to the increased cleanliness of the water system. Ultimately, a portion of the expensive fibers may be replaced by inexpensive filler. In addition, a lesser consumption of retention chemicals may be obtained. (Liukkonen, 2012)

1.1 Multilayer Board

Uncoated multilayer board A is a product of Stora Enso. It is a multilayer liquid packaging board with a total weight of 253 g/m². It is used for manufacturing aseptic brick-style liquid packages such as milk, wine and juice cartons. This type of board consists of 3 separate layers, together creating a rigid I-beam structure. The bulky mid layer is made from unbleached softwood pulp and it forms about 60% of the total weight, and nearly 70% of the total thickness of the board. The function of the mid layer is to provide the basic strength properties for the end product. The back layer is made from more refined unbleached softwood pulp, which provides improved stiffness. In the converting process the back layer is laminated with aluminum and coated with polymer in order to achieve the required barrier properties. The top layer is manufactured purely from dried bleached birch pulp. It is also highly refined for achieving high tensile stiffness. The function of the top layer is not only to support the rigidness, but also to act as the printing base for the retail package. In the converting process the board is typically printed with the flexography printing method and polymer coated afterwards to achieve moisture protection properties. In manufacturing Multilayer board A, calcined kaolin is used as filler on the top layer to improve its opacity.

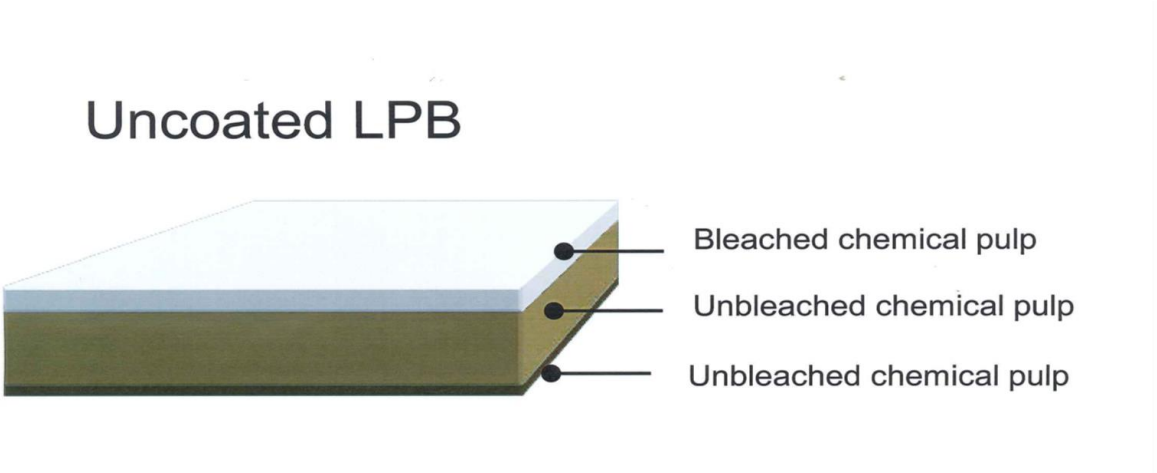

Picture 1. Structure of Stora Enso uncoated multilayer board A (Stora Enso Archives 2012)

1.1.2 Key properties of uncoated liquid packaging board

The function of the packaging is not only to protect the content, but also to act as a retail package. To manufacture a package that sells well, requires a high quality raw material which thereby enables a visually effective product. A common problem of non-coated paper qualities is their relatively low whiteness and poor top ply opacity which leads to the unbleached central layer to shining through. The most important feature of the multilayer board A is its bending stiffness. If the stiffness of the board is not at a desirable level, it has a direct effect on the usability of the end product. Besides the stiffness, other key properties of the multilayer board include surface smoothness, tear strength, elasticity and the internal sizing related edge wicking index. Key optical properties are brightness, opacity, mottling and visual formation. As multilayer board A is intended for aseptic packaging, the cleanliness and product safety are high priority issues.

1.1.3 SBS board

Solid bleached sulfate board is used as a raw material in various consumer goods packaging applications. Typical end uses are such as paper cups and plates, trays, liquid packages and folding cartons. SBS board is preferred when the board is in close contacts with food products as it usually does not cause problems with odor and taint. SBS board can be produced as single or multilayer and in some applications mechanical pulp is added into the middle layer to increase bulk properties. In other applications, unbleached pulp may be used as the middle layer and SBS only on the surface layer for its whiteness and good strength properties.

In many applications the board is coated either on one or both sides with polymer to form moisture, and other barrier properties. The board may be printed on either before or after the polymer coating. In applications such as cosmetics packages, the board is mineral coated in order to improve printability.

1.2 Trumpjet®

TrumpJet® is an innovative device for effective mixing of papermaking additives and chemicals into the main process stream of a paper machine. TrumpJet® is based on tubular shaped parts of which the innermost is fed with mixing liquid and the outermost with injection liquid. The chemical is fed in the middle, consequently flowing out in between and being instantly mixed effectively before entering to the main stream. Internal process circulation waters can be used as injection and mixing liquids therefore eliminating the need for fresh water. This type of mixing improves the chemical distribution and therefore reduces the need of retention aids. There is a selection of different type of mixers available for various kinds of applications.

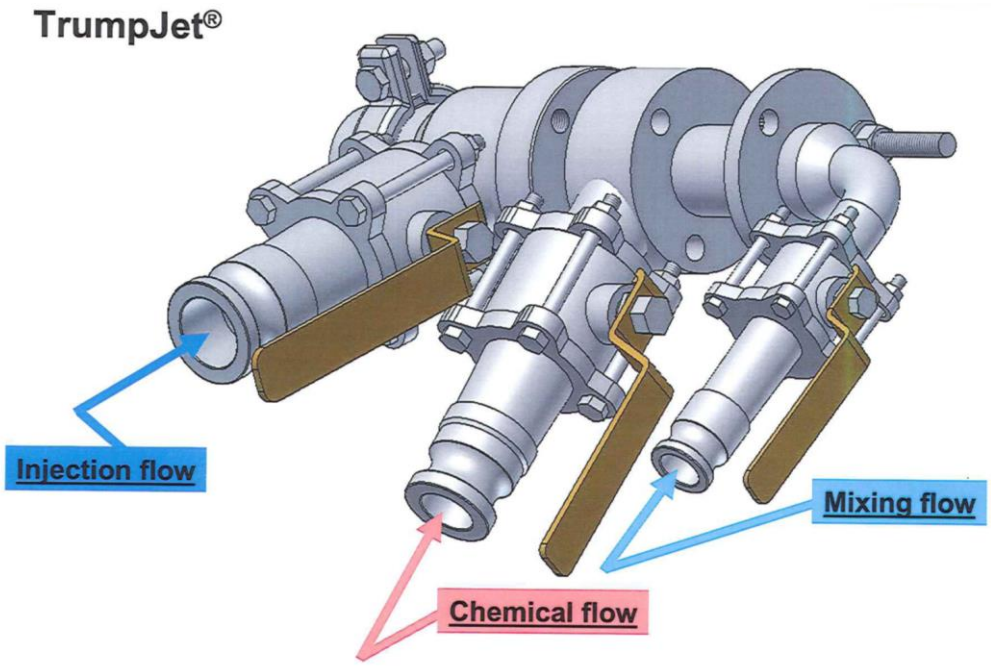

Picture 6. TrumpJet® chord operating principle (www.wetend.com)

1.3 Fillers in papermaking

The type filler and its level of use depend on the grade of the paper. Fillers used in papermaking are commonly characterized by their composition, particle size, morphology and distribution, brightness and refractive index. These characteristics can be used to predict how the pigment will perform in various paper applications. Typically used fillers are presented in table 1.

Table 1.Typical physical properties of widely used fillers (Peel 1999)

TYPE	Grade	Chemical Structure	Source	Particle Shape[10]	Composition[4] Weight % by Particle Sizes in µm,					Density	Refractive Index	Bright-ness	s[(2)]	k	Specific Surface Area[11]
					>10	10 – 2	2 – 1	1 – 0.25	<0.25	Kg/m^3		(ISO) %	m^2/kg	m^2/kg	m^2/g
China Clays (Kaolins)	Standard	Hydrated Aluminum Silicate	Natural [1,7]	Platelets Individual & in stacks	10	40	15	27	8	2400 – 2600	1.57	77 – 82[7]	150 / 120	2 – 4	7 – 9
	Fine				0	20	20	45	15		1.57	~ 86	– / 200	2 – 4	12 – 14
	Calcined	Dehydroxylated at ~ 980°C		Irregular (from platelets)	1	9	20	65	5	2700	1.59	90 – 93	340 / 290	1.2 – 1.7	14
Ground Calcium Carbonate	Standard	~ 97% $CaCO_3$ ~ 2% $MgCO_3$	Limestone[8] (Marble)		1	39	25	25	10	2650 –2710	1.57 1.66	95		0.3 – 0.7	7
	Fine				0	10	25	> 20	< 45			95			13
	Standard		Chalk		5	50	20	24	1			84 – 91	140 / 120	2 – 4	3
PCC[3]	Scaleno-hedral	~ 98% $CaCO_3$	Manufactured	Aggregated Crystals		20	20	40	10	2700 – 2900	1.58	95 – 96			7 – 9
Talc	Standard	Hydrated Magnesium Silicate	Natural[5]	Irregular Platelets	30	53	12	3	2	2700	1.54 – 1.59	83 – 86		2 – 4	6 – 9
	Fine				10	30	30	28	2						12 – 20
Titanium Dioxide	Anatase	TiO_2 80 – 95% pure	Manufactured[6]	Irregular Spherical			2	86	8	3900	2.55	97[9]		< 0.2	10 – 20
	Rutile									4200	2.72	96[9]			30

1.3.1 General

Mineral fillers used in the paper industry are fine white pigment powders with a typical particle size variation of 0.5 - 10µm. (Roberts 1991) They are manufactured from natural minerals or synthetically from various raw materials and have long been used in papermaking. Initially fillers were used mostly just to fill the voids between fibers with less expensive material. As such, fillers had a relatively small impact on the final sheet. Today as paper grades have evolved, the role of mineral fillers has expanded as there are several functional reasons for using them. (Alen, 2007)

In general, this has resulted in larger variety of the mineral products on the market offering different optical and physical properties. Reducing costs by replacing the expensive fiber by less expensive filler was initially, and is still, one of the main reasons for using fillers. The price of bleached chemical fiber is roughly five to seven times as much as typical filler prices (Maloney, 2010). Considerable savings can thereby be achieved by filler usage. According to Norström from the chemical company BASF, in 2008, just 1% of filler increase instead of fibers resulted in a 1,5€ to 3 €/ ton increase in fiber savings. (Norström, 2008) In addition, other properties such as brightness, opacity, smoothness, optical formation, improved printing properties and machine runnability have increasingly supported the incremental use of fillers. (Holik, 2006) The properties of filler pigments are totally different compared to fibers, so improvements are not the only effects fillers have on the paper quality. As a denser material than fiber, the fillers generally have a negative effect on the bulk. In addition, fillers do not form similar bonds as fibers, so the strength and stiffness properties typically decrease when filler content increases. Additionally, the use of mineral filler may have a significant impact on the dynamics of the paper machine such as chemical demand, drainage, speed and drying rate. The amount of fillers in the paper has a strong impact on the sheet properties. For cost effective optimization of the level of filler usage, and understanding of the characteristics of fillers and their impact in both the paper sheet and the paper machine is required (Thorn, 2009). From the paper converting point of view, it is important to have the same filler level on both sides of the paper as this has an impact on the coating of the paper (Gullichsen et al, 2000).

Table 2. Paper properties vs. calcium carbonate properties (Imerys, 2010)

	Finer particle size	Steeper particle size distribution	Aggregated crystal structure
Optics	+	+	+
Strength	-	+	-
Bulk	-	**O**	+
Stiffness	-	**O**	-
Porosity	-	**O**	+

(+ = increase, - = decrease, O = stays the same)

Table 2 illustrates how filler particle size; size distribution and crystal structure affects on the paper properties. When aggregated fillers such as scalenohedral or aragonite PCC are compared with solid particles like GCC or rhombohedral PCC at a similar particle size, the aggregated

particles provide greater light scattering. However, this is achieved by higher fiber de-bonding which leads to decreased paper strength. Scalenohedral and aragonite PCC provide good optics, bulk and surface smoothness, while rhombohedral PCC or GCC give better paper strength. The desired balance of paper properties may be achieved by varying the pigment particle size and morphology. Blending pigments of different size and morphologies can be used as an additional tool to achieve the required balance of paper properties. (Imerys, 2010)

1.3.2 Fillers and paper optics

Adding fillers to paper improves its optical properties in two ways. First, light scattering surface of the paper increases as the bonding degree decreases. Secondly, filler particles typically have a greater specific surface area than fibers. (Niskanen et al 1998)

The optical superiority of different types of fillers depends on multiple factors. The key factors include refractive index, particle size, size distribution, the shape and internal porosity. The particle morphology has an influence on light scattering by the number and size of air voids in the paper sheet. For different morphologies, there is a different optimum for light scattering in terms of particle shape. The shape and size of filler particles and their degree of packing or aggregation affect the light scattering coefficient. A small particle size and a large specific surface area are necessary for good opacity. The structure of a filler particle is best observed by scanning it with an electron microscope (Holik, 2006, Niskanen et al 1998).

Paper primarily consists of a fiber network, filler pigment particles and air. When light penetrates into a material such as filler or fiber, its velocity decreases. Refractive index is the relationship between the velocity of light in the material and in a vacuum. The higher the refractive index developed in the paper, the higher the amount of reflected and scattered light, which results in an increase of paper opacity.

Common fillers have a refractive index of 1.55 – 1.65(at the upper extreme titanium dioxide can be found with a refractive index of 2.55 – 2.75). For a comparison the typical refractive index of bleached chemical cellulose is 1.53 – 1.60. (Holik, 2006) The refractive index also determines how much light is reflected. (Pauler 2002) Light scattering consists of 4 phenomena; reflection, refraction, diffraction and absorption.

When light hits the paper, some of it reflects off of pigment and fiber surfaces in the surface layer and inside the paper structure. Light also penetrates into the fibers and filler particles and changes direction. A part of light is absorbed, but the remainder is reflected and refracted again by new fibers and pigments. A proportion of light reaches the paper surface again and is then reflected to all angles. Incremental diffraction occurs when the light meets particles or pores which are equal or smaller than the wavelength of the light. If the particles are smaller than half of the wavelength of the light, the diffraction decreases. Brightness is typically measured from the paper using a wavelength of 457 nm and light scattering using the wavelength of 420 nm. (Pauler, 2002) In general, the optical properties provided by filler are strongly influenced by its particle size and size distribution. To a certain extent, a finer filler particle size, as well as steeper particle size distribution produce more light scattering, hence more opacity. (Holik, 2006) In paper technology, high light scattering is considered positive as paper becomes more opaque and appears whiter. Light absorption measures how much light is absorbed. The higher the absorption value, the darker the paper appears. (Pauler 2002) The brightness and opacity of filled sheets can be calculated from formulas derived by Kubelka and Munk. The calculation is based on values determined for the light scattering and light absorption coefficients of the components, their proportions in the sheet and grammage.

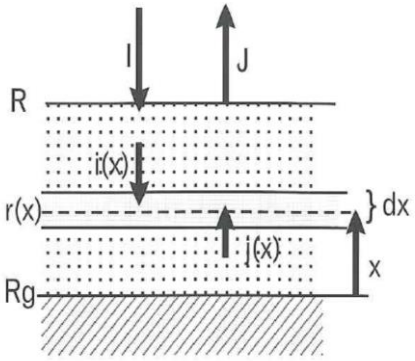

Picture 2. Basic model for the derivation of the Kubelka-Munk equation

The key elements in Kubelka-Munk theory are the quantities of light scattering (s) and light absorption (k). The derivation gives the relationship between the reflectance factor and light scattering and light absorption. (Alen, 2007)

Pauler presents the Kubelka-Munk theory as follows. The light scattering s can be determined by measuring the reflectivity R_∞ of an opaque pad and then measuring the reflectance factor R when the sheet is placed over a background Rg

The light scattering s can be calculated from the equation

$$s = \frac{1}{w\left(\frac{1}{R_\infty} - R_\infty\right)} \ln\left(\frac{(1 - RR_\infty)(R_\infty - Rg)}{(1 - RgR_\infty)(R_\infty - R)}\right)$$

(1)

It is usual to use a black background Rg = 0

And R = R_0 and to calculate s from the equation

$$s = \frac{1}{w\left(\frac{1}{R_\infty} - R_\infty\right)} \ln\left(\frac{(1 - R_0R_\infty)R_\infty}{(R_\infty - R_0)}\right)$$

(2)

Light absorption k is calculated using the equation

$$k = \frac{s \cdot (1 - R_\infty)^2}{2 \cdot R_\infty}$$

(3)

Total light scattering is a combined result of partial contribution of pigments and fibers. A substantial part of opacity comes from increased light scattering resulting from fiber debonding. (Alen 2007) Fiber bonds break via the addition of fillers, so that the internal surface area associated with the fibers increases. Three components affect the light scattering value of pigment filled paper: light scattering 1. from non-bonded fibers, 2. from pigment particles and 3. from fines and fibrils (Pauler 2002)

1.3.3 Types of fillers

Nowadays, calcium carbonates and kaolin clays are the most commonly used fillers among papermakers. Calcium carbonates can be divided into three classes: chalk, ground or precipitated, while kaolins are divided into two classes, that is, hydrous and calcined.

Less commonly used fillers include talc, gypsum, titanium dioxide and amorphous silicates. Usage of each type of fillers varies based on the geographical, economic and machine chemistry considerations along with the final product performance requirements. (Thorn, 2009) In this study the focus is mainly on precipitated calcium carbonate.

1.3.4 Calcined Kaolin

Calcined Kaolin, also referred to as thermally engineered kaolin, is an anhydrous aluminum silicate produced by heating ultra-fine natural kaolin to high temperatures in a kiln. In the calcinations process, the water of hydroxylation is first driven off as vapor at temperatures of 500-700ºC. Then heating is continued up to 1000ºC where ultra-fine particles begin to agglomerate into larger particles. The final result is kaolin –air interfaces with a relatively large internal pore volume. After the calcination, clay is pulverized to remove any oversized agglomerates. The end product typically has a very narrow particle size distribution. Calcined kaolin is defined as specialty filler and is mainly applied in order to increase light scattering and opacity and also to reduce potential ink print through. Because it's relatively high price, used percentual amounts are low.
(Murray 1984, Lehtinen 2000)

1.3.5 Precipitated Calcium Carbonate (PCC)

Precipitated calcium carbonate, also known as PCC, is a synthetic product which differs considerably from natural calcium carbonate. It has a higher purity than natural or ground calcium carbonate as impurities are removed in the production process. Important qualities of the limestone used as a raw material for PCC are low manganese and iron content, as they have negative influence on the brightness of the product.

PCC is manufactured from crushed limestone which is then burned (calcined) in an oven at a temperature of 1000ºC, resulting calcium oxide. Calcium oxide is hydrated with water at temperatures of 30-80 ºC to form calcium hydroxide, also called slaked lime or milk of lime ($Ca(OH)_2$). After slaking, the slurry is screened to remove impurities. Calcium hydroxide is then

introduced with carbon dioxide in a controlled environment to generate precipitated calcium carbonate crystals. The CO_2 used in carbonating may be taken from the flue gas originating from the calcination process. The amount of CO_2 needed in the carbonating process is equal to the amount of CO_2 that was released in the calcination process (Alen, 2007)

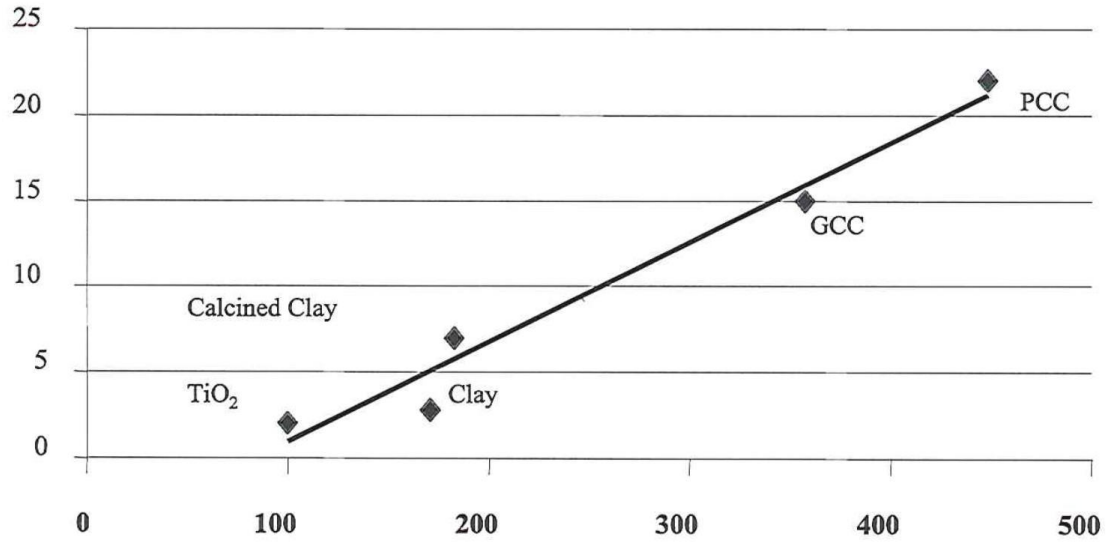

Picture 3. Brightness x Light scattering/Cost ratio with different pigments (Mueller, 2005)

According to Mr.Yeakey of the chemical company Omya, the consumption of PCC worldwide was over 6Mt in 2006, of which over 5Mt was used as filler. (Yeakey, 2009)

$$\mathbf{CaCO_3}\ (\text{Limestone}) + \mathbf{Heat} \Rightarrow \mathbf{CaO + CO_2}$$

$$\mathbf{CaO + H_2O \Rightarrow Ca(OH)_2}$$

$$\mathbf{Ca(OH)_2} + \mathbf{CO_2} \Rightarrow \mathbf{CaCO_3}\ (\text{PCC})$$

Formula 1. Chemical reaction in PCC manufacturing process

1.3.6 Crystallization of PCC

Calcium carbonate, $CaCO_3$ occurs in three different crystalline polymorphs, calcite, aragonite and vaterite. Calcite is the only thermodynamically stable form, while the other two are metastable and will eventually change into calcite when heated or exposed to water. The crystal

habits of aragonite usually observed are an elongated prismatic or acicular form. Vaterite also has the chemical formula $CaCo_3$. It is even more soluble than calcite and aragonite. When vaterite reacts with water at a low temperature, it turns into calcite, and when it reacts with water at a high temperature of 60º C or above, it transforms into aragonite. The crystal habit of vaterite usually observed is a spherical form (Hagemayer, 1984)

Crystallization is an organization of matter into solids of well-designed shapes. Crystals may form from a liquid solution, vapor or liquid melt. A crystal formation process involves two distinct steps; nucleation and growth. Nucleation can be described as a joining of molecules while growth is a process where more molecules are clustered to the crystal lattice. When these two phenomena occur simultaneously, and large enough crystals are formed to settle out of suspension, precipitation takes place. The key factor for precipitation is supersaturation, which can be achieved either by cooling the solution, evaporating the solvent or mixing two solutions. By altering reaction rates, a variety of different crystal shapes, sizes, size distributions and surface properties can be generated for fulfilling specific performance requirements.

All morphologies of PCC have been observed to affect some properties of the paper, for example a scalenohedral rosette-shaped type of PCC provides better bulk and caliper compared to ground calcium carbonate or kaolin, although strength properties are usually reduced. By combining different carefully selected morphologies, the properties of a specific paper grade can be optimized. (Thorn, 2009)

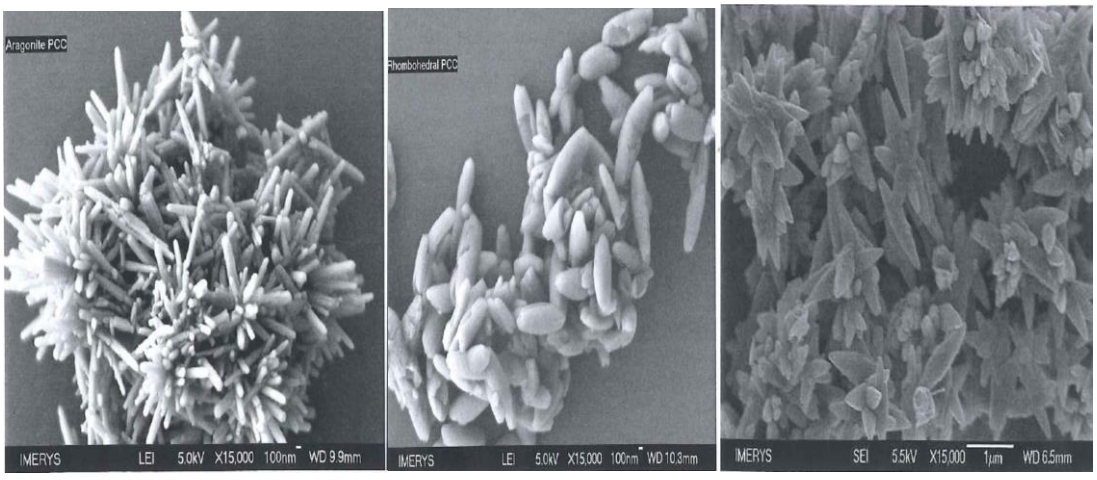

Picture 4. Common PCC crystal forms. From left to right: Aragonite (needle shaped), Rhombohedral (cubic shaped), Scalenohedral (rosette shaped) (Thorn, 2009)

1.3.7 PCC reaction rates

Reaction temperature, carbon dioxide partial pressure, the flow rate of carbon dioxide, lime slurry concentration and agitator speed are the most important factors in controlling the crystallization reaction. In general, cool temperatures during the addition of CO_2 tend to produce a rhombohedral crystal structure and warmer temperatures tend to form scalenohedral crystal structures. Experiments conducted in a study by Teir et al. for the Helsinki University of Technology showed carbonation temperatures between
41-90 ºC, resulting in a scalenohedral crystal. Between -1 to 10 ºC, rhombohedral crystal was formed and the threshold temperature for the aragonite structure was approximately
49 ºC. When the carbonation reaction starts, the pH of the lime slurry is at the range of 12 or higher, but decreases quickly as the reaction proceeds down to equilibrium pH 8 ± 1. The carbonation reaction is regulated by the solution equilibrium: When calcium ions precipitate to calcium carbonate, more calcium hydroxide dissolves to equalize the concentration of calcium ions. (Teir et al. 2005)

*The rate of dissolution of $Ca(OH)_2$ into Ca^2+ depends on the dissolution pressure and temperature, while the reaction rate of calcium ions combining with carbonate ions is instantaneous. Therefore, the rates of formation of calcium and carbonate ions are the primary limitations for the overall reaction rate. With a pressurized reactor, the overall
reaction rate is greater than with an atmospheric reactor, since the solubility of carbon dioxide is higher at elevated pressure. Pressures in the range 1–10 bar can be used, while 2–3 bar is the recommended value. The overall reaction rate for commercially used atmospheric PCC production processes is in the range 0.5–1.5 g/lmin of $Ca(OH)_2$* (Teir, et al. 2005) Overall, morphology and size distribution of particles are influenced mostly by the temperature and super saturation level of the system (Ukrainczyk et al., 2006)

1.3.8 Traditional method of manufacturing and application of PCC (Offline-PCC)

Generally, PCC is manufactured in plants located on-site at the paper mill. They are called satellite plants which may be owned and ran by a filler supplier. Carbon dioxide gas or CO_2

dissolved water is bubbled through slaked lime in large pressurized or atmospheric tanks and stirred simultaneously to set off the crystallization reaction. From the satellite plant the aqueous slurry of PCC at low solids is screened and led directly to the pulp preparation site via pipeline and then mixed with pulp among other chemicals. (Thorn 2009)

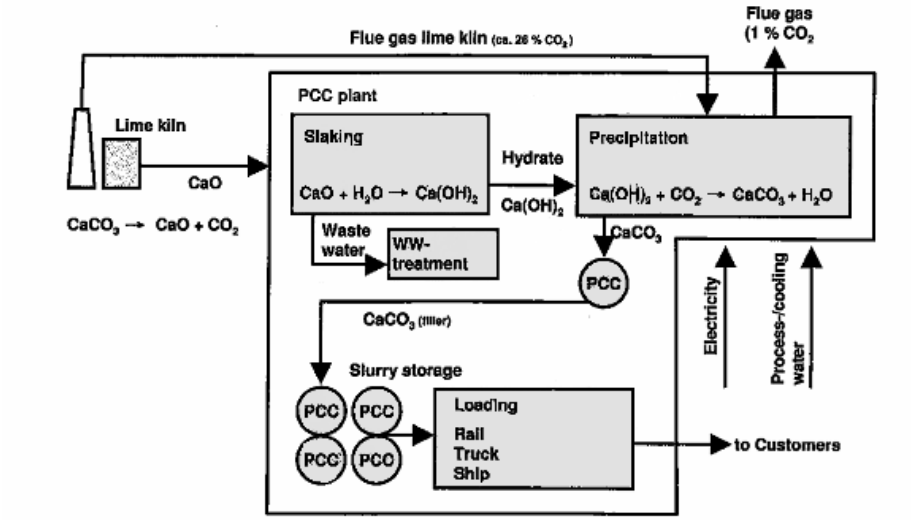

Picture 5. Typical offline-PCC manufacturing process

1.3.9 Inline PCC composite

Different approaches have been proposed and experiments done for increasing filler contents without diminishing paper quality. One of the latest innovations in the field of filler-fiber composite has been developed by the Finnish company Wetend Technologies.

With this invention, diluted pulp, calcium hydroxide solution and pressurized carbon dioxide are mixed in a specific reactor by using TrumpJet® technology. This technology enables an efficient dissolving of CO_2 to water by breaking down the bubbles and then spraying it to the short circulation. Simultaneously calcium hydroxide is led through another TrumpJet unit nearby where agglomerates are efficiently broken down for improved mass transfer from solid phase to water phase. As these two flows are introduced together with fibrous stock, precipitation in the reaction chamber occurs in seconds. With the described method, calcium hydroxide precipitates as a form of PCC in the reaction chamber instantly in the head box feed stock of the paper machine. Since paperboard fibers are present when the reaction occurs, the

fibers resemble a platform where calcium crystallizes firmly making a strong mechanical bond. (Imppola,WO Pat.2009/083633, Imppola et al.WO Pat.2011/110744)

1.4 Alternative methods of using PCC as filler

As stated earlier, a number of studies have been conducted and various technologies experimented with for improving the properties of paper when PCC is used as filler. A common problem in this field is poor retention, and inadequate strength properties of the end product. However, the general view of paper made from pulp where filler has been incorporated is positive. Several advantages in addition to savings in fiber material have been found, such as improvements in optical and surface properties as well as machine runnability.

1.4.1 Lumen and wall loading

The concept of lumen loading technology has been studied since the 30's. (Haslam et al 1936) Lumen loading is a technique, where filler, (calcium carbonate, or something else) is absorbed into the fiber cell and lumen, while in the conventional filler adding process, the filler particle is located between the fibers to fill the void spaces. The technique was developed to improve filler retention, and at the same time to enhance the stiffness of the paper. When filler is located within the lumens, it should not interfere fiber to fiber bonding. The disadvantages of the process include a decline in bonding properties as fiber cells stuffed with filler become less flexible. (Auranen et al 2006)

The principle of this technique is based on a mechanical diffusion of never dried pulp. Filler in aqueous solution is stirred with aqueous pulp for a period of time. During that time, the fiber and filler components are mixed together and some of the filler impregnates within the fiber lumens by mechanical diffusion. After fiber-filler components have been effectively mixed, a flocculating agent is applied. The flocculating agent causes the filler to form agglomerates of sufficient size to prevent diffusion outside of the lumens during the rest of the paper manufacturing process. In the described method, the type of mineral filler has a strong influence on the level of lumen loading as small filler particles will diffuse more easily than larger ones.

The concentration of fiber and filler solutions mixed together also has an effect on the extension of the loading level. (Hockman, Sohara, 1999)
With this method, approximately 0,08g filler in 1g fiber has been obtained. In applications where fibers have been pretreated with polyethylenimine or polyacrylamide among calcium carbonate, a filler level of 0,12g – 0,30g per a gram of fiber has been achieved. (Middleton et al. 2003)

1.4.2 In-situ loading

The aim of in-situ loading is fairly the same as that of lumen loading; only the method of loading differs slightly. Basically, there are two variations, of which in the first technique, calcium chloride solution or other soluble salt is impregnated into fiber. The excess is drained away and then another soluble salt, such as concentrated sodium carbonate, is added which then precipitates within the voids of the fiber cell wall. The downside of the method is that sodium chloride remains as a byproduct. (Middleton et al. 2003)
In the second variation, the basic idea is to impregnate fibers with calcium hydroxide suspension and then treat them with pressurized carbon dioxide gas to cause the precipitation reaction of calcium carbonate directly inside the fiber wall and lumen. Washing the fiber may be then required for removing the excess filler from the outside surfaces as it could interfere with fiber to fiber bonding. (Klungness et al). Both of the procedures also have disadvantages, such as irregular particle size distribution, and possible deviations in the process. (Middleton et al. 2003)

Picture 7. SEM microscopic image of cross section of a fiber within-situ precipitated calcium carbonate (Kumar et al. 2009)

1.4.3 Starch coated PCC

Starch has long been used as additive in papermaking, not only its improvements in strength, stiffness and absorption properties, but also due its relatively low price. In conventional starch application methods where starch is mixed with fibers and fillers, the absorption of starch results only in molecular level thickness on the surface of fillers and fibers. In this approach, the basic idea is to coat filler with swollen starch instead of molecular level starch as the behavior of swollen starch is considerably different. The dispersion of swollen starch forms a suspension which in papermaking conditions is very difficult to dissolve into solution. In this method, PCC is modified by mixing either native or modified starch powder (loading amount 12% of PCC weight) into a PCC suspension, which then is squeezed to remove excess water until required water content is obtained. The formed paste is then heated in 90ºC for 3 hours which results in a partially cross linked, water insoluble starch gel. The gel coats the filler surface and binds the filler together. In order to ensure uniform coating, the cooked mixture is grinded in mortar. Before being added to the pulp, the ground mixture is broken up in water solution resulting in small and strong aggregates. The use of cationic retention aid is required.
When comparing certain key properties of hand sheets by either using the starch coated PCC technique or the conventional PCC loading technique, starch coated PCC has been found to improve tensile and tearing strength and folding endurance. However, the optical properties were slightly lower (Zhao et al, 2005)

1.4.4 PCC cellulose composite

Subramanian et al. (2007) approached the issue of using PCC as filler by treating a 2:1 mixture of fiber fines and calcium hydroxide suspension with a stoichiometric amount of carbon dioxide. The precipitation was accomplished by altering the reaction rates described by Yamada & Hara, and thereby they were able to amend the crystal shape and size in order to achieve different properties for formed sheets. (Yamada & Hara 1985 $_{a\text{-}c}$). Subsequently, they mixed the formed PCC- fiber fines composite and retention aid with base pulp and then used it as filler for loading the paper.

By altering the parameters in the precipitation, they were able to find differences in the properties of paper used for printing and writing. Similar observations were made by Silenius (2002) when he precipitated calcium carbonate on fibril fines made from beaten kraft pulp. The thicknesses of the fibrils used were approximately the same range as the diameter of filler particles. Sodium silicate and starch were used as retention agents. According to his studies, this technique results in a chainlike structure of PCC and provided an improved light scattering coefficient along with better tensile strength compared to traditional PCC loading techniques. He called the technology SuperFill.

1.5 Filler cost structure

Table 3 presents the average price of calcium in different forms and the price of calcined kaolin. A major part of the calcium price derives from the calcination process.

Table 3. Average price of calcium and calcined kaolin in 2004
(Teir et al 2005, Maloney 2010)

Mineral	**€ / ton**
Calcium carbonate (limestone lumps) for calcination	11
Offline-PCC (cheapest quality)	120
Calcium oxide (CaO)	100
Calcined kaolin	500

While there is not a major difference in the purchasing prices compared to calcium oxide and offline-PCC, on the production lines that already use PCC as filler, greater savings are expected to be achieved by replacing more expensive fillers with Inline PCC. In addition, savings through improved runnability of the machine, and thereby superior quality of the product, are expected, as the use of retention aids may be reduced (Liukkonen, 2012). In production where fillers are

not currently applied, the savings are related to replacing a portion of fibers with inexpensive filler.

2 MATERIALS METHODS AND EQUIPMENT

2.1 Pilot scale paper machine

Trial runs were performed with the Stora Enso research center pilot scale paper machine (picture 11). The machine is capable of speeds from 20m/min to 100m/min and base weights from 20g/sqm to 280g/sqm. Maximum net width of the web is 700mm and the production capacity approximately 360kg/h. The maximum diameter of a finished reel is 1100mm. Changes in recipe at the machine are relatively quick, which enables a number of trial points in one day. Starting from the beginning of the manufacturing process, the pilot machine consists of pulp handling, pulp refining, short circulation, head box, wire section, press section, drying section, size press, on-line measurement, calendar and pope.

Pulp may be either manufactured on site from dried cellulose in a 5m³ pulper, or is transported as slurry by a tank truck from a pulp mill. At the preparation section, a total amount of 50m³ pulp can be stored.

Fiber clusters are defibrillated with a fiberizer, enabling pulp to be refined with a conical or disc refiner in order to improve its bonding ability. Larger impurities are removed in a pressure screener and other impurities heavier than fibers are separated with Bauer centrifugal cleaners in the short circulation. Pulp is diluted and led to the Vaahto dilution head box which has adjustable valves. In between the head box and the pulp preparations there are several points where chemicals may be applied in short circulation.

Tap water or river water may be chosen for diluting.

The wire section is a fourdrinier type equipped with a shaking ability for better formation. Excess water is drained with 5 vacuum boxes and a suction roll. In the press section, there are 3 double felted presses each having a maximum load of 50 kN/m. The drying section consists of two drying groups including 12 fully steam heated cylinders with a maximum temperature of 155 ºC. A conventional type size press, which is located just before the end of drying section, can be used to apply starch. Starch improves surface strength, stiffness and absorption properties.

Measurements such as base weight, ash and moisture can be followed and recorded online with an EL-sensor unit. Before winding at pope, the web may be calendared in either hard or soft nip with a maximum load of 100 kN/m.

2.2 In-line PCC equipment

The Inline-PCC system is a separable loop positioned in between the main head box feeding pipe just before the centrifugal cleaners. It consists of two TrumpJet® forte units which are attached to the reactor pipe, an injection pump and manifold with flow meters, pH measuring unit, CO_2 reservoir with pressure and flow adjustment capability and an independent calcium hydroxide container.

The loop is enabled by opening the valves which lead to the head box feed stock, entering the inline-PCC system circulation and then back to the main line. A portion of the flow is led to an electric motor-powered pump which allows the adjustment of the injection flow through the manifold to the mixer units. The TrumpJet forte® mixing unit is based on two tubular shaped parts where the outer one is fed with the injection liquid and the inner part with either carbon dioxide or calcium hydroxide. Carbon dioxide is fed to the unit from a reservoir of 12-gas cylinders. Calcium hydroxide solution is pumped to another mixer unit from a separate container and its flow is measured with flow meter. Each of the TrumpJet units has a specific nozzle design which allows calcium hydroxide and carbon dioxide efficiently to mix with the injection liquid in time as the flow enters the reactor pipe.

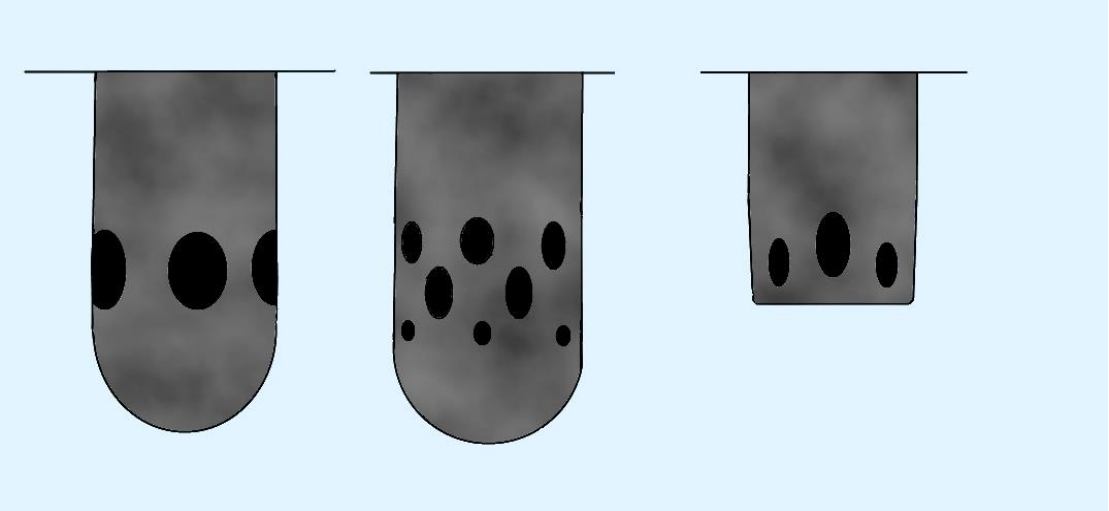

Picture 8. Different nozzles for carbon dioxide and calcium hydroxide.

Mixing reaction can be affected by the nozzle geometry and quantity and size of the orifices.

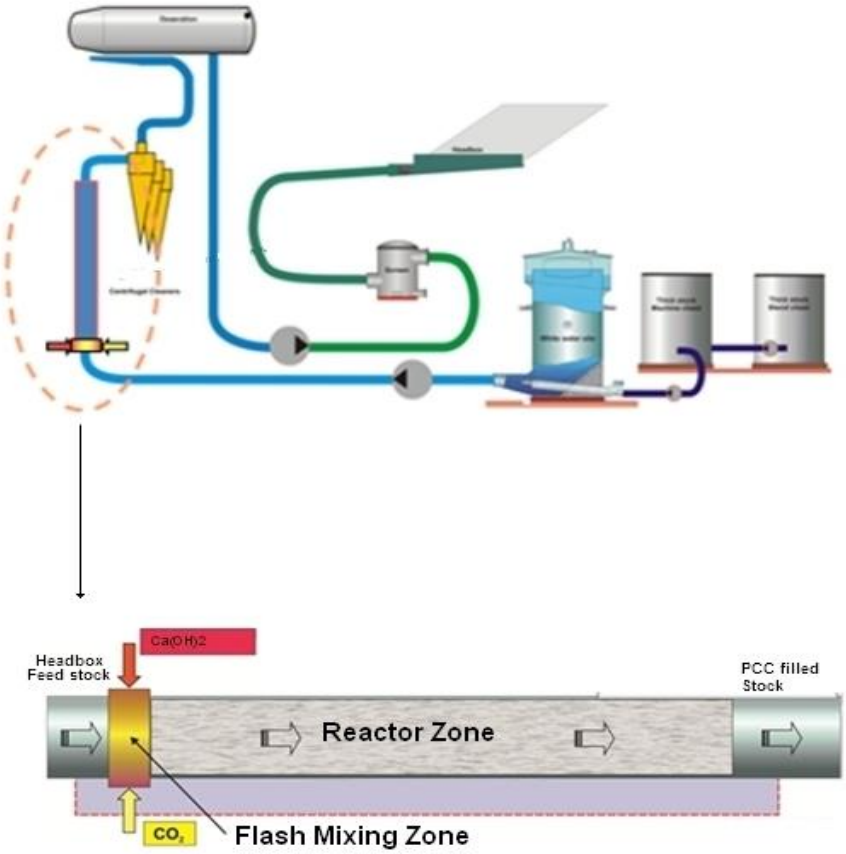

Picture 9. Inline-PCC system

2.2.1 Trumpjet® settings

The injection flow of Trumpjet® units can be altered by adjusting the pump revolutions. Injection flow adjustment is based on the depth in mass flow and the number of used Trumpjet units. In main feedstock flow, injected chemicals will mix according to the diameter of reactor pipe for a desired time period. By increasing the injection flow mass transfer from solid/gas phase to liquid phase can be accelerated. The precipitation of PCC occurs in the liquid phase. The injection flow is measured with a Siemens Sitrans Magflo magnetic flow meter. The feedstock flow setting is based on experimental knowledge, and can be amended when necessary. Flow differences between Trumpjet units can be equalized by slightly adjusting the manual valve on the injection manifold.

2.2.2 CO_2 settings

The carbon dioxide reservoir consists of twelve gas cylinders containing 60 bar and a total amount of 360 kg of liquefied gas. When pressurized liquid is discharged from the cylinders, the liquid changes to gas and simultaneously cools down. To prevent ice depositing, the gas is heated with an electric heater unit. Pressure adjustment of carbon dioxide gas is done with a pressure regulator. The pressure of the carbon dioxide has to be set above the pressure of the feedstock pipe to allow the flow. The pressure can be adjusted between 1-15 bar.

Picture 10. CO_2 reservoir

The gas flow can be manually adjusted with the Kytölä VE2A rotameter and measured with the Danfoss Massflo 2100 coriolis mass flow meter. Settings range between 1-80kg/h.

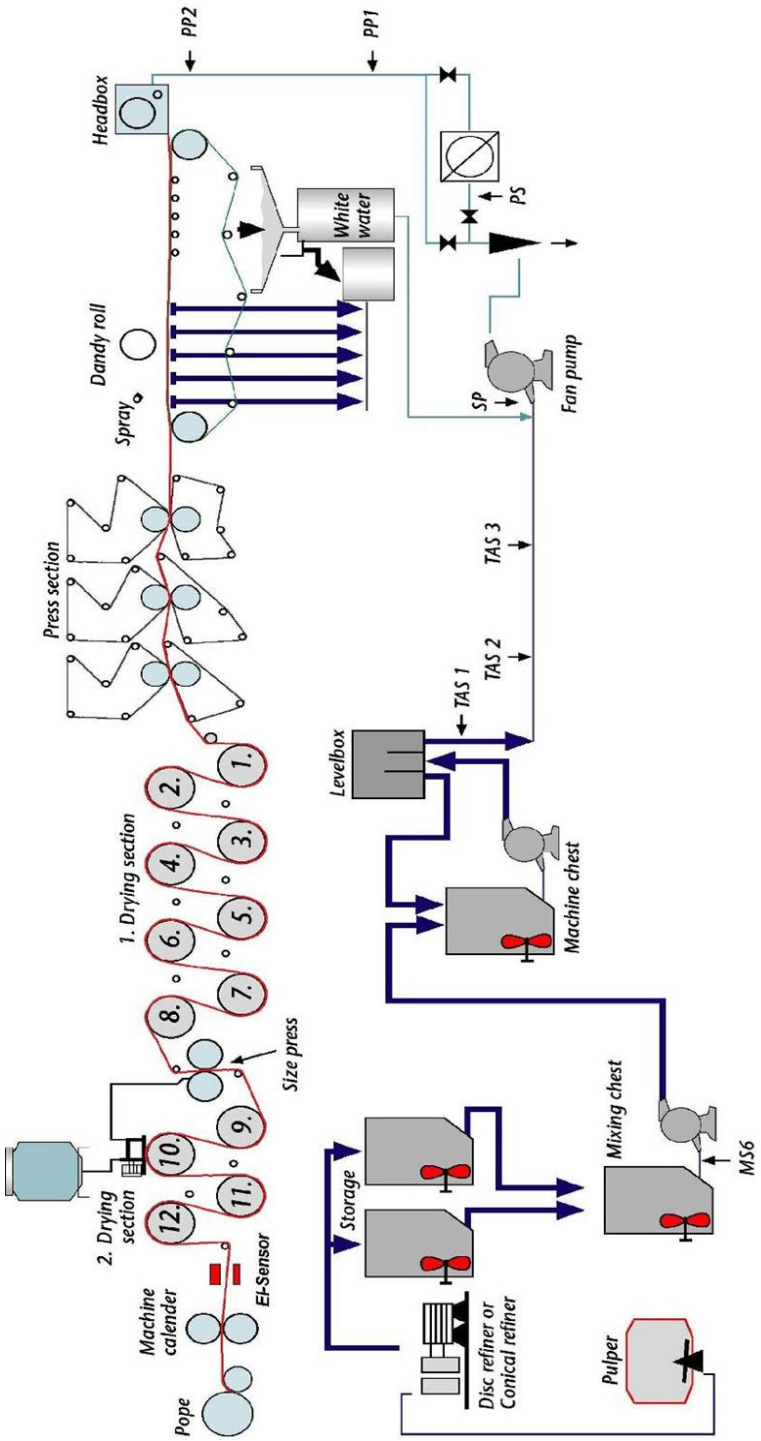

Picture 11. Stora Enso research centre pilot scale paper machine process scheme

2.2.3 Chemicals and recipes

Chemicals can be applied in multiple phases of the manufacturing process. In total, there are 10 chemical application points, which are illustrated in picture 11. Used chemicals in these trial runs include starch both as a strength improver and as a retention aid, hydrophobic agents such as ASA or AKD, alum for providing improved sizing, drainage, and retention of sizing agents. In addition, colloidal silica was applied as retention aid. In the 2nd and 3rd trial, CMC was used for improving the absorption and retention of cationic starch. In trial 4, bentonite crystalline silica was fed into the reactor injection line as seeds for a precipitation reaction. The fed amount of each chemical is monitored with magnetic flow meters and adjustments made by changing pump revolutions.

2.2.4 Milk of lime

Calcium hydroxide used in the trials originates from the Stora Enso Varkaus mill. It was delivered as a solution of which measured dry matter content was 8,5 - 10,4 % and density between 1,04 to 1,05. The solution was transported in 1m³ containers which is an adequate amount for one trial batch. The particle size distribution of the used calcium hydroxide was measured with a laser diffractometer at the Lappeenranta University of Technology.
According to research in the area made by Stora Enso Oyj, narrower size distribution and smaller particle size improve the precipitation reaction and thereby the runnability of the paper machine. The dosage of calcium hydroxide is made by adjusting a pump according to desired ash content in the paper. Flow is measured with a Siemens Sitrans Magflo magnetic flow meter.

2.2.5 Paperlab analysis

Paper samples were analyzed with the Metso Paperlab Plus 24 ASF, an offline testing system. Test modules include various optical and mechanical tests such as basis weight, caliber, roughness, porosity, gloss, whiteness, opacity, tensile strength, stretch, elasticity, tear and burst.

Paperlab testing modules comply with standards established by ISO and paper industry's major technical associations. More details of the standards used can be found in appendix 1.

2.2.6 White top Mottling

White top mottle, also called cloudiness of the paper, was analyzed using the Handy Measure v3 program. Measurement is based on the variation and size of reflectance value using a wavelength from 1 to 8mm. 5 points of 36mm x 36mm are measured from each sample sheet and their average value is calculated. In this thesis, white top mottling was measured against a brown background using Stora Enso's internal measuring method. (Ruohoniemi 2012)

2.2.7 Scanning Electron Microscope

Calcium hydroxide and paper samples were analyzed with a FEI Quanta 200 SEM/EDXA scanning electron microscope. The analyzed sample has to be either carbon or gold plated to make it conductive. SEM uses a focused beam of high-energy electrons to generate a variety of signals at the surface of solid specimens. The secondary and backscattered electrons that derive from electron-sample interaction are used for an imaging sample. Only solid and dried samples can be scanned. For this study, surface and Z-directional SEM images were taken from the samples.

2.2.8 Calcium hydroxide particle size measurement

Particle size distribution of the calcium hydroxide sample was measured by using a Beckman Coulter LS 13 320 particle size analyzer. Millipore water was used as a dissolution medium. During the measurements, an ultrasonic mixing rod was used for breaking possible agglomerates. Pump speed was maintained at 60 rpm. The measurement is based on laser diffraction, where particles of a given size diffract light through a given angle and intensity. Large particles scatter light at narrow angles with high intensity, whereas small particles scatter at wider angles but with low intensity. A series of detectors measure the light pattern produced over a wide range of angles. In laser diffraction, particle size distributions are calculated by comparing a sample's

scattering pattern with an appropriate optical model. The Fraunhofer optical model was chosen for these measurements.

2.2.9 Ash content measurement

Primarily, the ash content of the paper has been calculated before the manufacturing process and the settings have been adjusted accordingly, however there are a few methods in use for verifying this.

Ash content can be monitored with an EL-sensor which is located at the end of the drying section at the paper machine. This measurement cannot be considered as 100% accurate so normally adjustments are not made according to it. After manufacturing, the ash content of paper samples is measured in laboratory with a Makro TGA 701 thermo gravimeter. First the sample is placed in a pre-weighed ceramic crucible and into the furnace. The device raises temperature according to a variety of pre set programs. In the standard program, the temperature is first increased to 105ºC for 1 ½ hours at which time the moisture evaporates, and the sample becomes absolutely dry. The moisture percentage of the sample is recorded. Then the temperature is increased to 550ºC for 2 hours which is typically enough to burn all the organic material. The device is continuously measuring the changes in mass. A drawn curve of the changes in weight is available. The difference in weight between initial mass and ash mass, when taking moisture into account, reveals the filler content of the sample which is reported in percents. In this study, the ash content from all the samples was measured using the explained method.

In some cases, ash content may be measured by an express method during the trial runs. The measurement results based on this method are used for quick adjustments at the pilot machine if necessary. However, for speeding up the incineration process, the temperature has to be set very high which has an effect on the properties of the used filler. Therefore, specific correction factors are used.

2.2.10 Hand sheets preparation

The pulp of dry matter content of 2,8% was salvaged from trial 4, which was then diluted into 0,5% dry matter content and mixed both with and without cooked cationic starch of 20 kg/ton total content. The solution was heated to 45ºC on a hotplate. Calcium hydroxide which was also taken from trial 4's raw materials was injected among the solution with a syringe just before the carbonating process. The carbonating and mixing was completed with a Quantum Mark IV laboratory mixer. Hand sheets were prepared using an (MBF) moving belt former which is designed to simulate the water removing conditions of a paper machine while forming the sheet. (www.lut.fi) Hand sheets were pressed and drum dried according to the SCAN-C 26:76 standard. The target grammage of the prepared hand sheets was 65g/m² and the size of the sheets 190mm x 190 mm. SEM images of the produced hand sheets were taken for comparison.

Picture 12. Moving belt former (www.lut.fi)

2.2.11 Fourier transform infrared spectroscopy (FTIR)

Paper samples were analyzed with a Nicolet 6700 FT-IR. In FTIR analysis, the sample is subjected to infrared spectroscopy radiation. Each material has its characteristic vibration frequency. The analyzed sample absorbs some of the radiation and the part that passed through

the sample is collected in the detector. Spectrum shows the intensity of the absorbed radiation as a function of wave number. The sample is identified by the position, shape and intensity of the absorption lines. Specific databases are gathered for identifying the substances.

2.2.12 X-Ray diffraction (XRD)

Paper samples were analyzed using the Philips X'Pert Pro MPD powder diffractometer.
XRD is a non-destructive analytical technique that is used in identification of compounds. Diffraction yields information about crystalline structure and atomic arrangement. It is based on X-rays that scatter from atoms of the analyzed sample to the detector that interprets the diffraction based on their angle and intensity. The X-ray diffractometer consist of three basic elements: An X-ray tube, a sample holder, and an X-ray detector. X-rays are generated in a cathode ray tube by heating a filament to produce electrons, accelerating the electrons toward a target by applying a voltage, and bombarding the target material with electrons. When electrons have sufficient energy to dislodge inner shell electrons of the target material, characteristic X-ray spectra are produced. Every crystalline substance produces its own XRD pattern. Specific databases are gathered for identifying the substances.

2.3 Experimental

Each trial run is discussed separately in the following sections. A summary table of all the trial points from trials 1-5 can be found in appendix 10.

2.3.1 Trial 1

The objectives of trial 1 were to observe the overall functionality of the installed equipment, to find out whether inline-PCC would be a reasonable alternative for kaolin and how it would affect the optical and the strength properties of the paper at each ash content level. In addition, another objective was to find out the proper filler content level in contrast to the reference point.

The initial plan for trial 1 was to begin by producing a reference point with the pilot machine's standard recipe for modeling the surface layer of the uncoated multilayer liquid packaging board A. The recipe includes 5% calcined kaolin for improving the whiteness and opacity. After producing the reference point with the standard recipe, kaolin was replaced with the Inline-PCC while increasing the filler content in stages starting from 5% and ending at 20%. A target grammage of 65g/m² was kept constant. Fundamental goals during the 1st trial were to observe the runnability of the machine and the adjustment of carbon dioxide level according to the desired pH of the feed stock. A number of laboratory tests were performed on the paper samples and SEM images were taken.

8 trial points were prepared.

Table 4. Description and target of each trial point prepared

Trial point no		Target
1	Pilot machine standard recipe with 5% calcined kaolin	Reference
2	5% filler content with inline-PCC	Runnability & Paper quality
3	7,5% filler content with inline-PCC	Runnability & Paper quality
4	10% filler content with inline-PCC	Runnability & Paper quality
5	15% filler content with inline-PCC	Runnability & Paper quality
6	20% filler content with inline-PCC	Runnability & Paper quality
7	7,5% filler content with inline-PCC, -5% carbon dioxide from calculatory stoichiometric value	pH level check
8	7,5%filler content with inline-PCC, +5% carbon dioxide from calculatory stoichiometric value	pH level check

2.3.2 Trial 2

The objective of trial 2 was to improve the strength properties of the paper according to the received results in trial 1. A PCC concentration of 7,5% was chosen as the basis as trial 1 results indicated only minor degradation of strength properties while optical properties such as opacity and mottling were at desirable level. In addition, the porosity of the paper was found high which indicated potential for strength improvement.

The plan for trial 2 was to begin by producing a reference point with the pilot machine's standard recipe for modeling the surface layer of the uncoated multilayer liquid packaging board A. The recipe includes 5% calcined kaolin for improving the whiteness and opacity. After attaining the reference point, kaolin was replaced by 5% offline-PCC. Offline-PCC refers to an application of readymade PCC solution within the head box feed stock. This way a comparison between the traditional PCC application method and the Inline-PCC application method could be made. In trial 2, a scalenohedral offline-PCC was applied.

At trial points 5 and 6, cationic starch with carboxymethyl cellulose mixed among calcium hydroxide was experimented with. Carbon dioxide adjustment was done with the same setup as in trial 1. As there was an interest in finding out the effects of process water to the brightness and whiteness, tap water was used instead of the river water used in trial 1. A target grammage of 65g/m² was kept as a constant. A number of laboratory tests were performed on paper samples and SEM images were images taken.

6 trial points were prepared:

Table 5. Description and target of each trial point prepared

Trial point no		Target
1	Pilot machine standard recipe with 5% calcined kaolin	Reference
2	5% filler content with offline-PCC	5% Offline-PCC reference
3	5% filler content with inline-PCC	5% Inline-PCC reference
4	7,5% filler content with inline-PCC	7,5% Inline-PCC reference
5	7,5% filler content with inline-PCC, + 1% cationic starch among calcium hydroxide + 1% carboxymethyl cellulose (from total filler volume)	Strength improvement
6	7,5% filler content with inline-PCC, + 3% cationic starch among calcium hydroxide + 3% carboxymethyl cellulose (from total filler volume)	Strength improvement

2.3.3 Trial 3

The objectives of trial 3 were to specify the optimal filler content level and to learn how optical and mechanical properties would behave in contrast to each other while minor changes in filler content were made. Trial 2 results indicated starch as a potential strength improver, so the objective was to test whether the mechanical properties could be improved upon by increasing the dosage. In addition, it was noted that both filler pigments, that is, calcined kaolin and precipitated calcium carbonate, had positive unique features, therefore a mixture of them was experimented with.

The plan for trial 3 was to begin by producing a reference point with the pilot machine standard recipe for modeling the surface layer of the uncoated multilayer liquid packaging board A. The recipe includes 5% calcined kaolin for improving the whiteness and opacity. After obtaining the reference point, kaolin was replaced by 3% inline-PCC while increasing the filler content in stages until 7,5%. According to the results elicited from trial 2, an increased cationic starch dosage was experimented at trial point 6. At trial point 7, a mixture of different fillers with a total content of 5% and ratio of 2:3 was used. Trial point 8 was exactly the same as trial point 2. The reason for reproducing point 2, was to observe whether changes in paper occur when the machine has been running longer and the quantity of fiber fines increases. A target grammage of 65g/m² was kept as a constant. Carbon dioxide adjustment was done by starting +5% from the stoichiometric value and adjusted when necessary according the pH. River water was chosen as the process water. A number of laboratory tests were performed on the paper samples and SEM images were taken.

8 Trial points were prepared.

Table 6. Description and target of each trial point prepared

Trial point no		Target
1	Pilot machine standard recipe with 5% calcined kaolin	Reference
2	3% filler content with inline-PCC	3% Offline-PCC reference
3	5% filler content with inline-PCC	5% Inline-PCC reference
4	6% filler content with inline-PCC	6% Inline-PCC reference
5	7,5% filler content with inline-PCC	7,5% Inline-PCC reference
6	6% filler content with inline-PCC, + 5% cationic starch among calcium hydroxide + 2,5% carboxymethyl cellulose (from total filler volume)	Strength improvement
7	7. 5% total filler content including 3% inline-PCC and 2% calcined kaolin	Mixture filler, paper quality
8	8. 3% filler content with inline-PCC	Rerun of tp2

2.3.4 Trial 4

The initial objectives were tested in the 3 previous trials, so the objective of trial 4 was to find out the significance of factors other than filler content for paper properties and to the runnability of the machine. (According to the results from previous trials) 6% filler content level was chosen as basis for trial 4.

The plan for the trial 4 was to begin by producing a reference point with the pilot machine standard recipe for modeling the surface layer of the uncoated multilayer liquid packaging board A. The recipe includes 5% calcined kaolin for improving the whiteness and opacity values. After obtaining the reference point, kaolin was replaced by 6% inline-PCC. Previous trials had indicated that an elongated 1st inline PCC trial point is essential for improved accuracy of the machine settings, so the length of the trial point 2 was tripled compared to a regular trial point length. At trial point 3, calcium hydroxide was filtered with 80-micron bag filter in order to represent a highly homogenous raw material. At trial point 4 the temperature of the process water was reduced to minimum for enabling anticipated changes in the crystal structure of the

PCC. At trial point 5, bentonite was fed into the reactor injection line as seeds for a PCC precipitation reaction.

The objective of trial point 6 was to increase the conductivity of the process water by applying calcium chloride and sodium sulphate into the mixing chest. Carbon dioxide feeding pressure was increased at trial point 7.

Before trial 4, Trumpjet® nozzles were replaced with ones that have less orifices. This would presumably have a positive influence on the mixing effectiveness. A target grammage of 65g/m² was kept as a constant. Carbon dioxide adjustment was done by starting +5% from stoichiometric value and adjusted when necessary. River water was chosen as process water. A number of laboratory tests were performed on paper samples and SEM images were taken.

7 Trial points were prepared.

Table 7. Description and target of each trial point prepared

Trial point no		Target
1	Pilot machine standard recipe with 5% calcined kaolin	Reference
2	Elongated trial point of 6% filler content with inline-PCC	Elongated stabilizing period
3	6% filler content with inline-PCC using filtered calcium hydroxide	Highly homogenous calcium hydroxide
4	6% filler content with inline-PCC using minimum process water temperature	Crystal structure changes
5	6% filler content with inline-PCC + 100g/t Cloisite Na^+ bentonite	Precipitation seeding
6	6% filler content with inline-PCC, process water treated with calcium chloride and sodium sulphate	Increased conductivity
7	6% filler content with inline-PCC, increased carbon dioxide pressure	CO2 flow stability

2.3.5 Trial 5

The objectives of trial 5 were changing the morphology of the filler crystal and analyzing the impact on the paper. According to SEM images of 4 previous trials, it seemed that with the current setup, PCC crystallizes as spherical vaterite instead of the expected rhombohedral calcite. Based on positive results with mixture fillers and starch as a strength improver in trial 4, some of the trial points from earlier experiments were modified for improving certain areas of the properties. In addition, the difference between dried and undried pulp was tested. A 6% filler content was chosen as the basis.

The plan for trial 5 was to begin with undried pulp with 6% inline-PCC. Unlike the previous 4 trials, the calcined kaolin reference point was prepared at the end of the trial. The pilot machine standard recipe for surface layer of the multilayer liquid packaging board A includes 5% calcined kaolin for improving the whiteness and opacity values. The idea behind trial point 8 was to use purely undried pulp. The reason for the change in the running order was an attempt to keep the trial point with the undried pulp as pure as possible, as otherwise a small portion of dried pulp remains might have mixed together in the pulp mixing chest. Trial point 2 was an inline-PCC reference point with 6% filler content. At trial points 3 and 4, the Trumpjet® injection flow pump was adjusted first to double and then to half action with regards to the standard setting in order to find out possible changes in PCC crystal morphology.

At the 5th trial point, inline-PCC with 6% filler content was used and cationic starch added among the calcium hydroxide for improving strength properties. At trial point 6, a mixture of different fillers with a total content of 5% with ratio of 2:3 was experimented with.

At this trial point, cationic starch and CMC were applied among calcium hydroxide in order to affect the strength properties.

A target grammage of 65g/m² was kept constant. Carbon dioxide feeding was adjusted according to the desired pH of 7.8 - 8.0. River water was chosen as process water. A number of laboratory tests from paper samples were performed and SEM images were taken.

7 trial point were prepared

Table 8. Description and target of each trial point prepared

Trial point no		Target
1	Pilot machine standard recipe with 5% calcined kaolin	Reference
2	6% filler content with inline-PCC as reference point two	6% Inline-PCC reference
3	6% filler content with inline-PCC, increased Trumpjet® injection flow	Crystal structure changes
4	6% filler content with inline-PCC reduced Trumpjet® injection flow	Crystal structure changes
5	6% filler content with inline-PCC using undried birch pulp	Strength properties comparison
6	6% filler content with inline-PCC + 10% cationic starch among calcium hydroxide (from total filler volume)	Strength improvement
7	7.5% total filler content including 3% inline-PCC and 2% calcined kaolin + 4% cationic starch and 2% CMC among calcium hydroxide (from total filler volume)	Strength improvement

2.3.6 Starch experiments

As a secondary objective, some hand sheets were prepared as a thus far unknown veil or glue-like substance could be seen on the close-range SEM images of the paper samples. The veil was found in between and partially on top of PCC particles (e.g. picture 13). The idea was to find out whether the veil is related to the starch that is typically used as dry strength improvement. The experiment was carried out by preparing a batch of 20g/kg cationic starch and 7,5% calcium hydroxide mixed into the diluted pulp. Precipitation was carried out with a laboratory mixer. Another batch was prepared in the same way, but without the starch. The results were examined according to SEM-images.

2.3.7 Paper sample morphology analysis

Based on the SEM images of paper samples containing inline-PCC, filler particles consists mainly of spherical shaped crystals. According to previous experiences at Stora Enso Varkaus

mill, and tests made by Wetend OY, the expected dominant particle shape would have been a rhombohedral calcite, which is typically cubic shaped. (Stora Enso internal communication 2012) According to the literature within the field, the vaterite polymorph of calcium carbonate often exhibits in spherical shapes. (Specialty minerals, 2012) As a directional pre-test, a paper sample from trial 3 was divided into two pieces. One piece was soaked in RO-water over the weekend and dried in room temperature. The other piece was treated as a reference. A visual comparison of changes in morphology from both of the pieces was made according to SEM images. The definitive analysis was made using FTIR and XRD. Selected paper samples were analyzed to find out the proportions of vaterite and calcite from calcium carbonate in the paper samples. In addition, the influence of changes in process parameters to the morphology could be verified this way.

2.3.8 Filler particle analysis from a paper sample

The objective of this analysis was to determine the particle size distribution of the inline-PCC crystals. Fibers and other organic material were burned from the selected paper samples using a Macro TGA thermo gravimeter. Theoretically fillers such as calcium carbonate should not be affected by temperatures less than 500ºC, but practice has shown that even in temperatures over 400ºC particles tend to aggregate into larger clusters which consequently may distort the measurement results. Therefore, the incineration was first carried out in an oxygen atmosphere and temperature was set to 300ºC.

The Macro TGA is able to sense when organic material has burned out based on the weight stabilization of the sample and automatically stops the incineration. In this case the stabilizing took approximately 50 minutes.

It was found out that the residual coal of fiber was not completely burned at the temperature of 300 ºC in the said time period, even though the weight of the sample indicated the removal of most organic material. Therefore, the burning period was first extended manually to 6 hours but as the results were still not satisfactory, the incineration was extended to another hour at 500 ºC.

The residual filler ash was then mixed with Millipore water and the particle sizes measured with a Coulter LS 13 320 particle size analyzer. An ultrasonic rod was used in the beginning to break up the possible agglomerates.

3 RESULTS AND ANALYSIS

3.1 Trial 1 results

The most essential paper properties and ash measurement results of trial one are presented in tables 9-13. Paper properties are divided into surface properties, optical properties, optical properties against a brown background and strength properties. SEM images of surface and Z-direction from the most interesting trial points of trial one paper samples are presented in pictures 13-21. Picture 22 represents the SEM image of calcium hydroxide used in trial 1, while its particle size distribution is seen in diagram 1.

Table 9. The most important surface properties of trial 1

Trial point		**1**	**2**	**3**	**4**	**5**	**6**	**7**	**8**
	Unit								
Air resistance Gurley	s/100 ml	33	21	15	13	10	9	18	11
Bendtsen-roughness, ts + bs avg	ml/min	326	288	276	282	287	193	319	320
PPS 0.5, ts + bs avg	µm	6,1	6,1	6,1	6,1	6,0	5,9	6,1	6,2
PPS 1.0, ts+ bs avg	µm	5,9	5,9	5,9	5,8	5,7	5,5	5,9	5,9
PPS 2.0, ts + bs avg	µm	5,3	5,3	5,3	5,2	5,2	4,9	5,3	5,4

Table 10. The most important optical properties of trial 1

Trial point		**1**	**2**	**3**	**4**	**5**	**6**	**7**	**8**
	Unit								
Opacity C/2° +UV, ts + bs avg	%	78,3	77,4	79,6	81,3	83,5	85,6	80,2	80,0
Light scattering coefficient +UV, ts+ bs avg	m²/kg	35,9	32,7	37,6	40,9	50,1	58,1	38,7	40,3

Table 11. The most important optical properties against brown background of trial 1

Trial point		**1**	**2**	**3**	**4**	**5**	**6**	**7**	**8**
	Unit								
Brightness R457 C/2° +UV, ts+ bs avg	%	71,8	68,0	70,6	72,7	75,0	77,3	71,1	71,2
Brightness R457 D65/10° +UV, ts + bs avg	%	71,8	68,0	70,6	72,7	75,0	77,3	71,2	71,2
CIE whiteness C/2° +UV, ts + bs avg	%	66,9	58,0	61,8	64,7	68,2	71,4	62,7	63,6
CIE whiteness D65/10° +UV, ts + bs avg	%	67,0	58,4	62,0	65,0	68,4	71,6	63,0	63,9
White top mottle		1,419	1,231	1,083	1,123	1,043	1,068	1,230	1,243

Table 12. The most important strength properties of trial 1

Trial point		**1**	**2**	**3**	**4**	**5**	**6**	**7**	**8**
	Unit								
Tensile strength, Geom.avg. md+cd	kN/m	3,8	3,7	3,3	2,9	2,0	1,4	3,0	2,9
Stretch, Geom.avg. md+cd	%	3,3	3,4	3,2	3,0	2,6	2,2	2,9	2,9
Tensile index, Geom.avg. md+cd	Nm/g	56	56	50	43	32	22	46	46
Tensile stiffness, Geom.avg. md+cd	kN/m	444	409	417	388	307	221	409	370
Tensile stiffness index, Geom.avg. md+cd	MNm/kg	6,5	6,1	6,3	5,8	4,9	3,5	6,2	5,8
E-modulus, Geom.avg. md+cd	MPa	5048	4809	4844	4511	3569	2602	4759	4304

Table 13. Ash content measured from trial 1 paper samples by burning in 550 ºC

Trial point	P1	P2	P3	P4	P5	P6	P7	P8
%	5,0	4,7	7,2	9,9	14,9	21,0	7,6	7,8

Picture 13. 800x magnification SEM top image of the trial 1 paper sample containing 7,5% Inline-PCC

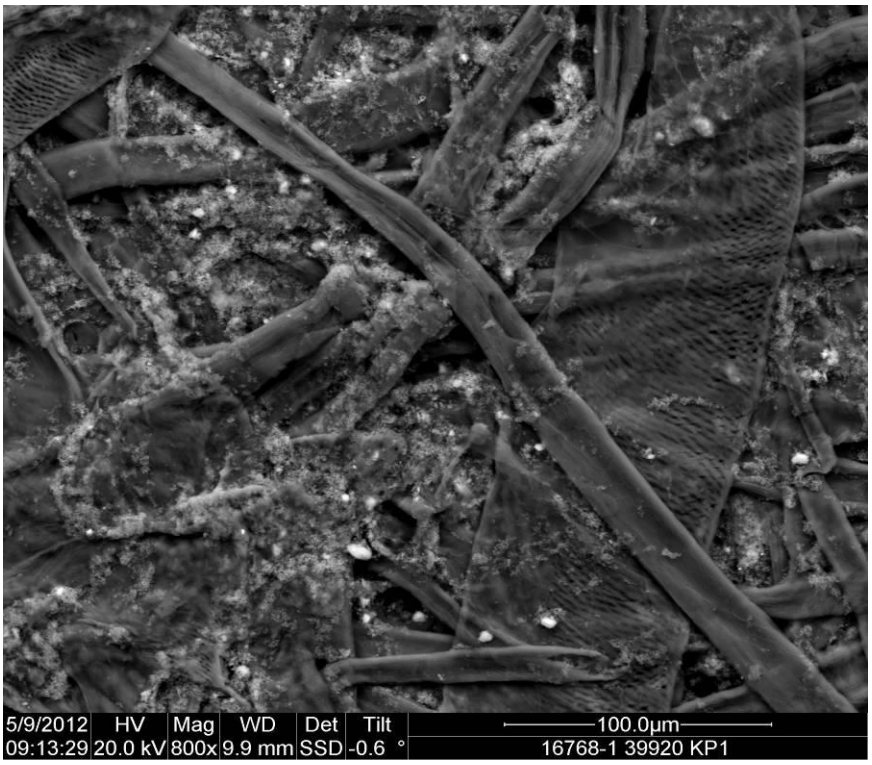

Picture 14, 800x magnification SEM top image of the trial 1 paper sample containing 5% calcined kaolin

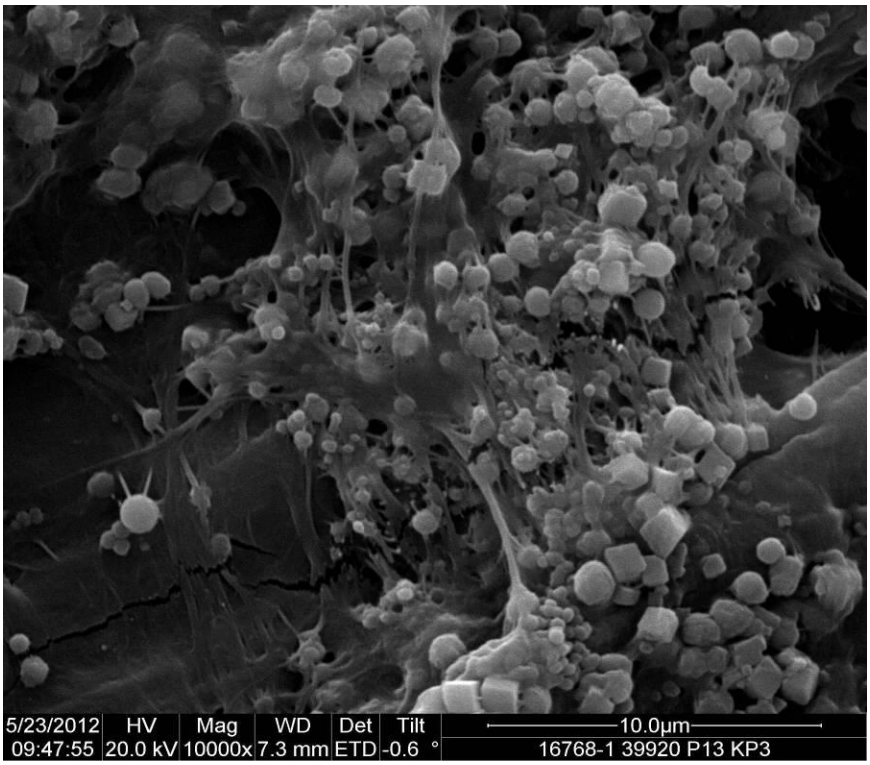

Picture 15. 10 000x magnification SEM top image of the trial 1 paper sample containing 7,5% Inline-PCC

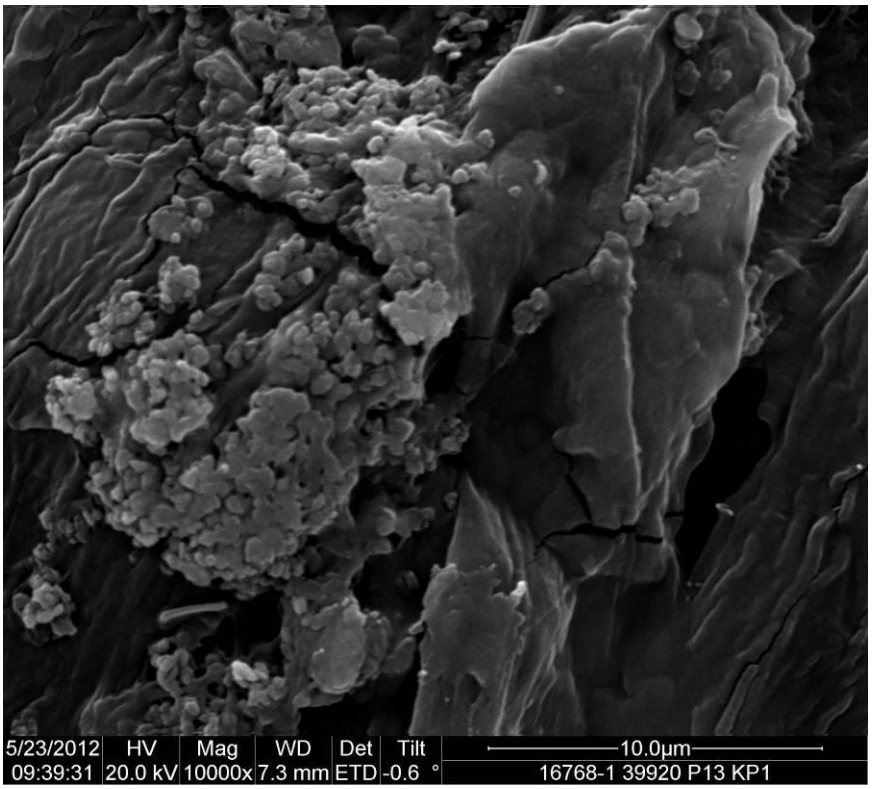

Picture 16, 10 000x magnification SEM top image of the trial 1 paper sample containing 5% calcined kaolin

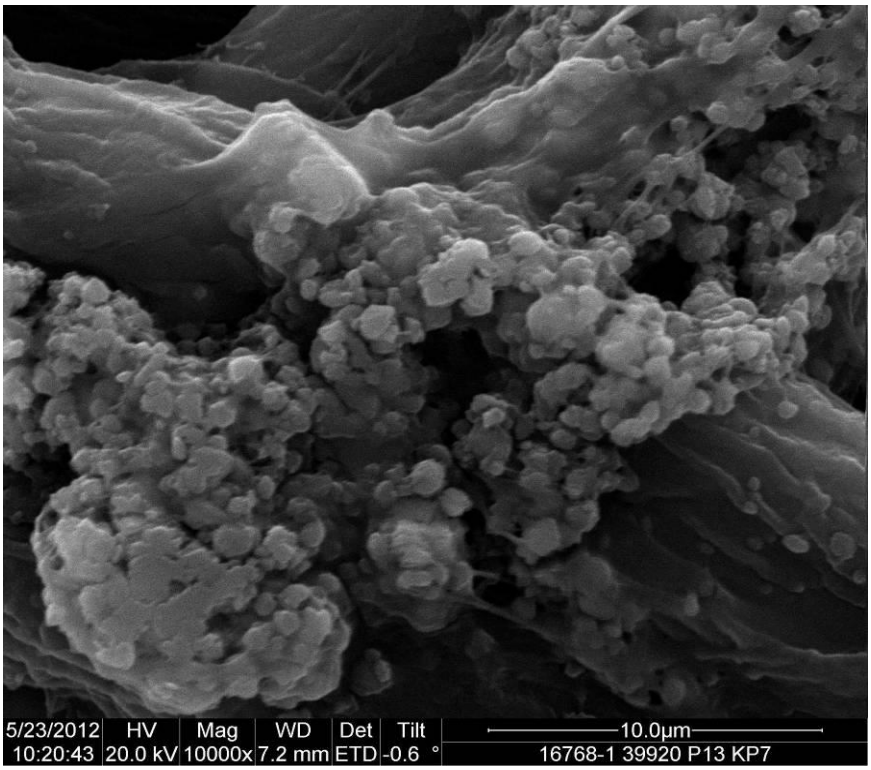

Picture 17, 10 000x magnification SEM top image of the trial 1 paper sample containing 7,5% Inline-PCC -5% CO_2 undersupply from calculated stoichiometric value.

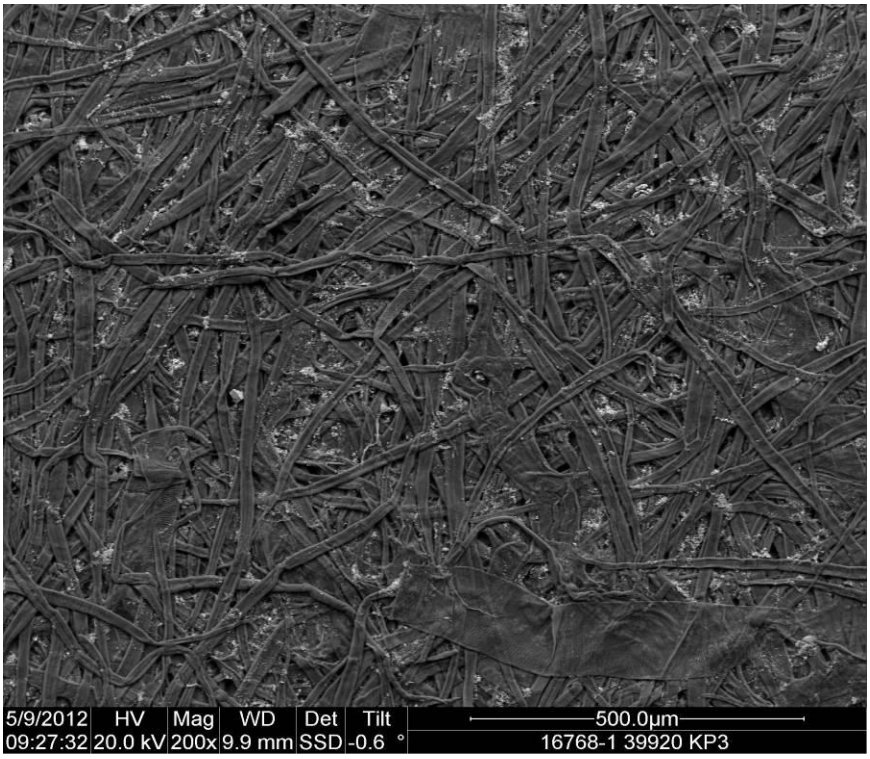

Picture 18, 200x magnification SEM bottom image of the trial 1 paper sample containing 7,5% Inline-PCC

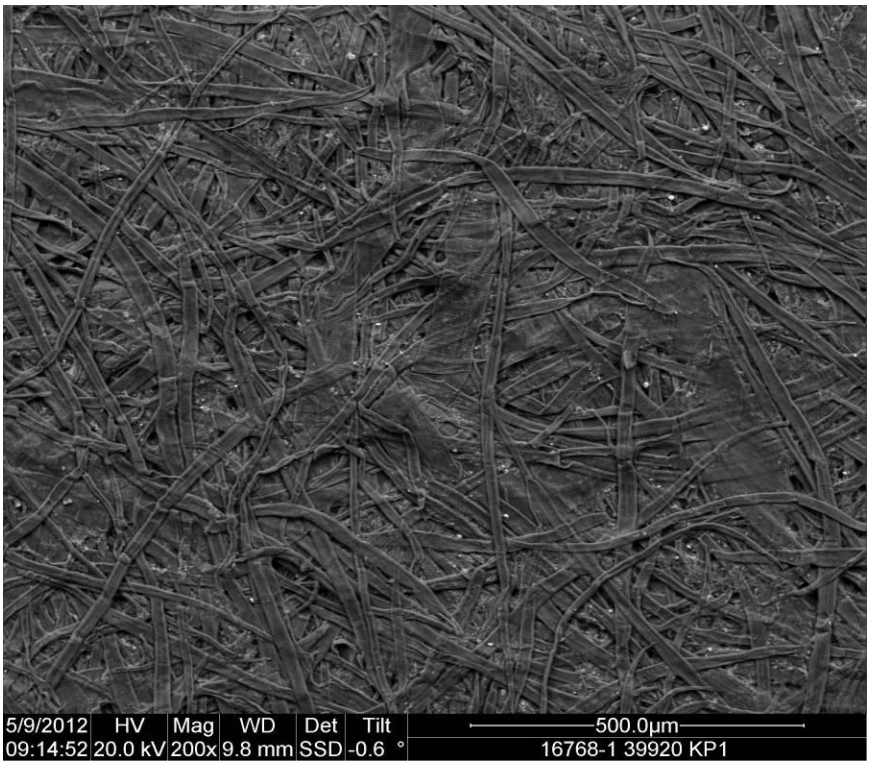

Picture 19, 200x magnification SEM bottom image of the trial 1 paper sample containing 5% calcined kaolin

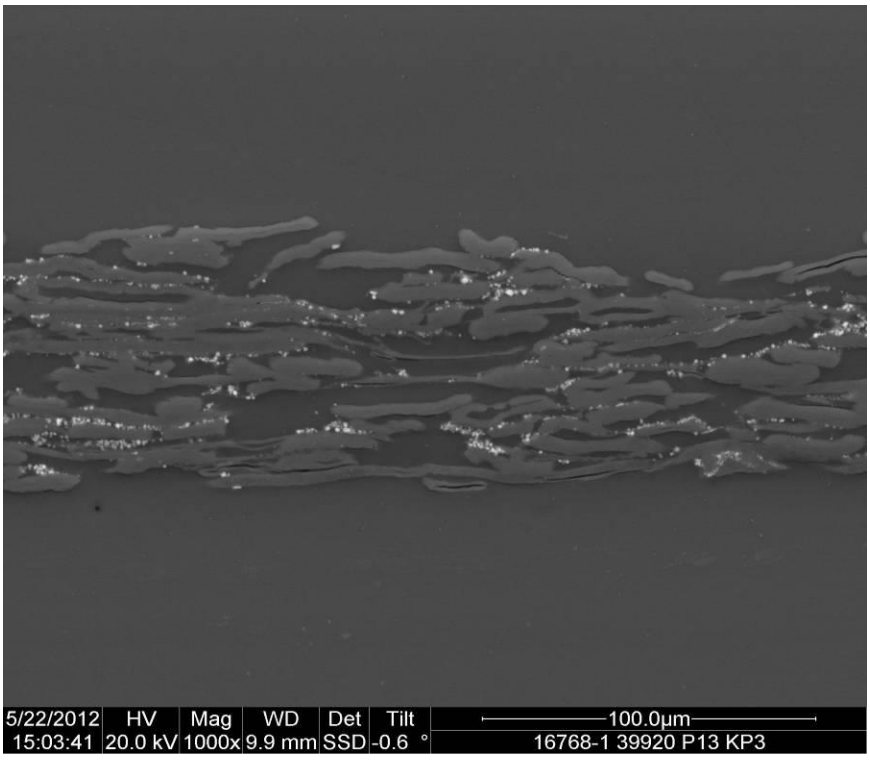

Picture 20, 1000x magnification SEM -cross section image of the trial 1 paper sample containing 7,5% Inline-PCC

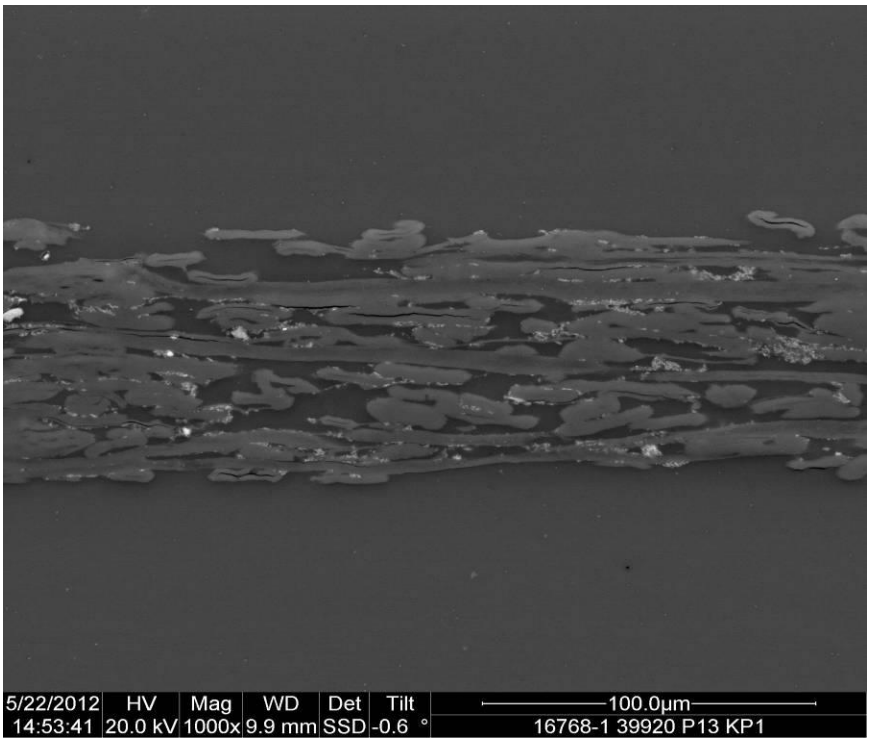

Picture 21, 1000x magnification SEM -cross section image of the trial 1 paper sample containing 5% calcined kaolin

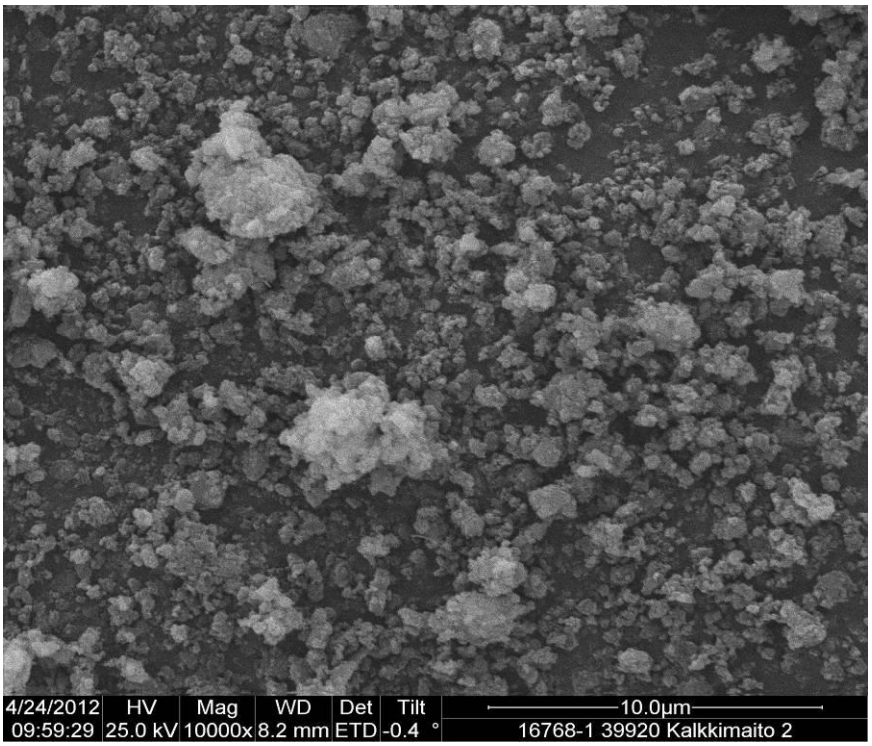

Picture 22, 10 000 x magnification of the trial 1 calcium hydroxide sample

Volume Statistics (Arithmetic)			120529_28_01.$ls	
Calculations from 0.040 µm to 2000 µm				
Volume:	100%			
Mean:	36.28 µm		S.D.:	43.58 µm
Median:	11.91 µm		Variance:	1899 µm^2
Mean/Median ratio:	3.045		C.V.:	120%
Mode:	12.40 µm		Skewness:	1.158 Right skewed
			Kurtosis:	0.090 Leptokurtic

<10%	<25%	<50%	<75%	<90%
1.043 µm	4.952 µm	11.91 µm	66.39 µm	108.1 µm

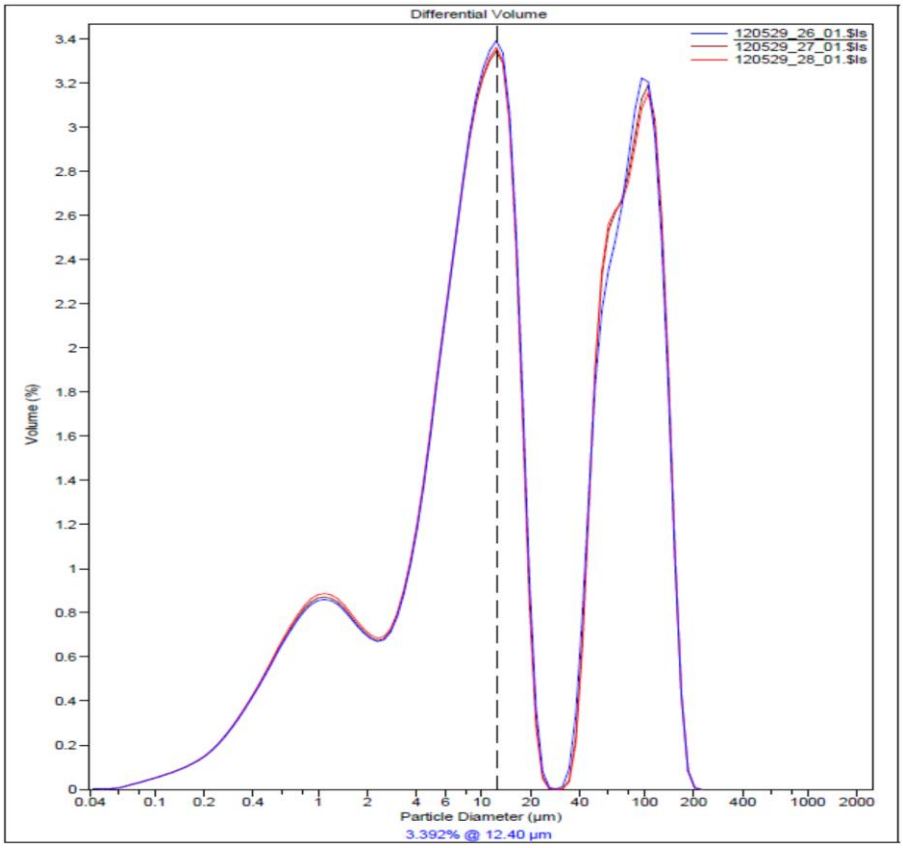

Diagram 1, Trial 1 Calcium hydroxide particle size distribution measured using Millipore water as dissolution medium

3.2 Trial 1 analysis

The main objectives of trial 1 were to observe the overall functionality of the installed equipment and to find out how different filler content levels would affect the runnability of the paper machine and the properties of the produced paper.

Soon after changing the filler from calcined kaolin to inline-PCC it was noted that for reaching the pursued pH level of 7,8, a relatively high dose of carbon dioxide had to be fed into the system. There was no obvious explanation as to whether this was due to a measurement error with the mass flow meter, or some other issue in the reaction.

According to the Paperlab results, optical, surface and strength properties were most balanced with 5 - 7,5% filler content. Strength properties decrease dramatically when filler content is increased to 10% or over, but on the other hand the optical properties rise considerably. According to the high resolution SEM images, PCC tend to crystallize as cubical or spherical shaped particles measuring approximately 1-2 micrometers, attached together with fibers by a glue-like substance. According to the SEM images, calcined kaolin seem to cluster on top of the fibers in very small particles measuring approximately 0,5 – 0,8 micrometers. 800 x magnification reveals calcined kaolin spreading out more evenly on the surfaces of the fibers, while PCC seemed to agglomerate mostly in between the fibers filling the gaps (pictures 13 & 14). This can also be observed from the cross-section SEM images. Cross directional SEM images show the filler particle distribution and the particle size difference between PCC and calcined kaolin. When carbon dioxide was undersupplied -5% from the stoichiometric value at trial point 7, the pH started to increase up to nearly 10. SEM images disclosed that a CO_2 undersupply results in a smaller than average PCC particle size (picture 17), which tends to lead to accumulation as framboidal clusters. Paperlab analysis also indicated a slight decrease in strength properties. Calcium hydroxide, which was used as raw material for PCC, was analyzed using SEM, with particle size distribution measured using a laser diffractometer. However, at the time when the particle size distribution measurement was performed, the sample had been preserved in a container for 6 weeks. It has been discovered, that calcium hydroxide tends to agglomerate into larger blocks relatively soon after manufacturing.

This was confirmed at the laser diffractometer which indicated high peaks at 100µm, 12µm and a low peak at 1µm. Median size was measured as 11,9µm. SEM imaging revealed a large variety

of size distribution, though much smaller particles starting from 0,1 µm up to 2µm. Even the use of ultrasonic rod during the measurement could not break the agglomerates. When comparing the received results with the reference point, significant differences between calcined kaolin and inline-PCC were found in such properties as Gurley air resistance, mottling and tensile strength. In addition, the filler retention level was notably lower with calcined kaolin than with inline-PCC. Therefore, further investigations were made in order to find out the reason for this. It was later discovered that many of the results received from calcined kaolin in trial 1, were deviant from the other 4 trials, thereby the results received from the inline-PCC trial points could not be directly compared with the reference point. One noteworthy reason for these deviations was the waterline at the web forming section. In a normal situation the visible waterline disappears just after the edge of the first vacuum box (Picture 23). At the trial 1 reference point, the waterline reached far beyond the edge of the 1st vacuum box. The shaking ability of the wire section is designed to reach the 1st vacuum box, and if the waterline reaches beyond, the fibers tend to flocculate forming clumps which then affects the formation among other properties.

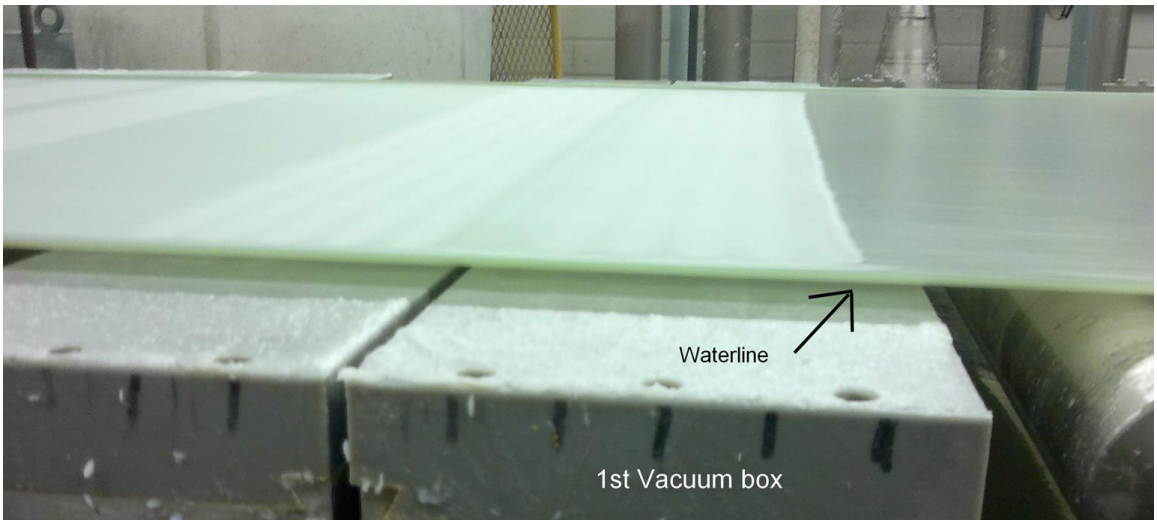

Picture 23. Normal waterline at the web forming section

This can be observed as a cloudy appearance of the paper (picture 24) and from SEM bottom images almost totally lacking filler particles. A comparison between the SEM bottom images

can be made between picture 18, which is inline-PCC, and picture 19, which is calcined kaolin. The exact reason for the further waterline could not be found, but a possible cause might be the change of the calcined kaolin brand. Originally the idea was to prepare a comparison chart where different trial points were compared with the reference point, but in light of the evidences that supports the reference point being unusable, the comparison was made between 5% of inline-PCC and higher filler contents of inline-PCC.

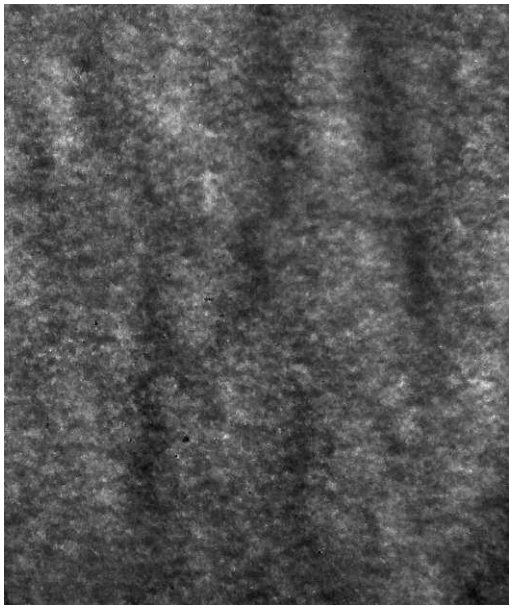

Picture 24. Trial 1 tp 1. Paper sample on a light desk. Color saturation adjusted

As stated earlier, increasing the filler content over 7,5%, dramatically decreases the strength properties, but at the same time improves the surface properties and optical properties.
Increasing the filler content from 5% to 7,5% appears to push up the whiteness for 1,5-2% and brightness for approximately 3,5%. Due to improved opacity, the significance is even clearer against a brown background. Mottling improves when filler content is raised from 5% to 7,5%, but then stabilizes. Beyond 7,5% the filler content does not seem to have yield any further improvements. (Appendix 2) These results indicated, that during the next trials, a filler content between 5% and 7,5% would be the level to aim for. Detailed Paperlab results can be found in appendix 3. No deviations were found in the runnability of the paper machine with a different filler content level. Altogether, the 1st trial went as initially planned without any major problems. A comparison of paper technical properties between 5% inline-PCC versus 7,5%, 10%, 15% and 20% inline-PCC is presented in the following matrix.

	Compared to the Trial point 2 (5% inline-PCC)
O	-3% - + 3%
-	- 3%- 10% deteriorated
- -	-10% -20% deteriorated
- - -	-20%... => deteriorated
+	+ 3% - 10% improved
+ +	+ 10% - 20%.. => improved
+ + +	+ 20%... => improved

Table 14. 5% inline-PCC vs 7,5 % , 10%, 15% and 20% inline-PCC

Measured Feature	7,5% offline pcc (tp 3)	10% inline pcc (tp 4)	15% inline pcc (tp 5)	20% inline pcc (tp 6)
Gurley air resistance	+ + +	+ + +	+ + +	+ + +
Bendtsen roughness	+	+	O	+ + +
PPS smoothness	O	O	O	+
Gloss	-	-	- -	+ +
Brightness	O	O	+	+
Whiteness	+	+	+ +	+ +
Opacity	+	+	+	+ +
Light absorption	O	-	O	-
Light scattering	+ +	+ + +	+ + +	+ + +
Stretch	-	- -	- - -	- - -
Tensile index	- -	- - -	- - -	- - -
Tensile stiffness index	+	-	- - -	- - -
E-modulus	O	-	- - -	- - -
Tensile energy absorption index	- -	- - -	- - -	- - -
Tear strength	-	- -	- - -	- - -
Tear index	-	- -	- - -	- - -
Burst strength	- -	- - -	- - -	- - -
Burst index	- -	- - -	- - -	- - -
Brightness against brown background	+	+	+ +	+ +
Whiteness against brown background	+	+ +	+ +	+ + +
Mottle	+ +	+ +	+ +	+ +

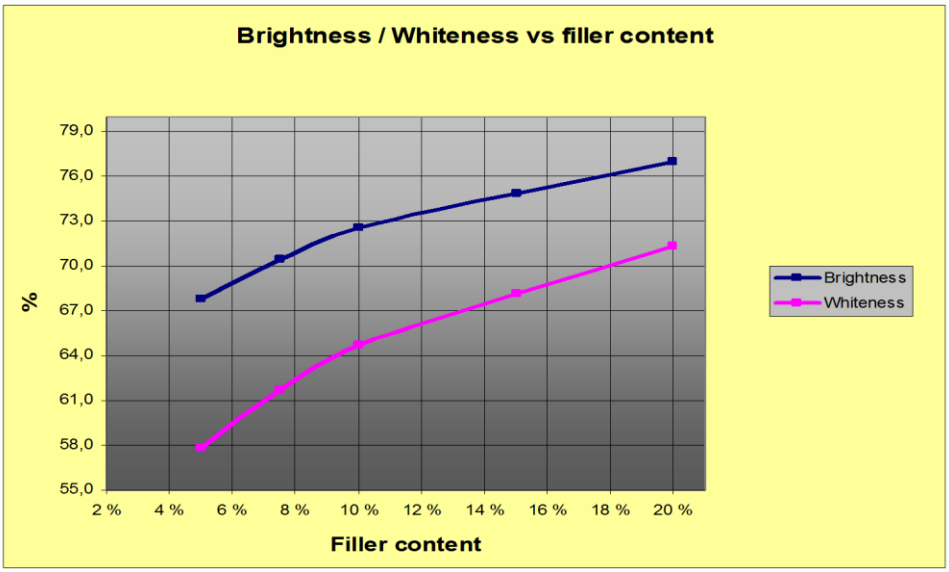

Diagram 2. Effects in brightness and whiteness when increasing the filler content

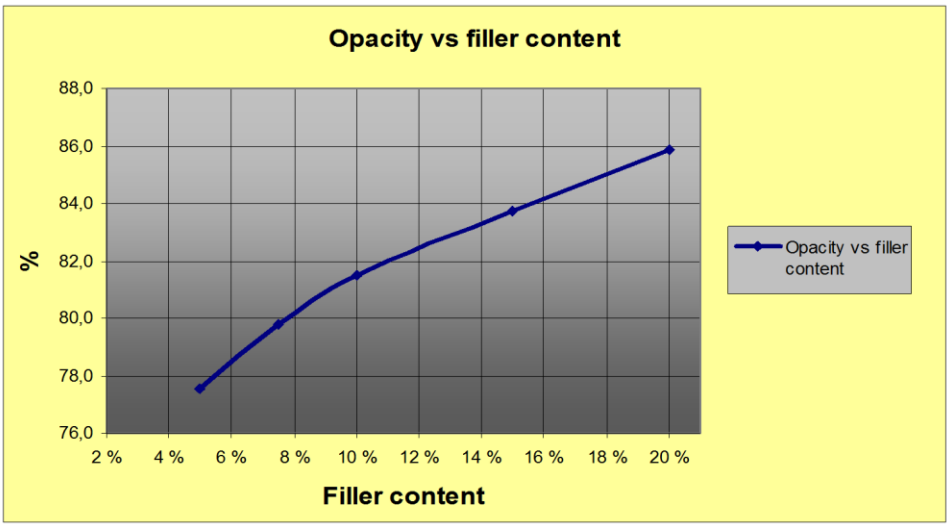

Diagram 3. Effects in opacity when increasing the filler content

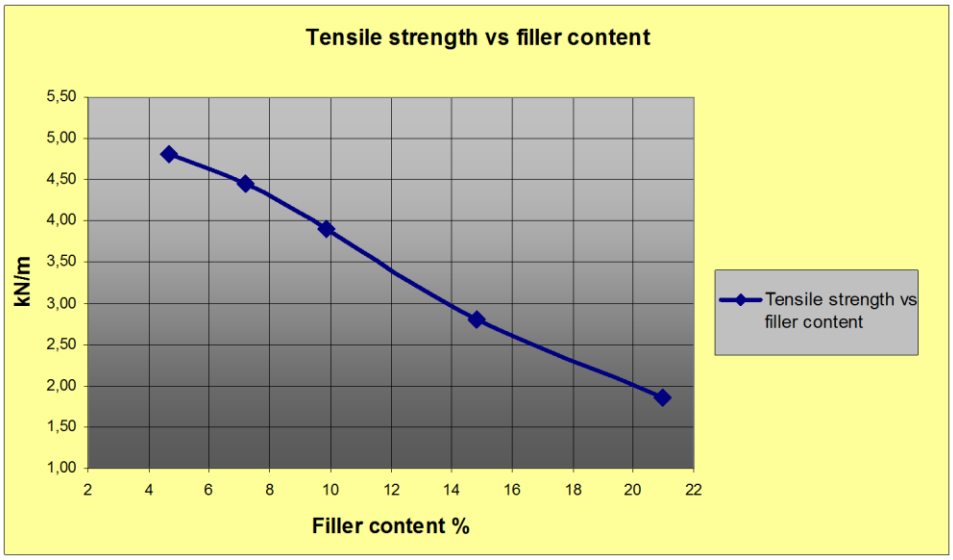

Diagram 4. Effects in tensile strength when increasing the filler content

3.3 Trial 2 results

The most essential paper properties and ash measurement results of trial two are presented in tables 15-19. Paper properties are divided into surface properties, optical properties, optical properties against brown background and strength properties. SEM surface and Z-directional images from the most interesting trial points of trial two paper samples are presented in pictures 25-28. Diagram 5 represents the changes in the particle size distribution of calcium hydroxide used in trial 2, and whether ultrasonic treatment was either used during the measurement or not. The SEM image of calcium hydroxide used in trial two is presented in picture 29.

Table 15. The most important surface properties of trial 2

Trial point		**1**	**2**	**3**	**4**	**5**	**6**
	Unit						
Air resistance Gurley	s/100 ml	10	11	12	11	12	15
Bendtsen-roughness, ts + bs avg	ml/min	286	277	275	276	223	224
PPS 0.5, ts + bs avg	µm	6,2	6,1	6,1	6,1	6,1	6,1
PPS 1.0, ts + bs avg	µm	5,9	5,9	5,9	5,9	5,8	5,8
PPS 2.0, ts + bs avg	µm	5,4	5,3	5,3	5,3	5,3	5,3

Table 16. The most important optical properties of trial 2

Trial point		**1**	**2**	**3**	**4**	**5**	**6**
	Unit						
Opacity C/2° +UV, ts + bs avg	%	78,8	78,5	78,2	79,8	78,7	78,1
Light scattering coefficient +UV, ts + bs avg	m²/kg	39,5	37,4	36,8	41,2	39,4	38,0

Table 17. The most important optical properties against brown background of trial 2

Trial point		1	2	3	4	5	6
	Unit						
Brightness R457 C/2° +UV, ts + bs avg	%	72,1	71,4	70,7	73,1	71,5	71,2
Brightness R457 D65/10° +UV, ts + bs avg	%	72	71,4	70,75	73,15	71,5	71,3
CIE whiteness C/2° +UV, ts + bs avg	%	67,6	65,2	64,2	67,6	65,2	64,9
CIE whiteness D65/10° +UV, ts + bs avg	%	67,7	65,5	64,5	67,9	65,5	65,2
White top mottle		1,20	1,20	1,18	1,16	1,15	1,07

Table 18. The most important strength properties of trial 2

Trial point		1	2	3	4	5	6
	Unit						
Tensile strength, Geom.avg. md+cd	kN/m	3,3	3,4	3,4	3,0	3,0	3,4
Stretch, Geom.avg. md+cd	%	3,0	3,0	3,2	3,1	3,1	3,3
Tensile index, Geom.avg. md+cd	Nm/g	51,2	51,4	51,0	45,9	47,5	52,4
Tensile stiffness, Geom.avg. md+cd	kN/m	376,6	372,6	382,5	346,9	329,3	356,3
Tensile stiffness index, Geom.avg. md+cd	MNm/kg	5,8	5,6	5,7	5,3	5,1	5,5
E-modulus, Geom.avg. md+cd	MPa	4231	4050	4347	3942	3829	4143

Table 19. Ash content measured from trial 2 paper samples by burning in 550 ºC

Trial point	P1	P2	P3	P4	P5	P6
%	5,49	5,02	5,20	7,35	7,75	7,09

Picture 25. 800x magnification SEM top image of the trial 2 paper sample containing 5% Offline-PCC

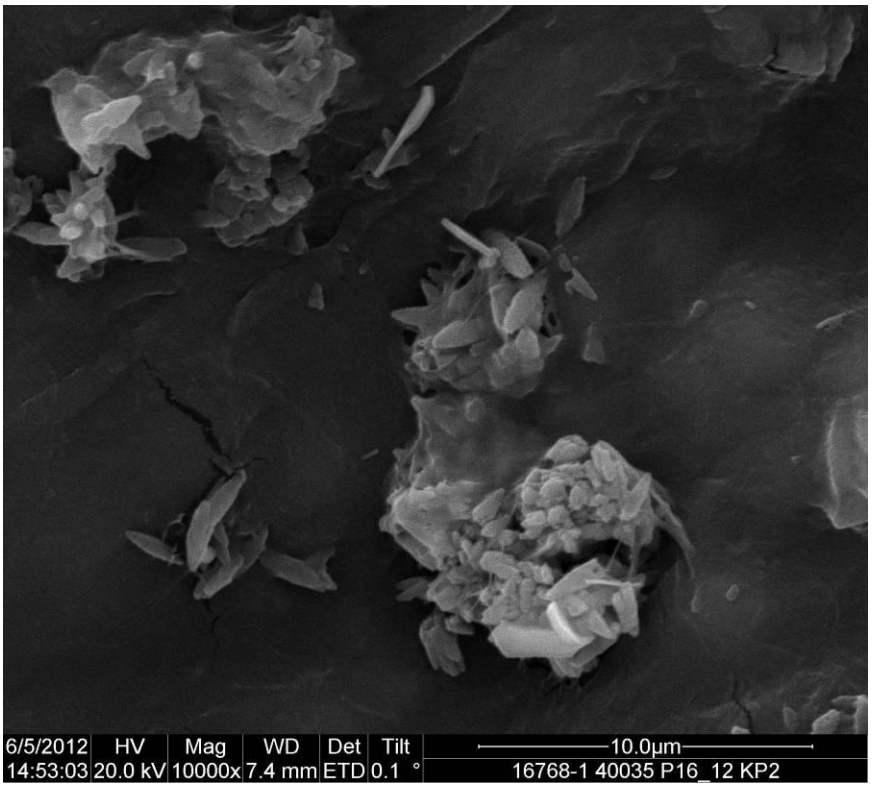

Picture 26. 10 000x magnification SEM top image of the trial 2 paper sample containing 5% Offline-PCC

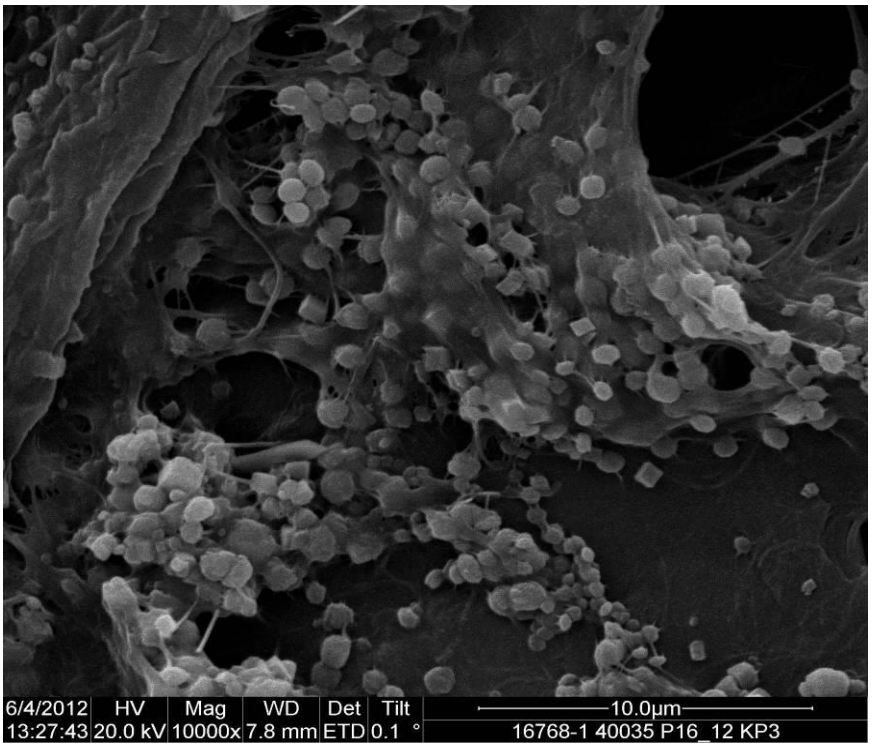

Picture 27. 10 000x magnification SEM top image of the trial 2 paper sample containing 5% Inline-PCC

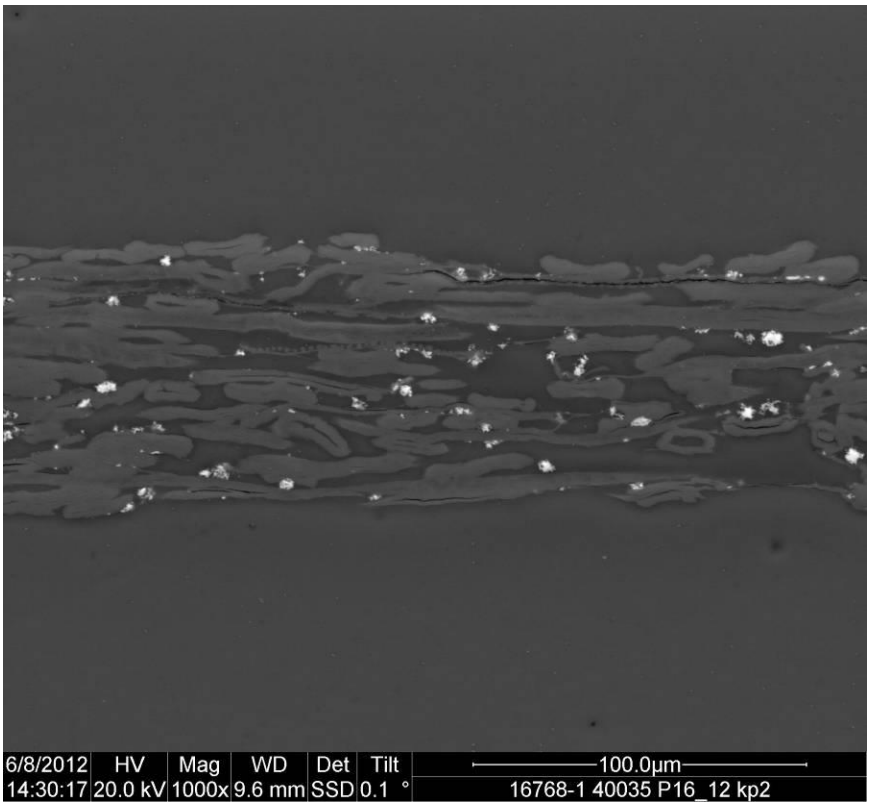

Picture 28, 1000x magnification SEM -cross section image of the trial 1 paper sample containing 5% Offline PCC

Volume Statistics (Arithmetic)			120529_46_01.$ls	
Calculations from 0.040 µm to 2000 µm				
Volume:	100%			
Mean:	48.66 µm		S.D.:	51.91 µm
Median:	22.09 µm		Variance:	2694 µm^2
Mean/Median ratio:	2.203		C.V.:	107%
Mode:	105.9 µm		Skewness:	1.348 Right skewed
			Kurtosis:	1.624 Leptokurtic
<10%	<25%	<50%	<75%	<90%
3.315 µm	8.446 µm	22.09 µm	81.78 µm	118.4 µm

Volume Statistics (Arithmetic)			120529_16_01.$ls	
Calculations from 0.040 µm to 2000 µm				
Volume:	100%			
Mean:	5.469 µm		S.D.:	3.971 µm
Median:	4.870 µm		Variance:	15.77 µm^2
Mean/Median ratio:	1.123		C.V.:	72.6%
Mode:	9.371 µm		Skewness:	0.519 Right skewed
			Kurtosis:	-0.761 Platykurtic
<10%	<25%	<50%	<75%	<90%
0.833 µm	1.787 µm	4.870 µm	8.502 µm	11.28 µm

Measurement 1

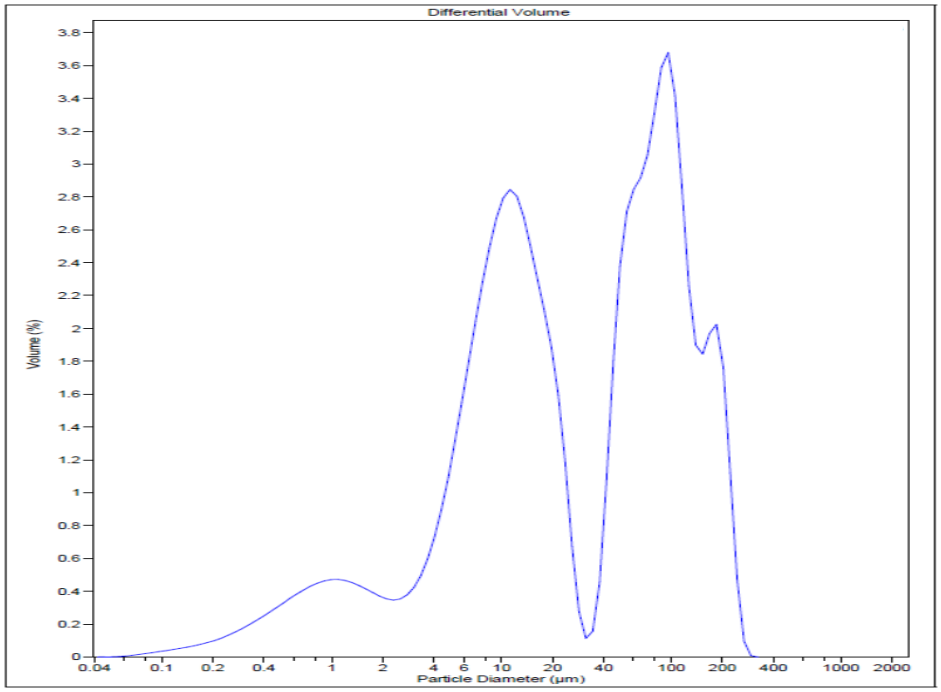

Measurement 2

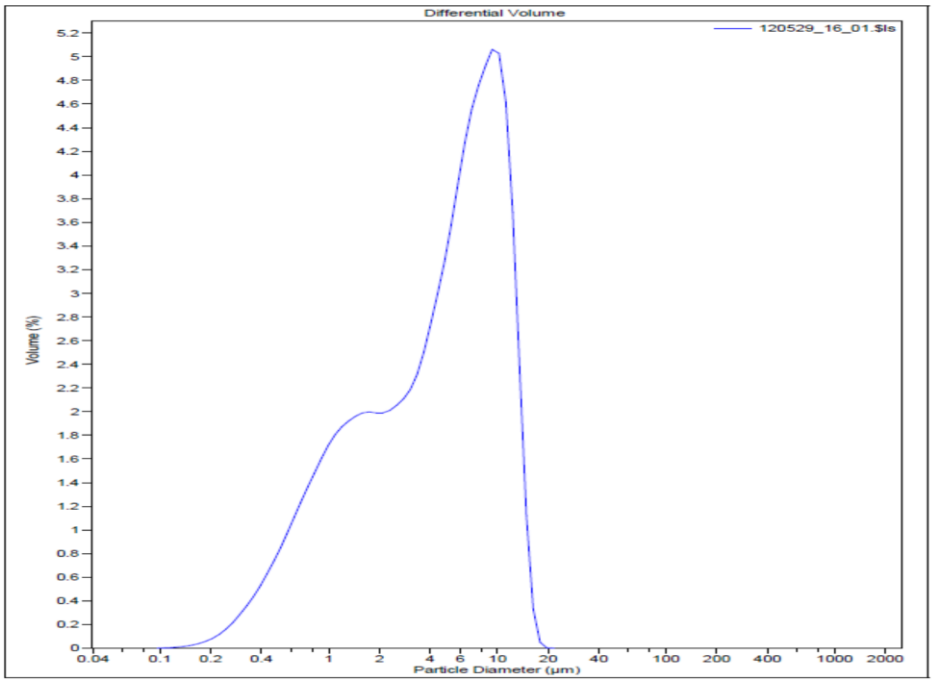

Diagram 5, Trial 2 Calcium hydroxide particle size distribution graph. 1st measurement without using ultrasonic. 2nd measurement using ultrasonic.

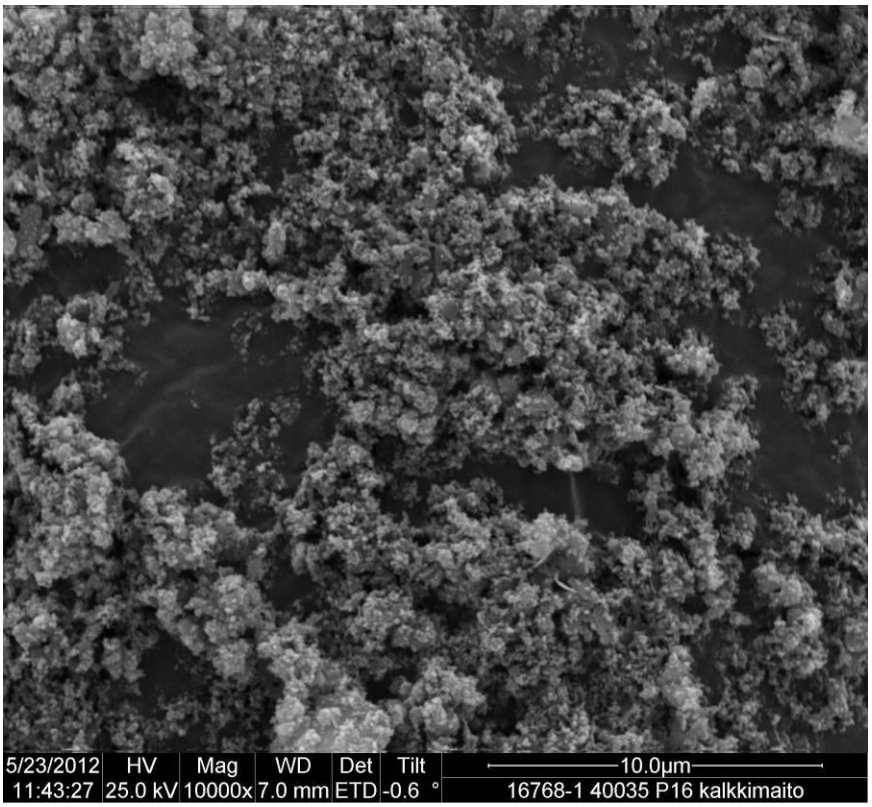

Picture 29. 10 000 x magnification of the trial 2 calcium hydroxide sample

3.4 Trial 2 analysis

The main objective of trial 2 was improving the strength properties of the paper using a suitable filler content level indicated by the results received from trial 1. According to the trial 1 results, strength properties declined radically when filler content was increased over 7,5%, although optical properties were still considerably low at a filler content of 5%. Therefore a 7,5% filler content was chosen as the basis for trial 2. Strength improvement was experimented with by adding cationic starch and carboxymethyl cellulose among the calcium hydroxide. The secondary objective of trial 2 was to find out the effect of process water to the properties of the paper. In trial 2, tap water was used instead of the river water used in trial 1. As an assumption, the optical properties would improve, but the purpose was to find out the extent of the improvement. Since one of the main purposes of this thesis was to examine whether inline-PCC could replace the calcined kaolin as filler, it also seemed essential to find out where offline-PCC stands in this comparison. Therefore, additional reference points were prepared using 5% scalenohedral offline- PCC and 5% Inline-PCC. When looking at the SEM images from the offline-PCC trial point 2 (pictures 25, and 26), it is clearly visible that the sample consists of small longish grain shaped particles that have clustered into larger rosette shaped bundles with a size range of 5 microns. Inline-PCC on the other hand has precipitated in cubical or spherical shaped crystals with a size range of 1 microns or less. Inline-PCC SEM images also indicated that the PCC particles seem to be partly covered by an unknown glue-like substance. This issue is discussed more closely in section 3.12. As in trial 1, the calcium hydroxide used as raw material for inline-PCC, was analyzed in trial 2. Only this time when particle size distribution was analyzed, the sample had been preserved in a container for less than 3 weeks. On the 1st measurement of the sample, the analyzer indicated two high peaks; one for approximately 100µm and another for approximately 10µm. After adding ultrasonic within the measurements, the agglomerates seemed to be broken down, leading to only one relatively narrow peak in the spectrum with a median size of 4,8 microns (Diagram 5). Thereby it can be inferred, that agglomeration occurs shortly after the manufacturing of calcium hydroxide, and within a certain time period, the change becomes permanent.

When comparing 5% inline-PCC with the calcined kaolin reference point, it becomes clear that in overall surface and strength properties Inline-PCC fares very well compared to calcined kaolin, being equal or even slightly better in for example e-modulus, tensile energy absorption and tear strength. However, it falls behind a few percentages in optical properties.

When considering the strength impact of starch and CMC added among the calcium hydroxide, utilizing a filler content of 7,5% Inline-PCC with 3% cationic starch and CMC provides equally good strength properties than plain 5% inline-PCC. In the same time better optical properties and 10% better mottling is achievable. When starch is applied, it also seems that the porosity of the paper decreases, but simultaneously the surface becomes smoother. Starch seems to affect the brightness and whiteness and by lowering them by just under 1% for brightness and about 1,5% for whiteness. Light scattering also decreases when starch is applied (diagram 6). The light scattering coefficient of the reference point with calcined kaolin is just over 3% better than with 7,5% inline-PCC with added starch and CMC, but over 3% worse than 7,5% Inline-PCC without added starch. Therefore, the correct balance in dosage has to be pondered carefully.

When comparing the calcined kaolin reference point against 7,5% inline-PCC with added starch and CMC (tp 6 and tp 1), the surface properties indicate that the porosity of Inline-PCC is notably lower, but smoothness however higher. Brightness and whiteness against a brown background are only fractionally inferior with the inline-PCC, mottling on the other hand more than 10% better. As to the strength properties, inline-PCC with added starch and CMC outweighs calcined kaolin distinctly in all areas except tensile stiffness and e-modulus. In tensile stiffness, the difference is roughly 5% in favor of calcined kaolin, while e-modulus is nearly at an equal level. Most significant differences in strength properties are found in tensile energy absorption, stretch and burst strength, all in favor of inline-PCC. A more detailed comparison between calcined kaolin and the most important trial points can be seen in table 20.

If a comparison is made between the calcined kaolin reference point (tp1) and 5% scalenohedral offline-PCC (tp2), it seems that both have very similar surface properties. Brightness and whiteness are slightly better with calcined kaolin while the difference in top side light scattering is approximately 8% in favor of calcined kaolin. With regards to the strength properties, calcined kaolin and offline-PCC are close to each other. Notable (8-12%) differences are found only in tear and burst strength, in favor of the offline-PCC.

The overall effect on optical properties, when using tap water as process water instead of river water, was approximately +5% for brightness and +12% for whiteness.

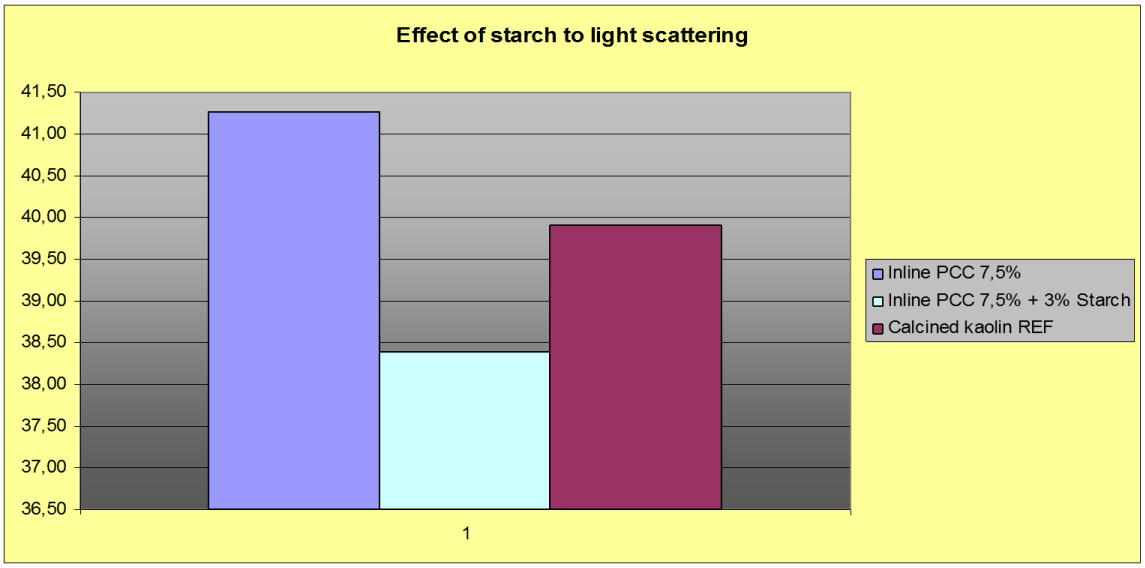

Diagram 6.Effect of starch to light scattering coefficient.

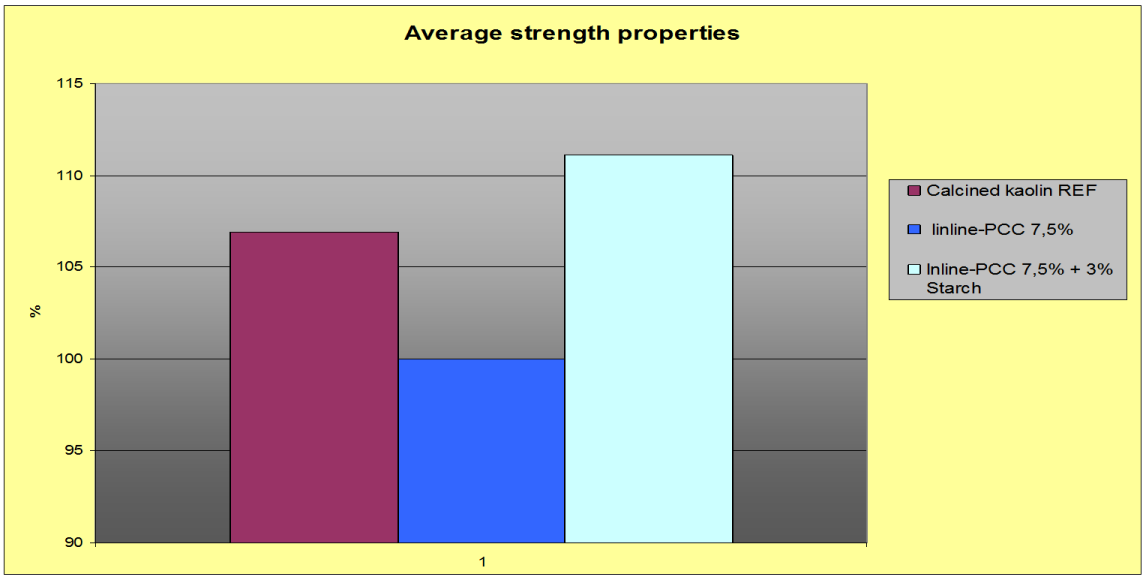

Diagram 7. Effect of starch to the overall strength properties.

A comparison of paper technical properties between 5% calcined kaolin versus the most important trial points of trial 2 is presented in the following matrix.

	Compared to the reference point 1
O	-3% - + 3%
-	- 3% -10% deteriorated
- -	-10% -20% deteriorated
- - -	-20%... => deteriorated
+	+ 3% - 10% improved
+ +	+ 10% - 20%.. => improved
+ + +	+ 20%... => improved

Table 20. Calcined kaolin (5%) reference point vs. most important trial points

Measured Feature	5% offline pcc (tp 2)	5% inline pcc (tp 3)	7,5% inline pcc (tp 4)	7,5% inline pcc + 3% cationic starch + 3% CMC (tp 6)
Gurley air resistance	-	- -	-	- - -
Bendtsen roughness	+	+	+	+ + +
PPS smoothness	O	O	O	O
Gloss	O	-	- -	O
Brightness	O	O	O	O
Whiteness	O	-	O	-
Opacity	O	O	O	O
Light absorption	O	+	O	O
Light scattering	-	-	+	-
Stretch	O	O	O	+
Tensile index	O	O	- -	+
Tensile stiffness index	-	O	-	-
E-modulus	-	+	-	O
Tensile energy absorption index	-	O	- -	+
Tear strength	+ +	+	+	+
Tear index	+	+	O	+
Burst strength	+	+	-	+ +
Burst index	+	O	-	+ +
Brightness against brown background	O	O	O	O
Whiteness against brown background	-	-	O	-
Mottle	O	O	+	+ +

3.5 Trial 3 results

The most essential paper properties and ash measurement results of trial three are presented in tables 21-25. Paper properties are divided into surface properties, optical properties, optical

properties against a brown background and strength properties. Pictures 30-33 illustrate SEM surface images of the most interesting trial points of the trial three paper samples.

Table 21. The most important surface properties of trial 3

Trial point		1	2	3	4	5	6	7	8
	Unit								
Air resistance Gurley	s/100 ml	14	13	12	11	12	13	13	18
Bendtsen-roughness, ts + bs avg	ml/min	185	269	257	248	262	280	275	271
PPS 0.5, ts + bs avg	µm	5,8	6,0	6,0	6,0	6,0	6,0	6,1	6,0
PPS 1.0, ts + bs avg	µm	5,5	5,7	5,7	5,7	5,7	5,8	5,8	5,8
PPS 2.0, ts + bs avg	µm	4,9	5,2	5,2	5,2	5,1	5,2	5,2	5,2

Table 22. The most important optical properties of trial 3

Trial point		1	2	3	4	5	6	7	8
	Unit								
Opacity C/2° +UV, ts + bs avg	%	79,7	77,2	78,2	80,1	81,4	79,6	80,8	76,7
Light scattering coefficient +Uv ts + bs avg	m²/kg	40,0	33,7	36,3	39,7	42,1	38,2	41,2	32,9

Table 23. The most important optical properties against brown background of trial 3

Trial point		1	2	3	4	5	6	7	8
	Unit								
Brightness R457 C/2° +UV, ts + bs avg	%	72,7	67,8	69,2	70,8	72,5	70,5	71,9	67,5
Brightness R457 D65/10° +UV, ts + bs avg	%	72,8	67,9	69,2	70,8	72,6	70,6	71,9	67,6
CIE whiteness C/2° +UV, ts + bs avg	%	67,2	57,3	59,6	61,8	64,0	61,0	63,7	57,1
CIE whiteness D65/10° +UV, ts + bs avg	%	67,4	57,7	59,9	62,1	64,3	61,3	63,9	57,5
White top mottle		1,056	1,252	1,214	1,122	1,135	1,129	1,065	1,271

Table 24. The most important strength properties of trial 3

Trial point		1	2	3	4	5	6	7	8
	Unit								
Tensile strength, Geom.avg. md+cd	kN/m	3,1	3,4	3,0	2,8	2,7	3,1	2,9	3,6
Stretch, Geom.avg. md+cd	%	3,4	3,3	3,2	3,1	3,0	3,3	3,1	3,6
Tensile index, Geom.avg. md+cd	Nm/g	47,3	52,5	47,9	43,8	40,9	47,1	45,5	55,6
Tensile stiffness, Geom.avg. md+cd	kN/m	340	328	337	333	348	341	360	361
Tensile stiffness index, Geom.avg. md+cd	MNm/kg	5,2	5,1	5,3	5,2	5,3	5,2	5,6	5,6
E-modulus, Geom.avg. md+cd	MPa	4006	3769	3963	3871	3955	3971	4134	4245

Table 25. Ash content measured from trial 3 paper samples by burning in 550 ºC

Trial point	P1	P2	P3	P4	P5	P6	P7	P8
%	5,9	3,1	5,0	6,5	8,0	6,8	6,6	2,7

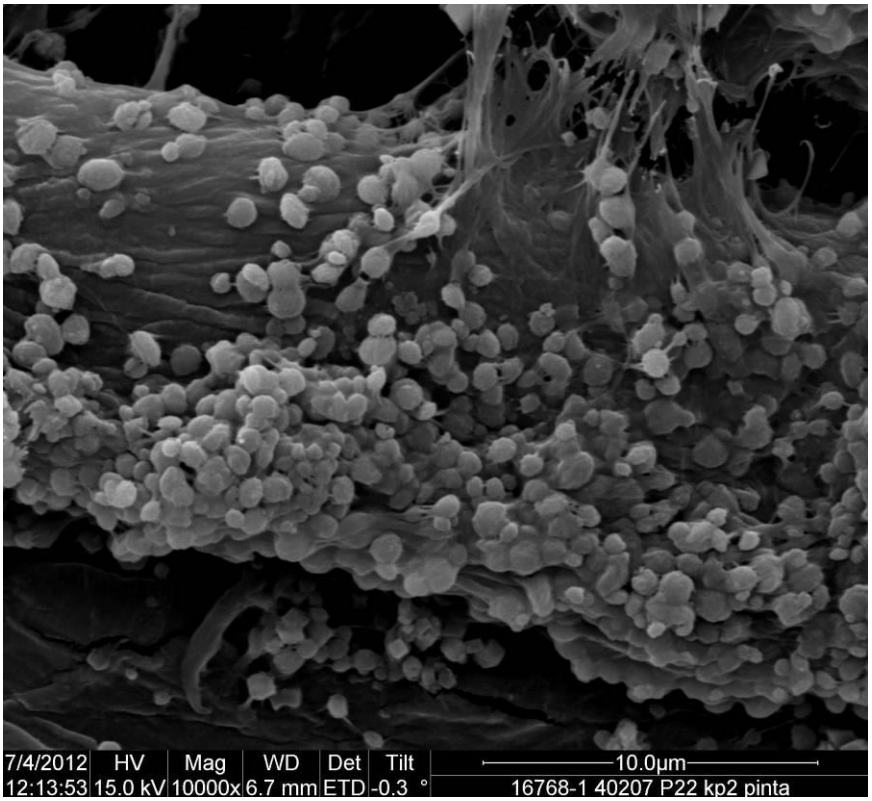

Picture 30. 10 000x magnification SEM top image of the trial 3 paper sample containing 3 % Inline-PCC. Manufactured in the beginning of the trials

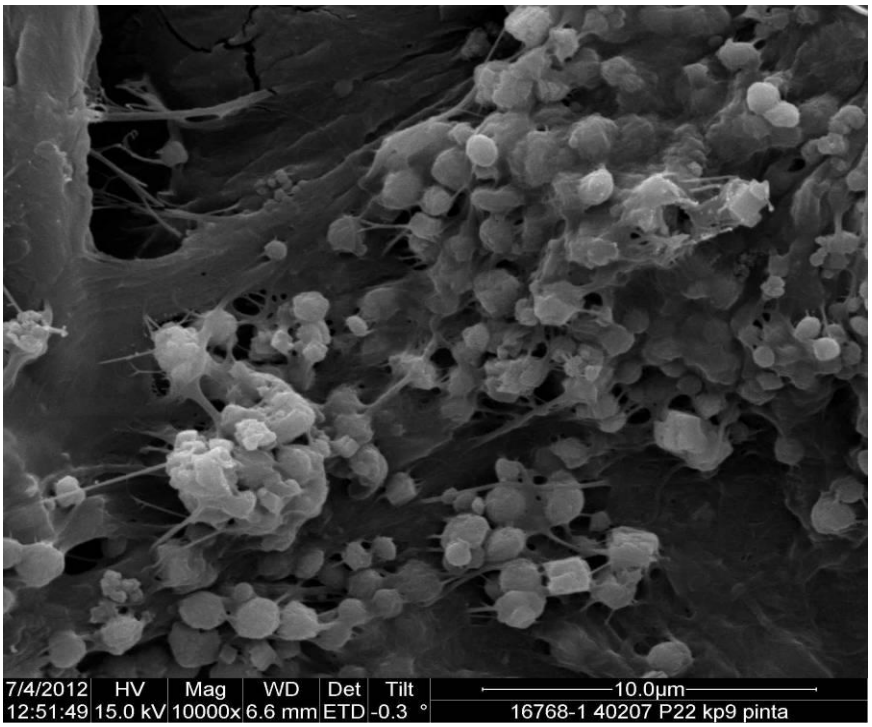

Picture 31. 10 000x magnification SEM top image of the trial 3 paper sample containing 3 % Inline-PCC. Manufactured by the end of the trials

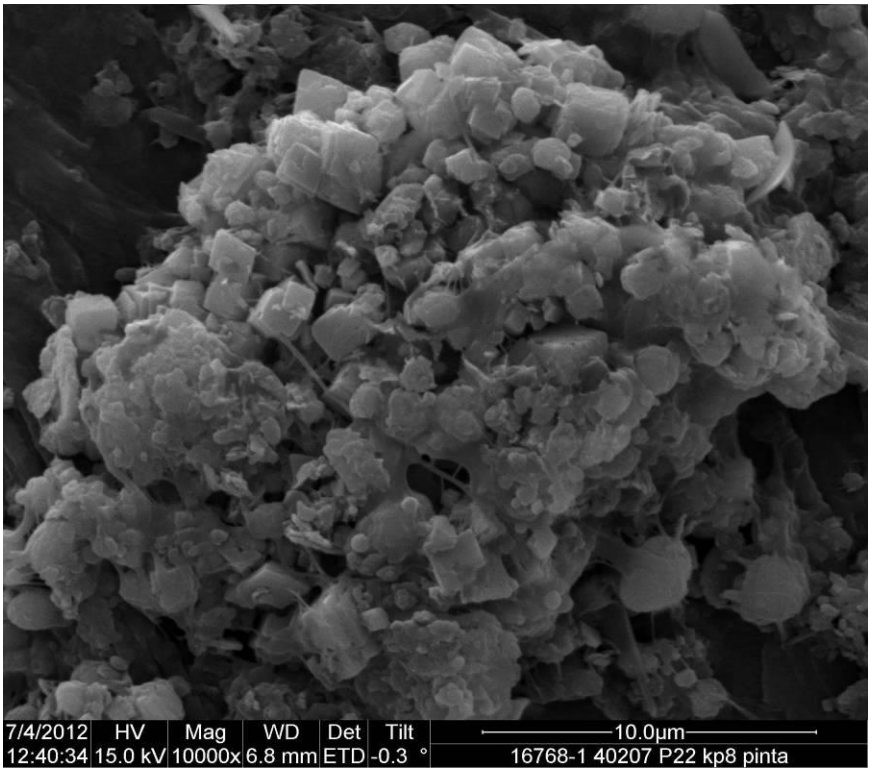

Picture 32. 10 000x magnification SEM top image of the trial 3 paper sample containing 2% calcined kaolin and 3% Inline-PCC

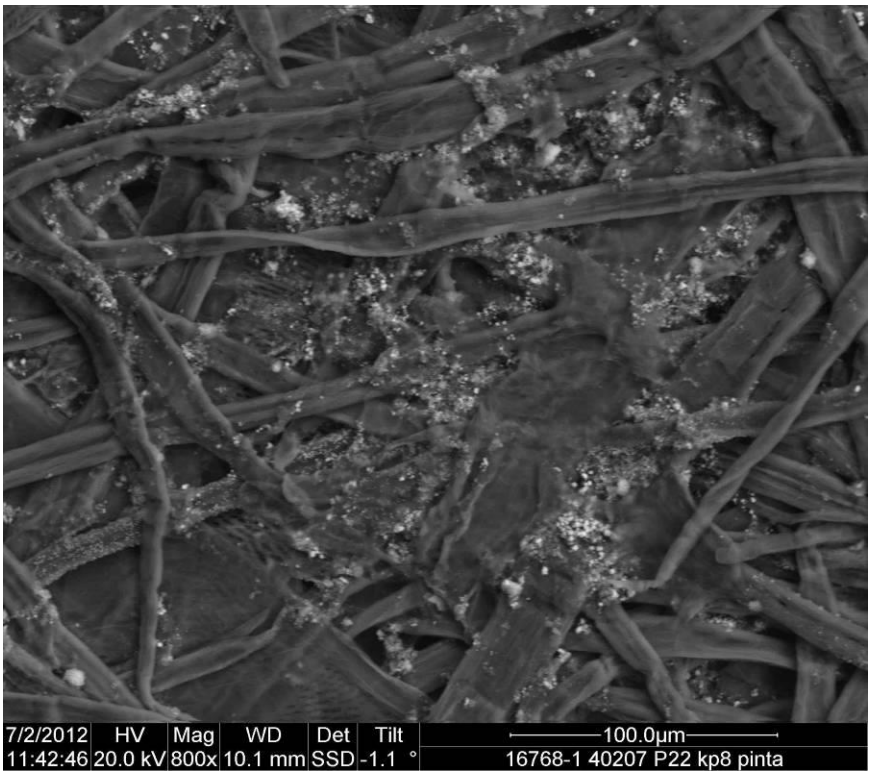

Picture 33. 10 000x magnification SEM top image of the trial 3 paper sample containing 2% calcined kaolin and 3% Inline-PCC

3.6 Trial 3 analysis

The main objectives of trial 3 were specifying an optimal filler content level and learning how optical, strength and surface properties vary while filler content is increased in stages from 3% to 7,5%. In addition, the effects in properties of an increased dosage of cationic starch and CMC among calcium hydroxide were tested. As an additional experiment, a mixture of calcined kaolin and Inline-PCC was prepared. In previous trials it was observed that according to the mass flow meter, a relatively high dose of carbon dioxide is needed to maintain the desired pH level of 8 ± 0,3. Therefore the CO_2 dosage was started at +5% from the stoichiometric value but soon increased higher, as otherwise pH would to climb up to 10. The exact reason for this was not resolved, but the difference with the stoichiometric value seemed to be approximately +1kg/h with all the prepared trial points at a desired pH level.

Trial point 2 was duplicated at the end of the trials as trial point 8. The idea was to find out whether running the paper machine longer has any effect on the pH or the properties of paper when the same amount of carbon dioxide is fed to the system. An increased amount of fiber

fines and carbon dioxide would be dissolved to the circulating process water towards the end of trials. According to the close-range SEM images (30, 31) the amount of fiber fines seems to have increased considerably. The fiber fines can be seen as yarns in between the filler particles. Also, a rather remarkable change in strength properties can be found in the Paperlab results, table 24. SEM images also reveal that particle size and shape seem to be slightly different, being smaller and more spherical at the trial point in the beginning of the run. The pH level was 0,5 units higher at the trial point in the beginning of the run even though the same amount of CO_2 was fed into the system.

Consequently, it can be stated that the amount of fines in the short circulation has affected the strength properties positively, but at the same time dissolved carbon dioxide has reduced the need for additional carbon dioxide to be fed. Therefore, the pH level was higher in the beginning and lower in the end. It has also been observed that the undersupply of carbon dioxide in inline-PCC manufacturing results in smaller, increasingly spherical shaped PCC crystals. Smaller filler crystal size commonly tends to weaken the strength properties compared to larger ones. Also as the trial point 8 was kept short due to running out of pulp stock, there seems to have been a possibility of some traces from the previous trial point which presumably would also affect the strength properties.

When looking at the close-range SEM images, an interesting filler structure can be seen in picture 32, where a mixture of calcined kaolin and inline-PCC is used. It seems that both filler pigments are merged with each other forming uneven clusters that contain particles of many shapes and sizes. This type of filler pigment structure has a positive effect on light scattering and opacity values. In a mixture of these two fillers (tp 7), the surface roughness is higher than the reference and brightness about 3% lower, but due to good opacity the optical properties against a brown background is quite similar. Regarding strength properties, when compared to calcined kaolin, the mixture filled paper falls slightly behind in all sections except tensile stiffness and e-modulus, being in average just over 3% inferior to the reference point. A closer examination shows that the total filler content of trial point 7 was higher than the aimed 5%, measuring in actually at 6,6%. However, when a comparison is made between 6% inline-PCC and the mixture filler, the latter prevails in all the sections excluding surface properties.

Based on the Paperlab results of trial 3, when calcined kaolin is used as a comparison point, the optimal Inline-PCC filler content level on behalf of optical properties is approximately 7,5%.

However, 7,5% inline-PCC falls behind in strength properties at an average of 7%. In contrast, 6% Inline-PCC has equal strength properties with the reference point, and adding starch and CMC among the calcium hydroxide, will increase the strength properties by additional 6-10%. A more detailed comparison of the reference point and the most important trial points can be seen in table 26 and 27. Comparison of paper technical properties between 5% calcined kaolin versus the most important trial points of trial 3 is presented in the following matrixes.

	Compared to the reference point 1
O	-3% - + 3%
-	- 3% -10% deteriorated
- -	-10% -20% deteriorated
- - -	-20%... => deteriorated
+	+ 3% - 10% improved
+ +	+ 10% - 20%.. => improved
+ + +	+ 20%... => improved

Table 26. Calcined kaolin (5%) reference point vs. most important trial points

Measured Feature	3% inline pcc (tp 2)	5% inline pcc (tp 3)	6% inline pcc (tp 4)	7,5% inline pcc (tp 5)
Gurley air resistance	+	+ +	+ + +	+ +
Bendtsen roughness	- - -	- - -	- - -	- - -
PPS smoothness	-	-	-	-
Gloss	+	-	-	-
Brightness	-	-	-	O
Whiteness	- -	- -	- -	-
Opacity	-	O	O	O
Light absorption	+ + +	+ + +	+ + +	+ + +
Light scattering	- -	-	O	+
Stretch	O	O	-	-
Tensile index	+ +	O	-	- -
Tensile stiffness index	-	O	O	+
E-modulus	-	O	-	O
Tensile energy absorption index	+	O	- -	- -
Tear strength	+	O	-	-
Tear index	+	O	-	-
Burst strength	+ +	O	-	-
Burst index	+ +	O	-	-
Brightness against brown background	-	-	O	O
Whiteness against brown background	- -	- -	-	-
Mottle	- -	- -	-	-

Table 27. Calcined kaolin (5%) reference point vs. most important trial points

Measured Feature	6% inline pcc + 5% cationic starch + 2,5% CMC (tp 6)	3% inline pcc + 2% calcined kaolin (tp 7)	3% inline pcc rerun (tp 8)
Gurley air resistance	+	+	- - -
Bendtsen roughness	- - -	- - -	- - -
PPS smoothness	-	-	-
Gloss	-	-	+
Brightness	-	-	-
Whiteness	- -	-	- -
Opacity	O	O	-
Light absorption	+ + +	+ + +	+ + +
Light scattering	-	O	- -
Stretch	O	-	+
Tensile index	O	-	+ +
Tensile stiffness index	O	+	+
E-modulus	O	+	+
Tensile energy absorption index	O	-	+ + +
Tear strength	-	-	+
Tear index	-	-	+ +
Burst strength	+	-	+ +
Burst index	+	-	+ +
Brightness against brown background	O	O	-
Whiteness against brown background	-	-	- -
Mottle	-	O	- - -

3.7 Trial 4 results

The most essential paper properties and ash measurement results of trial four are presented in tables 28 - 32. The Paperlab results are divided into surface properties, optical properties, optical properties against a brown background and strength properties. Pictures 34-37 illustrate SEM surface images of the most interesting trial points of the trial four paper samples.

Table 28. The most important surface properties of trial 4

Trial point		1	2	3	4	5	6	7
	Unit							
Air resistance Gurley	s/100 ml	11	12	10	10	11	12	10
Bendtsen-roughness, ts + bs avg	ml/min	226	215	215	199	538	237	242
PPS 0.5, ts + bs avg	µm	5,9	6,0	5,9	5,9	6,0	6,0	6,0
PPS 1.0, ts + bs avg	µm	5,6	5,7	5,6	5,5	5,7	5,7	5,7
PPS 2.0, ts + bs avg	µm	5,0	5,1	5,0	5,0	5,2	5,1	5,1

Table 29 The most important optical properties of trial 4

Trial point		1	2	3	4	5	6	7
	Unit							
Opacity C/2° +UV, ts + bs avg	%	80,1	81,9	81,5	81,2	81,3	81,4	81,6
Light scattering coefficient +UV, ts + bs avg	m²/kg	41,6	41,7	41,4	41,0	39,3	41,3	41,8

Table 30. The most important optical properties against brown background of trial 4

Trial point		1	2	3	4	5	6	7
	Unit							
Brightness R457 C/2° +UV, ts + bs avg	%	72,8	72,1	71,9	71,9	71,6	71,6	71,8
Brightness R457 D65/10° +UV, ts + bs avg	%	72,8	72,2	72,0	71,9	71,7	71,7	71,8
CIE whiteness C/2° +UV, ts + bs avg	%	67,1	63,1	63,0	63,4	62,7	62,8	62,7
CIE whiteness D65/10° +UV, ts + bs avg	%	67,3	63,3	63,3	63,7	63,0	63,1	63,0
White top mottle		1,026	1,039	1,071	1,042	1,049	1,028	1,083

Table 31. The most important strength properties of trial 4

Trial point		1	2	3	4	5	6	7
	Unit							
Tensile strength, Geom.avg. md+cd	kN/m	3,0	2,7	2,7	2,6	2,6	2,8	2,9
Stretch, Geom.avg. md+cd	%	3,1	2,9	3,1	3,0	2,8	2,9	3,1
Tensile index, Geom.avg. md+cd	Nm/g	46,9	42,1	41,4	39,7	39,1	43,2	44,5
Tensile stiffness, Geom.avg. md+cd	kN/m	238	297	275	315	283	332	273
Tensile stiffness index, Geom.avg. md+cd	MNm/kg	3,7	4,6	4,2	4,8	4,2	5,1	4,2
E-modulus, Geom.avg. md+cd	MPa	2738	3419	3161	3667	3212	3732	3104

Table 32. Ash content measured from trial 4 paper samples by burning in 550 ºC

Trial point	P1	P2	P3	P4	P5	P6	P7
%	5,9	6,9	6,9	6,8	6,3	6,4	6,6

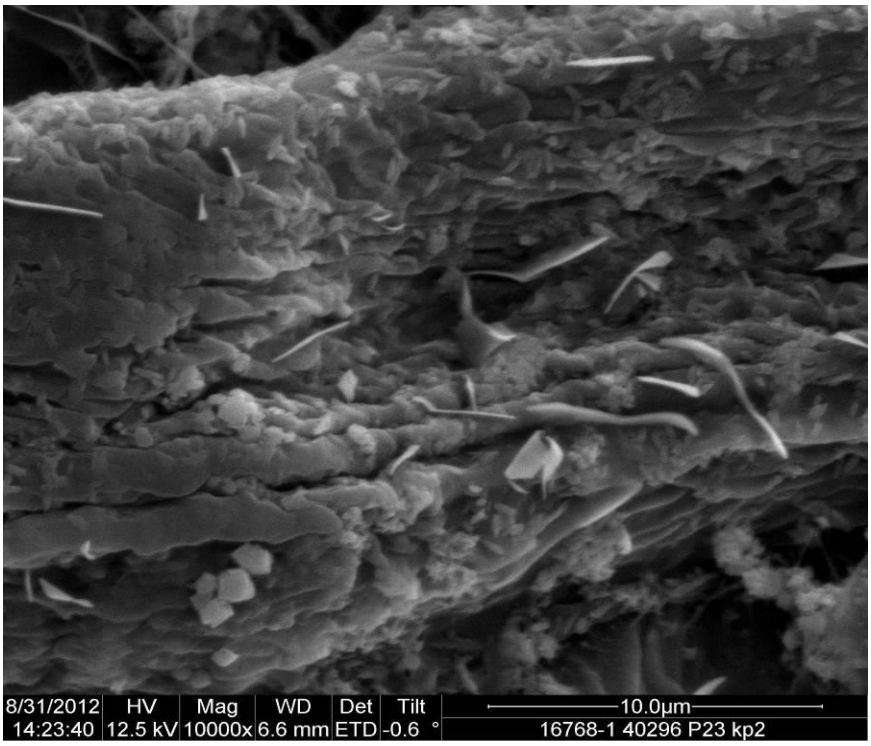

Picture 34. 10 000x magnification SEM top image of the trial 4 paper sample containing 6% Inline-PCC. Manufactured with high pH level.

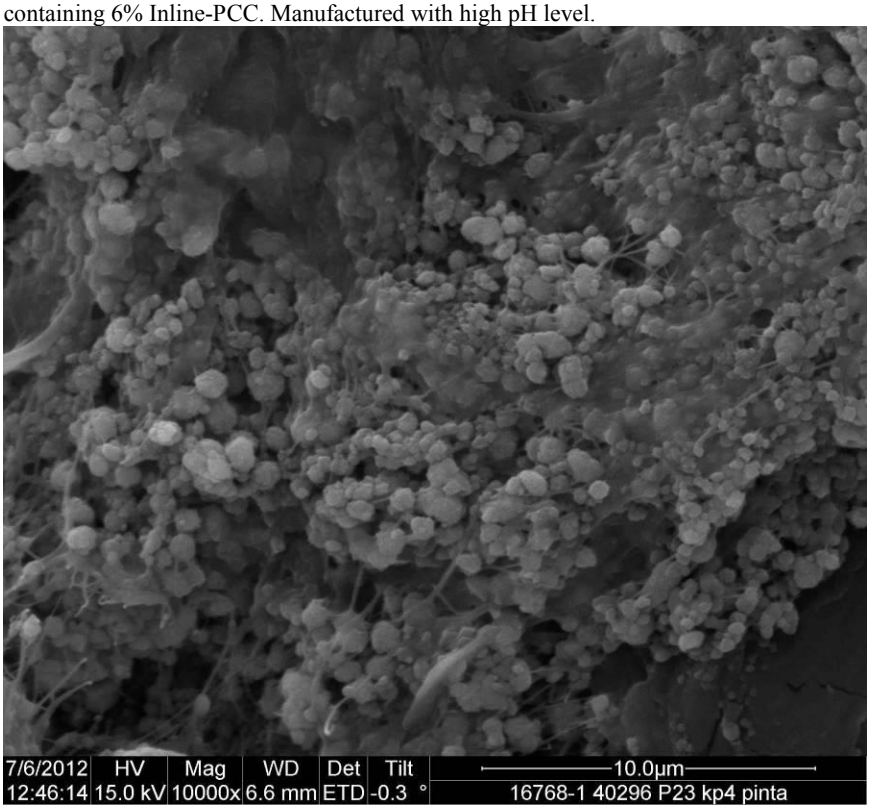

Picture 35. 10 000x magnification SEM top image of the trial 4 paper sample containing 6% Inline-PCC manufactured with low process water temperature

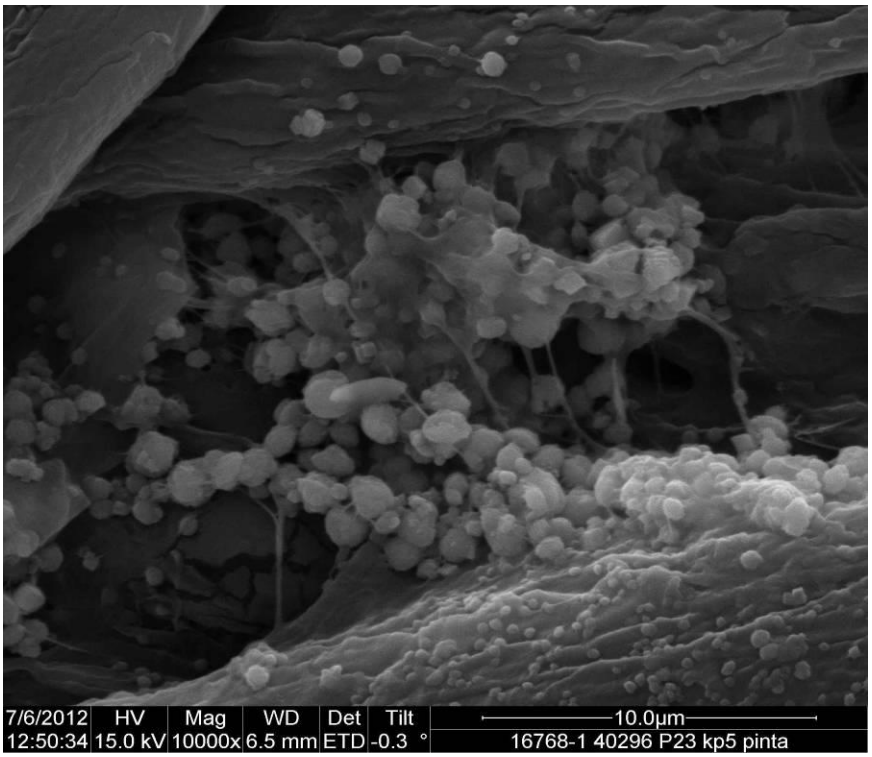

Picture 36. 10 000x magnification SEM top image of the trial 4 paper sample containing 6% Inline-PCC and bentonite

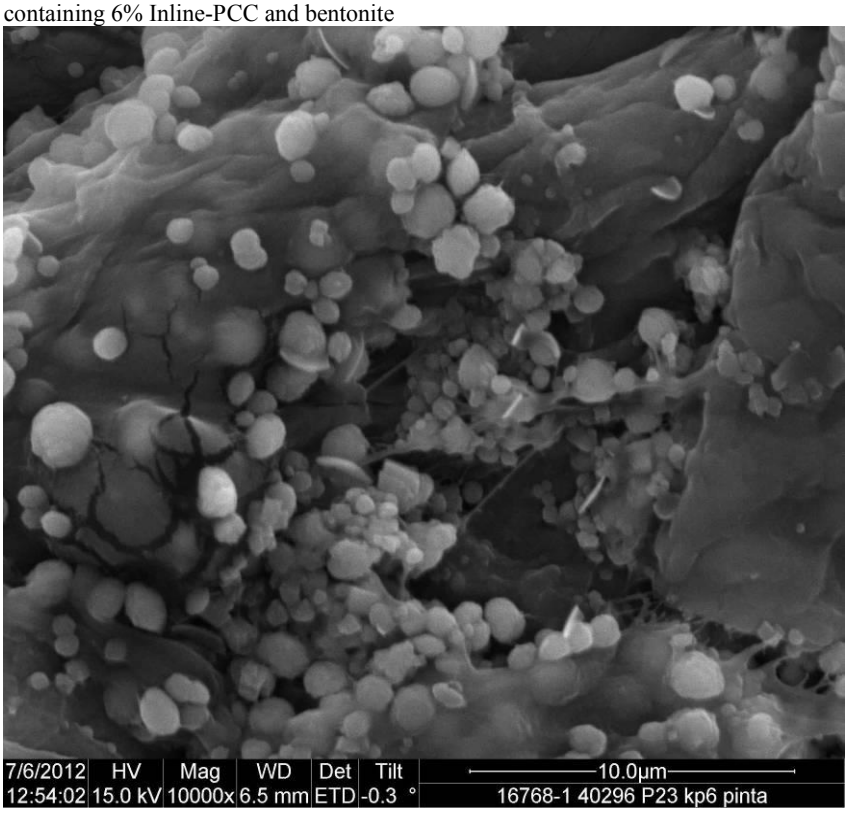

Picture 37. 10 000x magnification SEM top image of the trial 4 paper sample containing 6% Inline-PCC manufactured using highly conductive process water.

3.8 Trial 4 analysis

The main objective of trial 4 was to test the significance of factors other than filler content to paper properties and the runnability of the paper machine. A 6% Inline-PCC filler content was chosen as basis for the trials and in addition to the reference point, 6 other variables were experimented with. The 1st trial point after the reference was originally meant to take 3 times longer than a normal trial point in order to let the machine stabilize thoroughly. However due to the sudden freezing of the carbon dioxide pressure regulator, the fed amount of CO_2 decreased causing an undersupply of carbon dioxide which resulted in a high 10,4 pH value. The CO_2 undersupply seems to have also had an effect on the inline-PCC crystallizing reaction as according to the trial point 2 SEM images, PCC particles were formed as grain or ribbon shaped figures, a result so far unforeseen in this application. When comparing the paper technical properties of trial point 2 to the reference point, it can be noted that the surface properties are very similar. With regards to optical properties, the opacity of inline-PCC is slightly better than calcined kaolin. Other optical properties are nearly equal. Brightness against a brown background is also close to equal, while whiteness with the inline-PCC remains 6% lower. There are no significant differences in mottling. As to the strength properties, inline-PCC surpasses calcined kaolin explicitly in tensile stiffness and e-modulus, while calcined kaolin is superior in other categories. The largest - over 10% - differences in favor of calcined kaolin are seen in tensile index.

In order to confirm the morphology at trial point 2, the paper sample was later analyzed with an X-ray diffractometer. This issue is discussed more closely in the section 3.13. The idea in trial point 3 was to filter the calcium hydroxide with an 80-micron bag filter. Filtered calcium hydroxide would represent a highly homogenous raw material. During the filtration, it was found that the product was challenging to filter. With a filtering system powered by a compressed air pump, the calcium hydroxide turned into PCC very quickly, thus clogging the filter. With manual filtering, if the bag was held stationary, calcium hydroxide tended to form an impenetrable film on the surface of the filter, thereby clogging the filter very easily. The only way to get the calcium hydroxide through was to rotate the filter back and forth constantly.

A Paperlab analysis revealed that there were no major differences in papers made with filtered and unfiltered calcium hydroxide. Greater effects might have been observed if filtration could have been made reliable with a preferably smaller pore sized filter. In addition, a single trial point is not enough for observing the overall effects on the runnability of the machine.

At trial point 4, process water temperature was reduced to 23 degrees instead of the normal 45 degrees. The target was to find out the effects of precipitation in a lower temperature to PCC crystal morphology. Compared to inline-PCC prepared at a standard process water temperature, the surface properties, such as smoothness, were enhanced while optical properties remained similar. In strength properties the greatest improvements are seen in cross directional tensile stiffness and e-modulus. Other strength properties remain close to the same or inferior values. Inline-PCC manufactured using low temperature process water yielded a smoother, more porous end product than the reference point, yet with similar optical properties. White top mottle and brightness against a brown background were close to equal, but whiteness approximately 6% lower than with calcined kaolin. Calcined kaolin provides better tensile strength and stretch by over 10%, but on the other hand has more than 30% lower tensile stiffness and e-modulus.

Based on the high magnification the SEM images of trial point 4, (Picture 35) lowering the process water temperature diminishes the PCC crystals from the size regularly seen while hardly any other crystal shapes than spherical can be found. In addition, this trial point was analyzed with an X-ray diffractometer, the results are discussed more closely in the section 3.13.

100g/t bentonite was pumped into the reactor injection line at trial point 5. The aim was to increase the amount of nuclei for precipitation reactions. The average particle size of bentonite is typically 30-70 nm, which is generally much smaller than PCC crystals. According to SEM images, bentonite has mostly attached on the surfaces of the fibers and has not affected the PCC crystallation (picture 36). Paperlab analysis confirms a decline in all key properties compared to plain inline-PCC.

When a comparison is made with the reference point, tensile stiffness and e-modulus remain the only properties that have improved with bentonite among Inline PCC.

At trial point 6, pulp was treated with calcium chloride and sodium sulfate in order to increase conductivity. This trial point was prepared to mimic the conductivity of full scale paper machine process waters. A conductivity meter indicated 3-4 times higher readings than during other trial points. According to the Paperlab results compared to plain inline-PCC, high conductivity

causes higher surface roughness, improved brightness and whiteness, but due to a slightly lower opacity and light scattering against a brown background, they slacken slightly lower. Increasing the conductivity by using salts amongst the pulp seems to improve most of the strength properties at an average range of 5%, with the most significant improvements observed in cross directional tensile stiffness and e-modulus. The changes in the paper technical properties may be related to reaction kinetics or to the reaction equilibrium, but this needs further examination for confirmation.

When a comparison is made between the trial point 6 with increased conductivity and the reference point, the surface properties indicate a slightly higher roughness at trial point 6, while more substantial differences are found in strength properties. Calcined kaolin is better at an average range of 7 % with regards to tensile strength and stretch, however, inline-PCC with increased conductivity clearly exceeds calcined kaolin in tensile stiffness and e-modulus being nearly 40% stronger.

Carbon dioxide pressure was adjusted from the normal 5 bar to 9,5 bar at trial point 7. This did not as such have any major impact on the paper technical properties, although, it did have a positive effect on the stability of carbon dioxide flow adjustment.

As an overall result of trial 4, it may be stated that with variables other than filler content, notable changes in paper technical properties can be achieved. Nevertheless, with regards to optical properties against a brown background, 6% inline-PCC filler content is not adequate compared to 5% calcined kaolin. A comparison between calcined kaolin and the other most important trial points can be seen in table 33

Comparison of paper technical properties between 5% calcined kaolin versus the most important trial points of trial 4 is presented in the following matrix

	Compared to the reference point 1
O	-3% - + 3%
-	- 3% -10% deteriorated
- -	-10% -20% deteriorated
- - -	-20%... => deteriorated
+	+ 3% - 10% improved
+ +	+ 10% - 20%.. => improved
+ + +	+ 20%... => improved

Table 33. Calcined kaolin (5%) reference point vs. most important trial points

Measured Feature	6% Inline-pcc (tp 2&3)	6% Inline-pcc + reduced temperature (tp 4)	6% Inline-pcc + bentonite (tp 5)	6% Inline-pcc + salts (tp 6)
Gurley air resistance	**O**	**+**	**O**	**-**
Bendtsen roughness	**O**	**+**	**-**	**-**
PPS smoothness	**O**	**O**	**O**	**O**
Gloss	**-**	**O**	**-**	**-**
Brightness	**-**	**-**	**-**	**-**
Whiteness	**- -**	**- -**	**- -**	**-**
Opacity	**O**	**O**	**O**	**O**
Light absorption	**+ + +**	**+ + +**	**+ + +**	**+ + +**
Light scattering	**O**	**O**	**-**	**O**
Stretch	**-**	**-**	**- -**	**-**
Tensile index	**- -**	**- -**	**- -**	**-**
Tensile stiffness index	**+ +**	**+ + +**	**+ +**	**+ + +**
E-modulus	**+ +**	**+ + +**	**+ +**	**+ + +**
Tensile energy absorption index	**- -**	**- -**	**- - -**	**- -**
Tear strength	**+**	**O**	**+**	**+**
Tear index	**O**	**-**	**O**	**+**
Burst strength	**- -**	**- -**	**-**	**-**
Burst index	**- -**	**- -**	**- -**	**- -**
Brightness against brown background	**O**	**O**	**O**	**O**
Whiteness against brown background	**-**	**-**	**-**	**-**
Mottle	**O**	**O**	**O**	**O**

3.9 Trial 5 results

The most essential paper properties and ash measurement results of trial five are presented in tables 34-38. Paper technical properties are divided into surface properties, optical properties, optical properties against a brown background and strength properties. Pictures 38-41 illustrate SEM surface images of the most interesting trial points of trial five paper samples.

Table 34. The most important surface properties of trial 5

Trial point		**1**	**2**	**3**	**4**	**5**	**6**	**7**
	Unit							
Air resistance Gurley	s/100 ml	10	12	11	10	20	15	15
Bendtsen-roughness, ts + bs avg	ml/min	208	196	184	198	199	201	215
PPS 0.5, ts + bs avg	µm	5,9	5,8	5,8	5,8	5,9	5,8	5,9
PPS 1.0, ts + bs avg	µm	5,6	5,5	5,5	5,4	5,6	5,5	5,6
PPS 2.0, ts + bs avg	µm	5,0	5,0	4,9	4,9	5,1	5,0	5,1

Table 35. The most important optical properties of trial 5

Trial point		**1**	**2**	**3**	**4**	**5**	**6**	**7**
	Unit							
Opacity C/2° +UV, ts + bs avg	%	80,2	80,0	80,5	81,8	78,1	79,3	79,1
Light scattering coefficient +UVt, ts + bs avg	m²/kg	41,1	37,8	39,0	40,5	33,9	37,1	35,9

Table 36. The most important optical properties against brown background of trial 5

Trial point		**1**	**2**	**3**	**4**	**5**	**6**	**7**
	Unit							
Brightness R457 C/2° +UV, ts + bs avg	%	72,7	70,0	70,5	71,9	68,6	69,6	69,8
Brightness R457 D65/10° +UV, ts + bs avg	%	72,7	70,1	70,6	72,0	68,7	69,7	69,8
CIE whiteness C/2° +UV, ts + bs avg	%	67,1	60,7	61,0	63,0	59,4	59,6	61,0
CIE whiteness D65/10° +UV, ts + bs avg	%	67,3	61,2	61,4	63,4	59,8	60,0	61,3
White top mottle		1,064	1,061	1,064	1,020	0,995	1,090	1,071

Table 37. The most important strength properties of trial 5

Trial point		1	2	3	4	5	6	7
	Unit							
Tensile strength, Geom.avg. md+cd	kN/m	2,8	3,2	3,0	2,9	3,5	3,4	3,6
Stretch, Geom.avg. md+cd	%	3,1	3,2	3,1	2,9	3,7	3,4	3,5
Tensile index, Geom.avg. md+cd	Nm/g	44,9	48,5	46,2	42,6	52,7	53,2	53,5
Tensile stiffness, Geom.avg. md+cd	kN/m	298	390	373	362	383	384	380
Tensile stiffness index, Geom.avg. md+cd	MNm/kg	4,7	6,0	5,8	5,4	5,8	5,9	5,7
E-modulus, Geom.avg. md+cd	MPa	3507	4539	4382	4114	4675	4518	4364

Table 38. Ash content measured from trial 5 paper samples by burning in 550 ºC

Trial point	P1	P2	P3	P4	P5	P6	P7
%	5,8	5,2	5,6	6,1	5,3	5,4	4,4

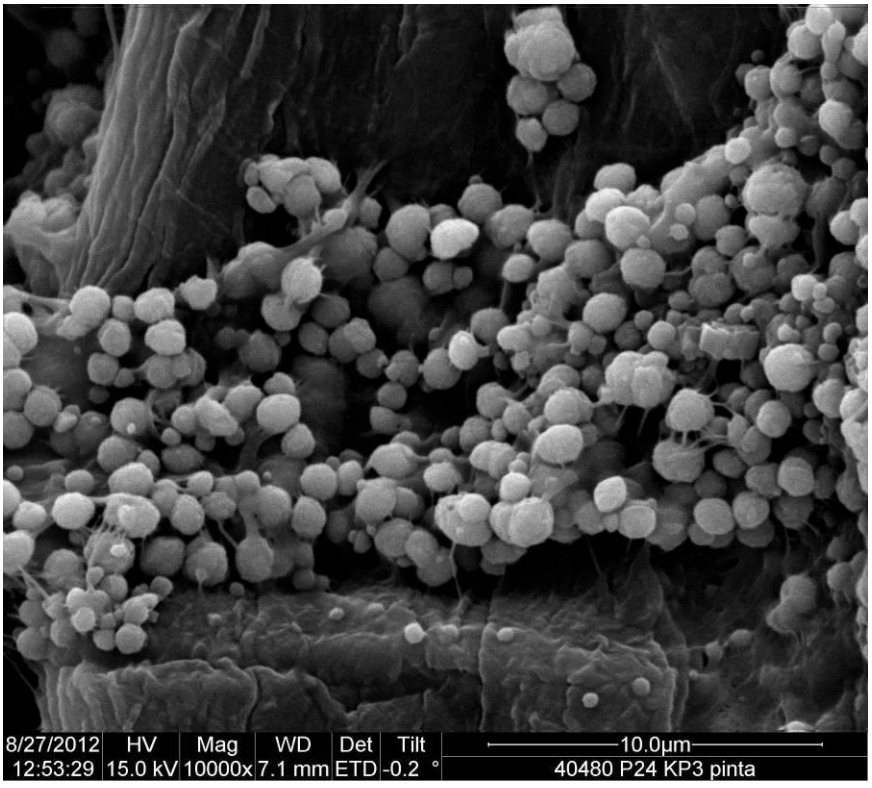

Picture 38. 10 000x magnification SEM top image of the trial 5 paper sample containing 6% Inline-PCC. Trumpjet® injection flow increased

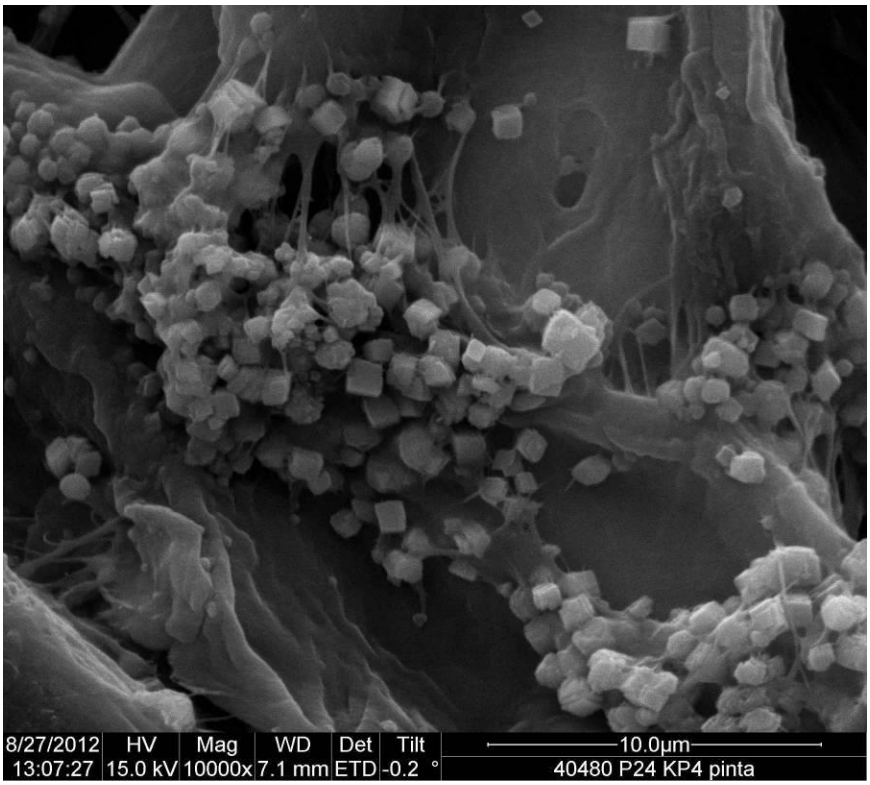

Picture 39. 10 000x magnification SEM top image of the trial 5 paper sample containing 6% Inline-PCC. Trumpjet® injection flow decreased

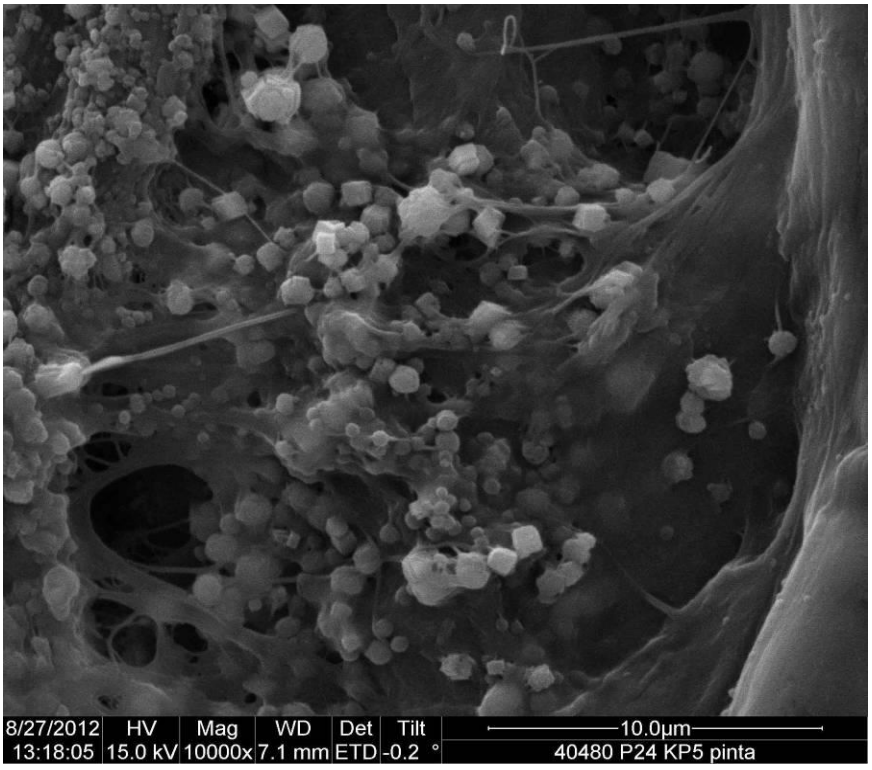

Picture 40. 10 000x magnification SEM top image of the trial 5 paper sample containing 6% Inline-PCC. Manufactured from undried pulp

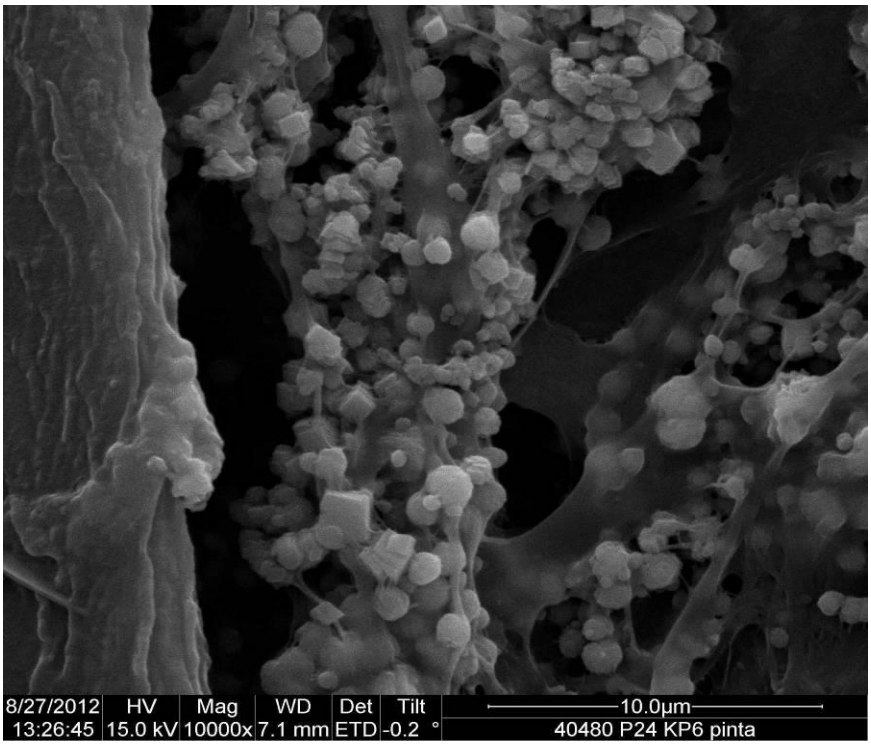

Picture 41. 10 000x magnification SEM top image of the trial 5 paper sample containing 6% Inline-PCC. Manufactured with 10% cationic starch among the calcium hydroxide

3.10 Trial 5 analysis

The main objectives of trial 5 were an attempt to have an impact on the PCC crystal morphology, to analyze the divergence of dried and undried pulp and to apply starch for strength improvement to some of the previously experimented trial points. 6% Inline-PCC filler content was chosen as basis for the trials. The previous 4 trials have shown that inline-PCC crystallizes most often into a spherical form.

The idea of trial points 3 and 4 was to alter the Trumpjet® injection flow and thereby to either hasten or slacken the precipitation reaction in order to elucidate the possible changes in crystal morphology. The standard setting for injection flow is 2 l/s which is estimated as optimal for the current reactor diameter and feedstock flow. At trial point 3, the flow was increased to 4 l/s and at trial point 4 it was reduced to 1 l/s. When looking at the high-resolution SEM images (pictures 38 and 39), it is clearly seen that with different injection flows, the shape of precipitated calcium carbonate crystals differs notably. When the injection flow was increased, more spherical PCC crystals formed. When the injection flow was decreased, more cubical crystals formed.

Trial points 1, 2 and 3 were analyzed with an X-ray diffractometer, to confirm the proportions of each polymorph. Divergences are also found in the paper technical properties: Paperlab analyses reveal slightly improved opacity, light scattering and optical properties against a brown background when the injection flow was decreased. On the other hand, most of the strength properties are improved with the increased injection flow. The difference in strength properties is in average of 6%. Strength properties however are not any higher with an increased injection flow than with the standard 2 l/s injection flow. The differences may explain not only the changes in crystal shape, but also changes in crystal size. According to the SEM images, lower injection results in slightly smaller PCC particles than with a higher injection flow. When a comparison is made between the reference point and 6% inline-PCC, the paper including inline-PCC has a slightly smoother surface, nearly 10% better overall strength properties, yet approximately a 2,5% lower brightness and an 8% lower whiteness. This result would suggest an increase of filler content for obtaining equal optical properties with the reference point, while strength properties can afford to be slightly compromised from.

All the previous trials were prepared using dried cellulose, thus there was an interest to determine the difference between dried and undried cellulose. Undried pulp contains an increased amount of micro fibrils which improve strength properties considerably. In addition, the fiber structure has not hornificated as much as with dried pulp. Relative to inline-PCC manufactured from dried pulp, the opacity and light scattering coefficient are considerably lower, but all the strength properties excluding cross directional tensile stiffness and e-modulus are much higher. A few degrees raised Shopper Riegler value at trial point 5 indicated a higher beating level of the pulp, which has resulted in denser fiber structure and lower porosity, but on the other hand very good mottling. In total, the average improvement of strength properties compared to dried pulp was just over 10%.

Based on the positive experiences of employing starch among calcium hydroxide as a strength improver in earlier trials, the experiment was duplicated at trial point 6. This time the starch dosage was increased to 10% of the filler content, and CMC was left out. Similar to previous experiments, starch densified the paper structure, lowered the porosity and light scattering coefficient, yet improved all the strength properties by an average of +5%. Unlike earlier experiences in trial 3, starch without CMC did not seem to have such a major impact on the brightness and whiteness values.

In trial 3, a mixture of calcined kaolin and inline-PCC was experimented with. Due to very good results in light scattering and opacity values, a rerun with added starch and CMC was experimented with in trial 5. The idea was to improve some of the strength properties, such as tensile strength and stretch, which was found inferior, compared to calcined kaolin. Trial 5 analysis reveals that the filler retention had dropped because of starch and CMC from 82,6% in trial 3 to 74,6% in trial 5. Therefore, total filler content had also dropped from the intended 5% to 4,3%. Low filler content has on one hand obviously affected the optical properties negatively, yet on the other hand affected positively on the strength properties. With regards to strength properties the mixture filler surpasses plain calcined kaolin and plain inline-PCC in every section. Despite the low filler content, optical properties are not bad at all, when compared to 6% inline-PCC. This result would suggest a mixture filler experiment with a total filler content of for example 7% including 2% calcined kaolin and 5% inline-PCC.

A comparison between calcined kaolin and the other most important trial points can be seen in tables 39 and 40. Comparison of paper technical properties between 5% calcined kaolin versus the most important trial points of trial 5 is presented in the following matrixes.

	Compared to the reference point 1
O	-3% - + 3%
-	- 3%- 10% deteriorated
- -	-10% -20% deteriorated
- - -	-20%... => deteriorated
+	+ 3% - 10% improved
+ +	+ 10% - 20%.. => improved
+ + +	+ 20%... => improved

Table 39. Calcined kaolin (5%) reference point vs. most important trial points

Measured Feature	6% inline pcc (tp 2)	6% inline pcc increased injection flow (tp 3)	6% inline pcc decreased injection flow (tp 4)
Gurley air resistance	**- -**	**-**	**O**
Bendtsen roughness	**+**	**+ +**	**+**
PPS smoothness	**O**	**O**	**O**
Gloss	**+**	**+**	**O**
Brightness	**-**	**-**	**O**
Whiteness	**- -**	**- -**	**-**
Opacity	**O**	**O**	**O**
Light absorption	**+ +**	**+ + +**	**+ +**
Light scattering	**-**	**-**	**O**
Stretch	**+**	**O**	**-**
Tensile index	**+**	**O**	**-**
Tensile stiffness index	**+ + +**	**+ + +**	**+ +**
E-modulus	**+ + +**	**+ + +**	**+ +**
Tensile energy absorption index	**+ +**	**O**	**-**
Tear strength	**+**	**+**	**+**
Tear index	**O**	**O**	**O**
Burst strength	**+**	**O**	**-**
Burst index	**+**	**O**	**- -**
Brightness against brown background	**-**	**-**	**O**
Whiteness against brown background	**-**	**-**	**-**
Mottle	**O**	**O**	**+**

Table 40. Calcined kaolin (5%) reference point vs. most important trial points

Measured Variable	6% inline pcc Undried pulp (tp 5)	6% inline pcc + 10% cationic starch (tp 6)	3% inline pcc + 2% calcined kaolin + 4% starch + 2% CMC (tp 7)
Gurley air resistance	- - -	- - -	- - -
Bendtsen roughness	+	+	-
PPS smoothness	O	O	O
Gloss	-	+	+
Brightness	-	-	O
Whiteness	-	- -	-
Opacity	O	O	O
Light absorption	+ +	+	+
Light scattering	- -	-	- -
Stretch	+ + +	+	+ +
Tensile index	+ +	+ +	+ +
Tensile stiffness index	+ + +	+ + +	+ + +
E-modulus	+ + +	+ + +	+ + +
Tensile energy absorption index	+ + +	+ + +	+ + +
Tear strength	+ +	+	+ +
Tear index		+	+
Burst strength	+ + +	+ + +	+ + +
Burst index	+ +	+ +	+ +
Brightness against brown background	-	-	-
Whiteness against brown background	- -	- -	-
Mottle	+	O	O

3.11 Hand sheet experiment results

The SEM images from hand sheets manufactured using cationic starch as an internal sizing agent are presented in pictures 42 and 43. Pictures 44 and 45 represent the SEM images of the hand sheets manufactured without internal sizing.

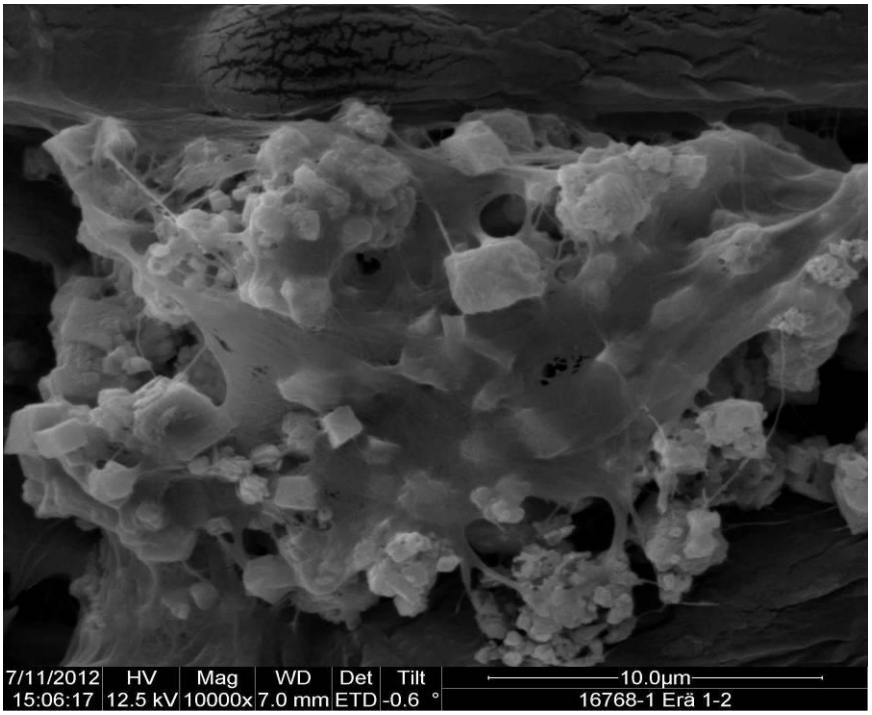

Picture 42. 10 000 x magnification SEM image from hand sheet with 20kg/t cationic starch

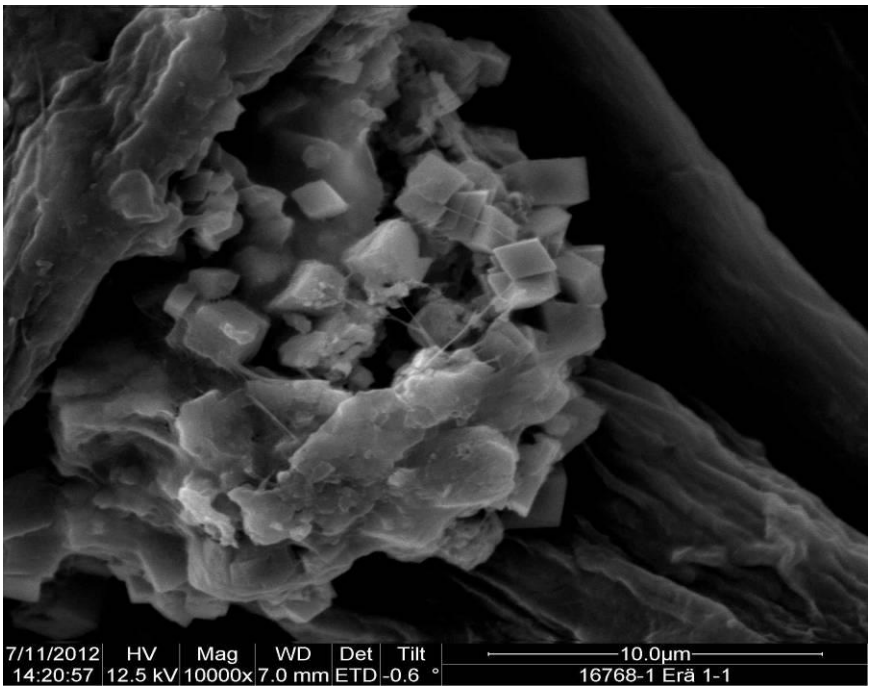

Picture 43. 10 000 x magnification SEM image from hand sheet with 20kg/t cationic starch

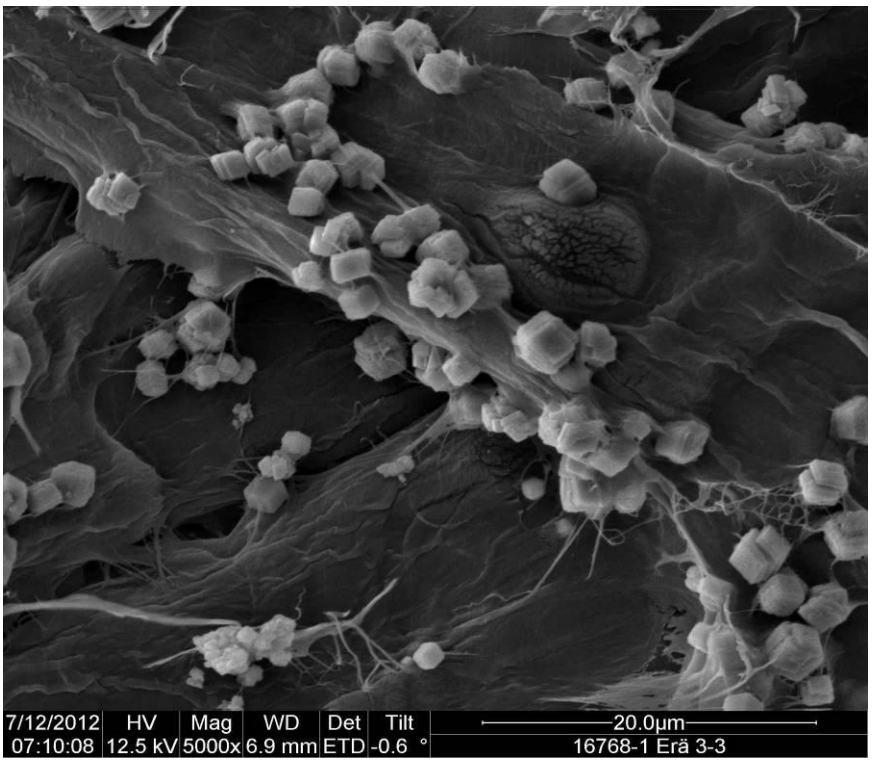

Picture 44. 10 000 x magnification SEM image from hand sheet without starch

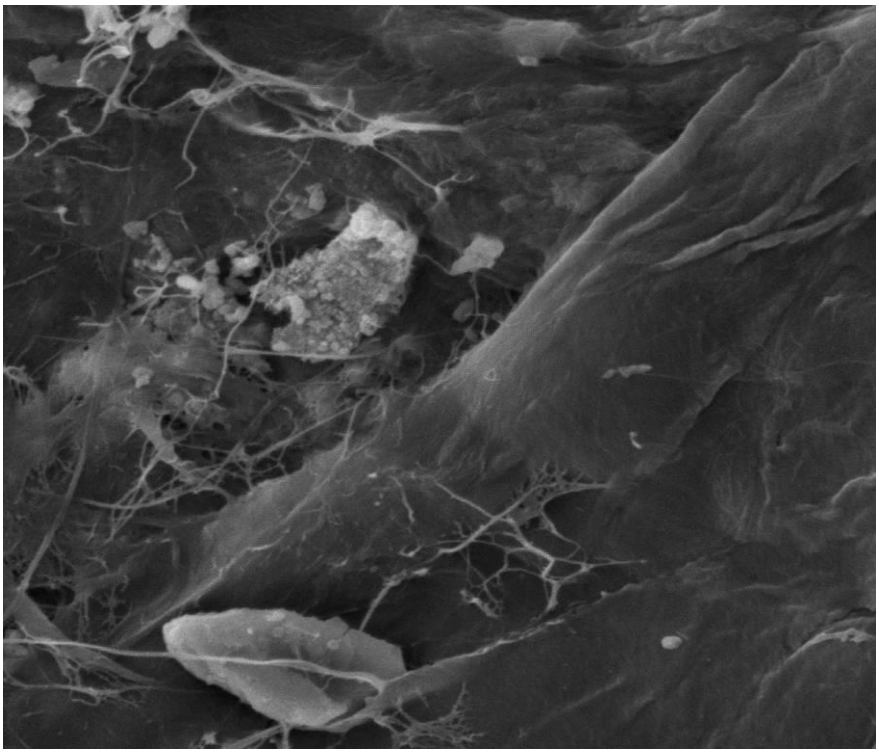

Picture 45. 5000 x magnification SEM image from hand sheet without starch

3.12 Hand sheet experiment analysis

According to the SEM images from the first trial onwards, a glue-like substance was observed as a veil or film surrounding PCC particles. The substance was perceived as a positive phenomenon as it seemed to firmly attach the filler particles into the fiber. The idea of these tests was to find out whether the substance is related to the starch that is used as internal sizing agent. The experiments were conducted by preparing hand sheets including and excluding starch and examining the results from SEM images. An important detail was to have the starch mixed with the pulp before PCC was precipitated in. PCC was precipitated in with a Quantum laboratory mixer. When comparing the SEM images 42 and 43 which contain starch, with 44 and 45 which do not contain starch it seems obvious that starch is the key element of the film. Web-like structures of fiber fines can be seen in pictures 44 and 45 which presumably act as a base where starch can attach to, yet no film can be observed.

3.13 Morphology results

The morphology of the selected points from the pilot trials was analyzed with 3 different methods. Picture 46 represents the SEM image of the reference sheet manufactured at the pilot paper machine. Picture 47 represents the SEM image of the same sheet which is subsequently soaked in RO-water and dried in room temperature. FTIR results are presented in diagram 8. The results of XRD analysis are presented in diagram 9. The diagram presents the proportional distribution of calcite, vaterite and aragonite form of $CaCO_3$.

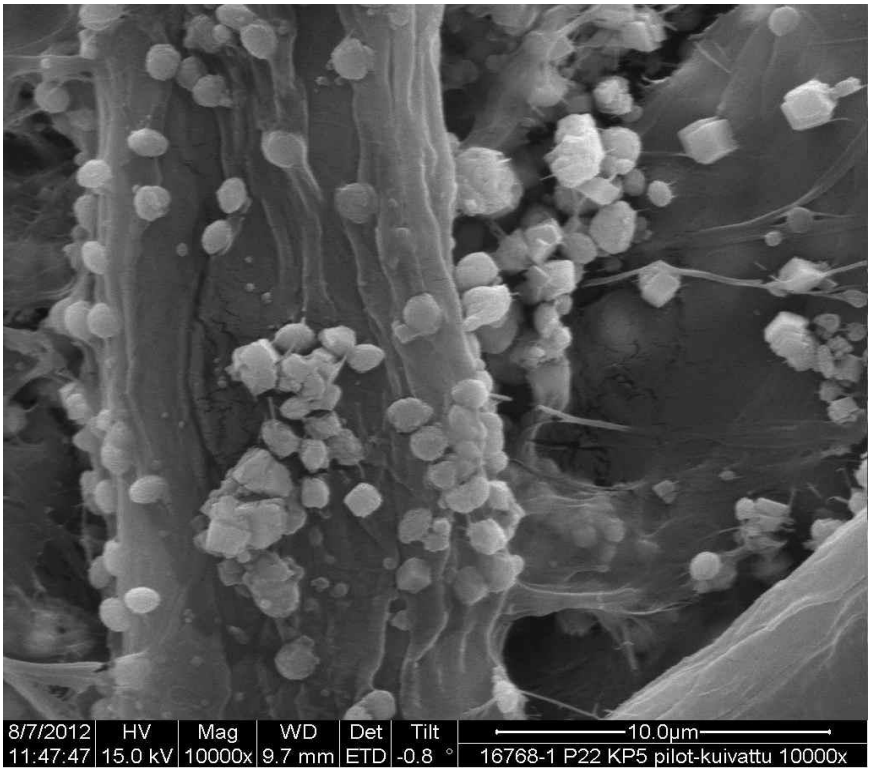

Picture 46. 12 000 x magnification SEM image from trial 3 pilot paper machine paper sample

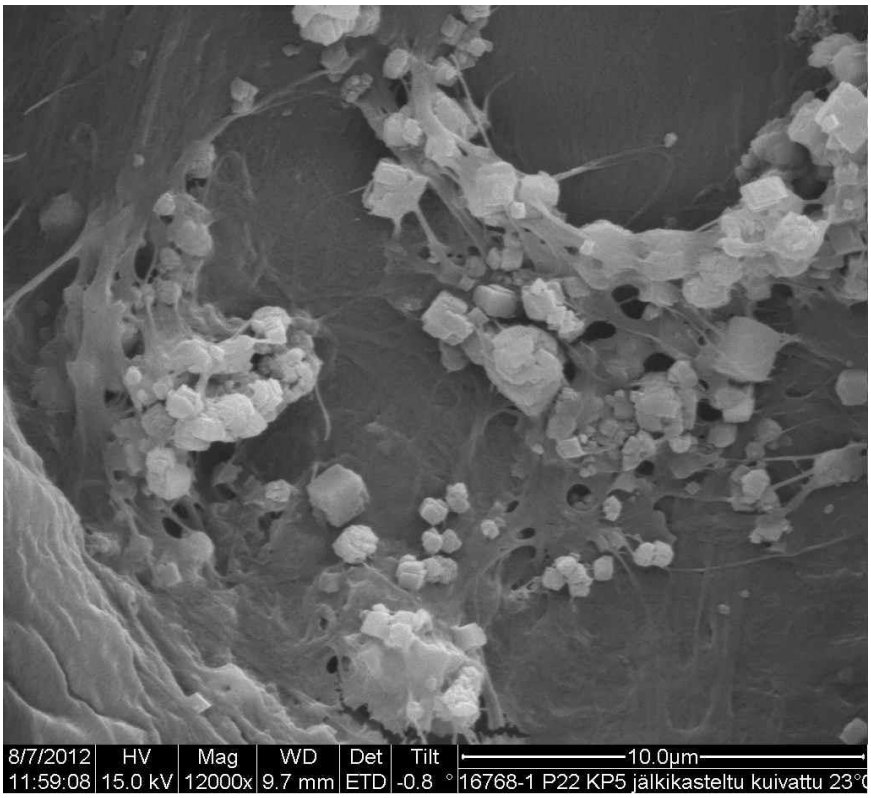

Picture 47. 12 000 x magnification SEM image from trial 3 paper sample.
Subsequently RO-soaked and room temperature dried.

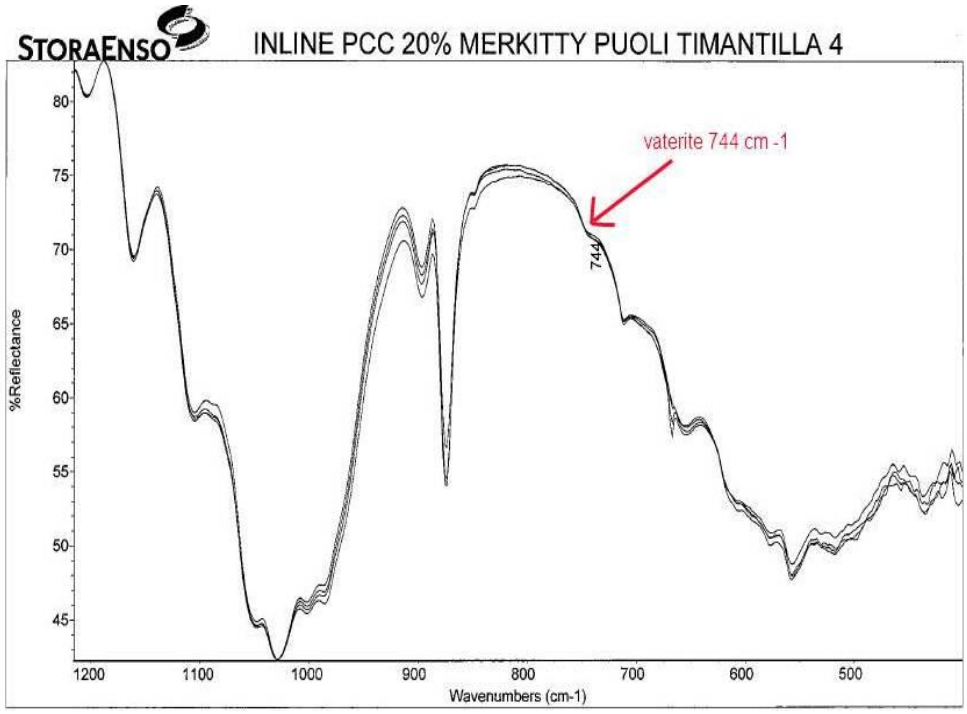

Diagram 8. Trial 1 tp 6 (20% inline-PCC) FTIR spectra

Table 41. $CaCO_3$ polymorph phase proportions [m-%]

Sample	Calcite	Vaterite	Aragonite
P23kp2	38,6 %	0,0 %	61,40 %
P23kp3	49,6 %	50,4 %	0,0 %
P23kp4	4,2 %	95,8 %	0,0 %
P23kp5	42,8 %	57,2 %	0,0 %
P23kp6	43,7 %	56,3 %	0,0 %
P23kp7	40,5 %	59,5 %	0,0 %
P24kp2	54,5 %	45,5 %	0,0 %
P24kp3	46,0 %	54,0 %	0,0 %
P24kp4	62,6 %	37,4 %	0,0 %

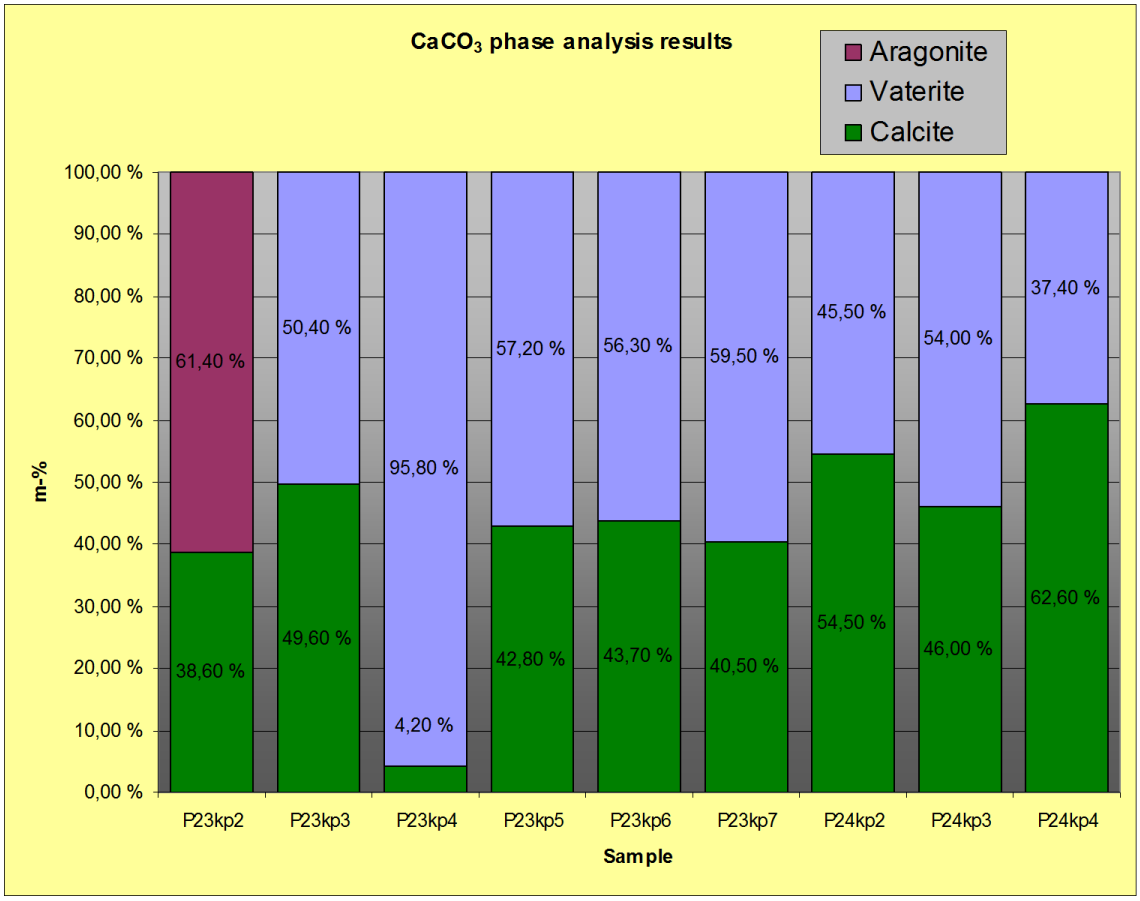

Diagram 9. Trial 4, trial points 2-7, Trial 5, trial points 2-4 XRD analysis

3.14 Morphology analysis

SEM images from all 5 trials indicated that filler particles precipitated with the inline-PCC method form more or less spherical shapes instead of the expected rhombohedric cubical shapes. According to previous experiences concerning inline-PCC, the typical polymorph is a cubical calcite. Vaterite typically has a spherical polymorph and when exposed to water or heat, it will eventually change into either calcite or aragonite. The polymorph of calcium carbonate produced in these trials was tested with three different methods.

Pictures 46 and 47 reveal the changes in crystal shape when exposed to water. PCC particles have distinctly converted from spherical to a more cubical shape. This discovery supported the theory of produced vaterite and therefore an FTIR analysis was performed.

To be able to have reliable results from FTIR, the sample would have to contain preferably 10% or more of the targeted polymorph. Consequently, trial point 6 in trial 1 was chosen to be analyzed as it contained 20% PCC. In FTIR, different polymorphs of calcium carbonate can be identified by the unique peaks on the spectrum, in the case vaterite the peak being 744 cm-1. The vaterite peak can clearly be identified from Diagram 8, though it is not very intense which indicates the vaterite content being half of the total amount of PCC or less. Finally, the polymorph was confirmed with X-ray diffractometer.

Trial points 2-7 from trial 4 and trial points 1-3 from trial 5 were chosen to be analyzed.

XRD analysis verified the other completed tests which indicated that a notable portion of calcium carbonate consists of vaterite. Surprisingly, the XRD results indicated an aragonite content of 61,4% in trial 4 trial point 1 where an undersupply of CO2 occurred which resulted in the pH level climbing to over 10. Another interesting discovery was made from the results of trial 4 trial, point 4 where the process water temperature was dropped to 23 degrees Celsius instead of the normal 45 degrees. The vaterite content of trial 4 trial point 4 was increased to 95,8%, while the rest of the trial points from trial 4 consisted of 50-60% vaterite and 40-50% calcite. In trial 5 the injector flow was adjusted in order to enable changes in crystal morphology. The test results revealed that the higher the mixing reaction, the more spherical vaterite crystals occur. The lower the mixing reaction, the more cubical calcite crystals occur. More research has to be done to find out whether the high vaterite content results from other ingredients in the experimented paper recipe or from other configurations at the inline-PCC reactor. XRD-analysis

was conducted in the laboratory of industrial physics at Turku University. The original report of the Trial 4 measurements is found in appendix 8

3.15 Calcium carbonate particle size measurement results

The particle size distribution of calcium carbonate particles is presented in Diagrams 10-12. Calcium carbonate has been separated from the fiber by incinerating the selected paper samples according to the method described in section 2.3.8.

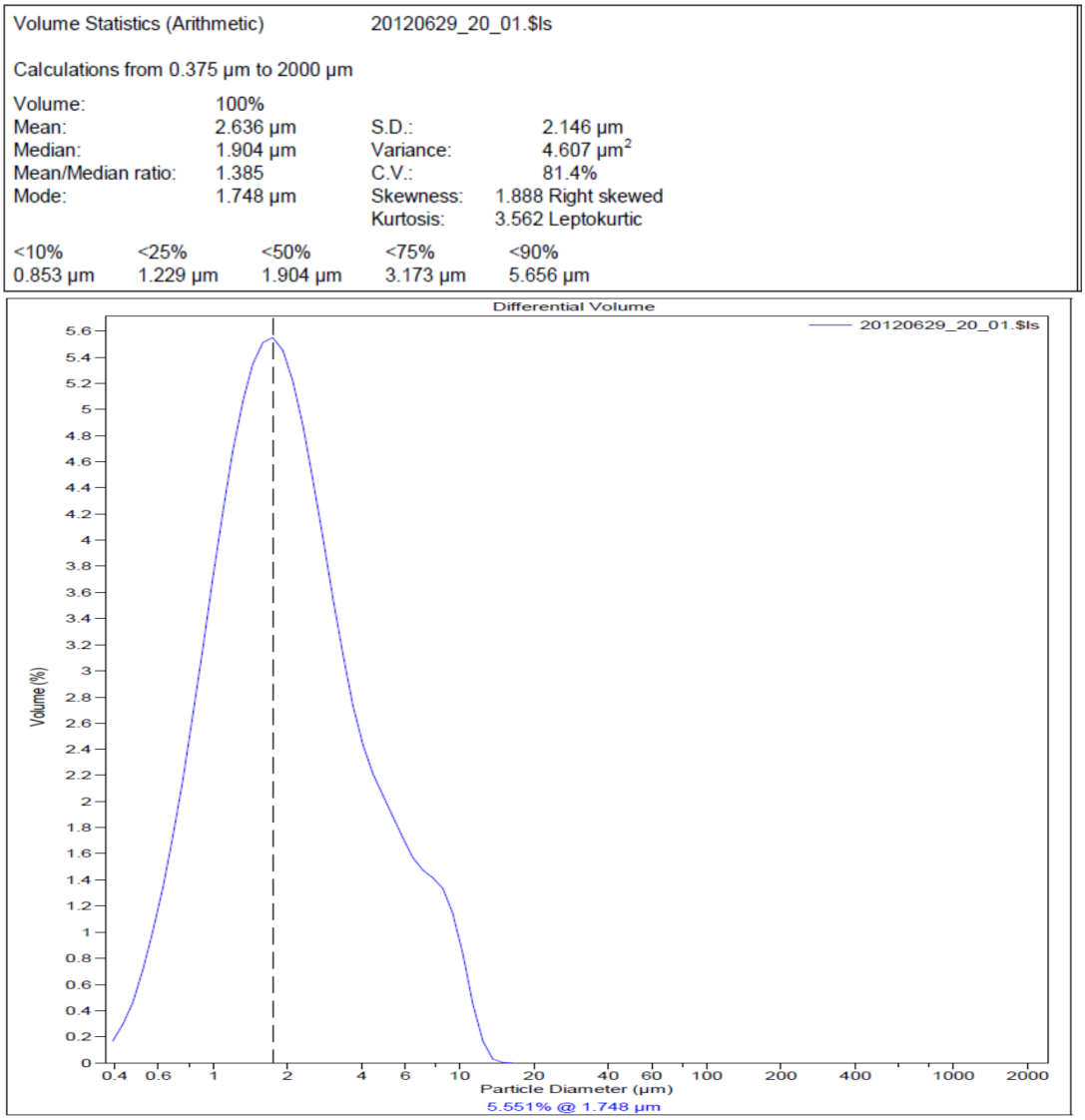

Diagram 10. Trial 1, tp 3. Incinerated paper sample particle size measurement graph.

Volume Statistics (Arithmetic)			20120629_29_01.$ls	
Calculations from 0.375 µm to 2000 µm				
Volume:	100%			
Mean:	1.673 µm		S.D.:	1.869 µm
Median:	1.296 µm		Variance:	3.492 µm²
Mean/Median ratio:	1.290		C.V.:	112%
Mode:	1.322 µm		Skewness:	5.837 Right skewed
			Kurtosis:	39.77 Leptokurtic

<10%	<25%	<50%	<75%	<90%
0.678 µm	0.919 µm	1.296 µm	1.804 µm	2.424 µm

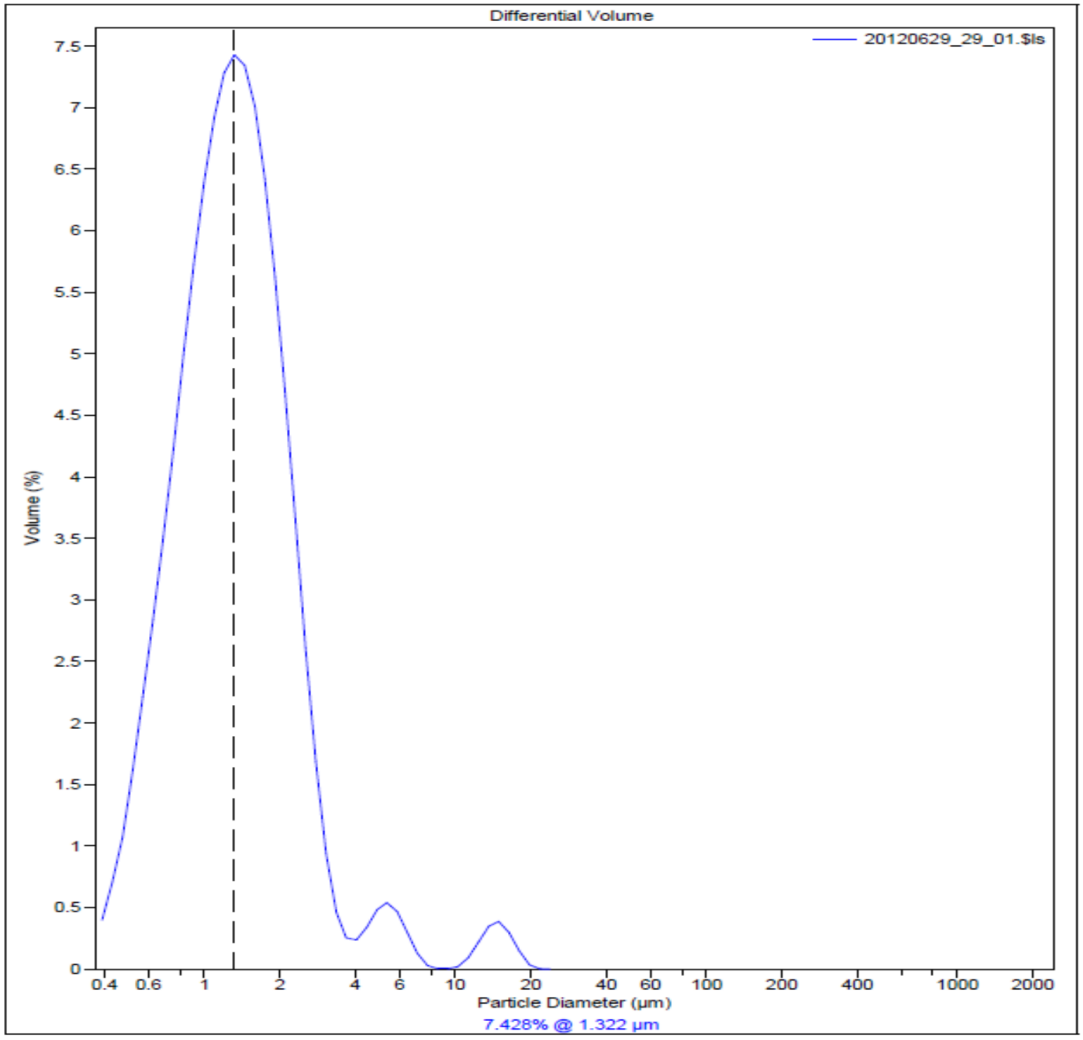

Diagram 11. Trial 1, tp 7. Incinerated paper sample particle size measurement graph.

Volume Statistics (Arithmetic)

Calculations from 0.375 µm to 2000 µm

Volume:	100%		
Mean:	4.511 µm	S.D.:	4.235 µm
Median:	3.462 µm	Variance:	17.93 µm^2
Mean/Median ratio:	1.303	C.V.:	93.9%
Mode:	5.355 µm	Skewness:	2.640 Right skewed
		Kurtosis:	9.107 Leptokurtic

<10%	<25%	<50%	<75%	<90%
0.951 µm	1.711 µm	3.462 µm	5.920 µm	8.503 µm

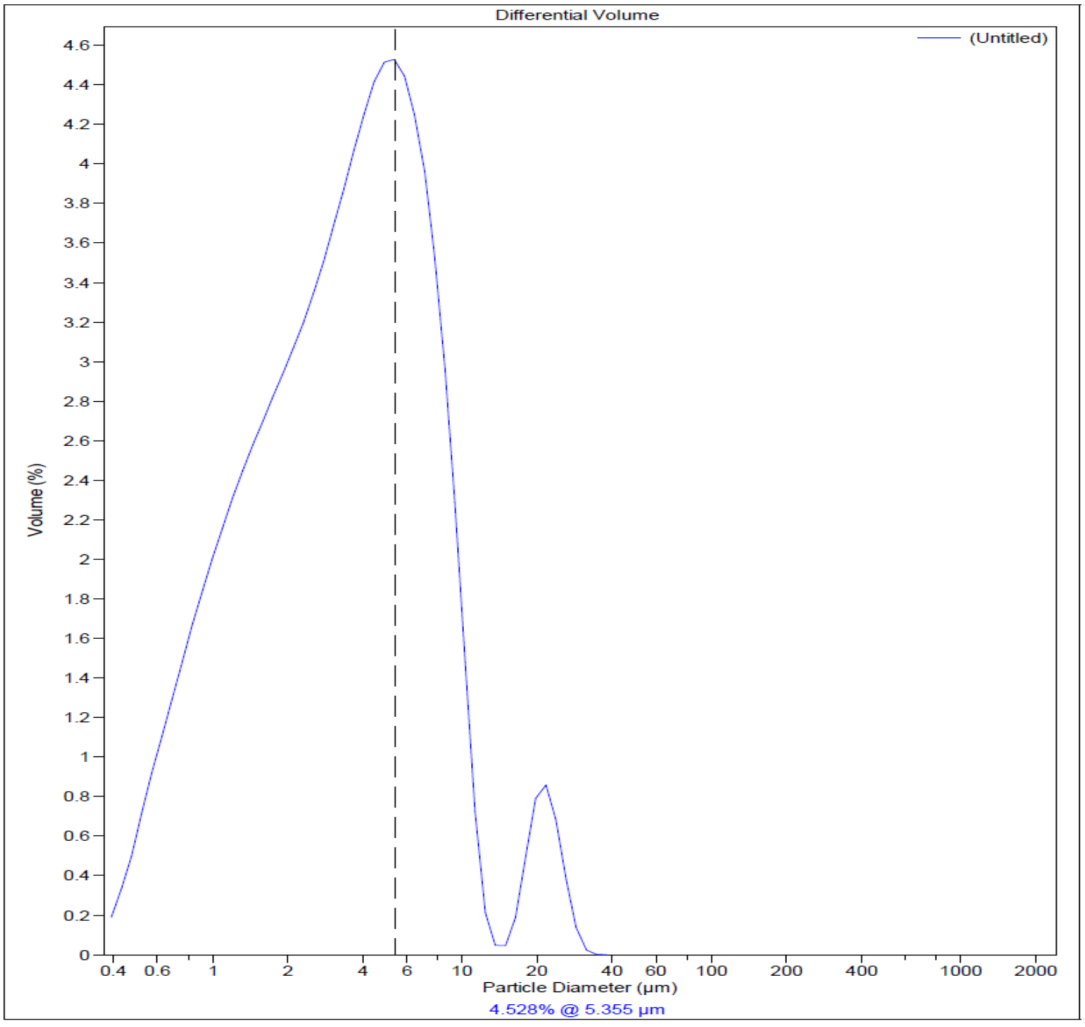

Diagram 12. Trial 2, tp 2. Incinerated paper sample particle size measurement graph.

3.16 Calcium carbonate particle size measurement analysis

As discussed earlier in the section 1.2.2, in theory, filler particle sizes have a significant impact on the optical properties of paper. PCC particles were separated from selected paper samples by burning and the particle size distribution was measured with a Coultier LS13 320 laser diffractometer. Eliminating the organic material from the paper sample was found challenging as there is no proven method for preserving the original size and shape of PCC crystals while burning. Experiments have shown that agglomeration of the PCC particles occurs if the temperature is too high or if the period of burning is too long.

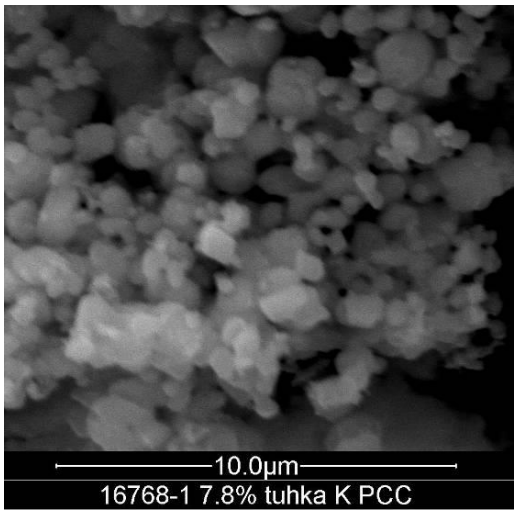

Picture 48. Trial 1 tp2. Ash SEM image

Insufficient temperature will result in excessive coal amongst the sample. Both cases lead to distorted measurement results. The most credible results were received with the incineration program of 1 hour/300 ºC in oxygen atmosphere, 6 hours/300 ºC in normal atmosphere and finally 1 hour/500 ºC in normal atmosphere. The measurement was conducted by mixing the residual ash with Millipore water just prior the analysis. Trial points 2 and 7 were selected from trial one as a comparison because referring to a visual examination of the SEM images, there seemed to be a slight difference in particle size. This way it could be confirmed whether the measurement results supported the visual conclusion. Offline-PCC trial point 2 from trial two was selected as the third sample. The measurement results (Diagram 10,11) indicated a median particle size of 1,90 µm for trial point 2 and a highest peak on the spectrum at 1,75µm. A median particle size of 1,29 µm was measured for trial point 7 while the highest peak on the spectrum

was at 1,32 µm. At trial point 7, carbon dioxide was undersupplied which resulted in the pH to climbing to nearly 10. Therefore, it may be concluded that the results confirm the observations and running with CO_2 undersupply results in a slightly smaller particle size. According to the trial 2 SEM images of trial point 2, Offline-PCC seems to cluster in approximately 5-micron bundles. The laser diffractometer confirms this as the median particle size was measured to be 3,46 µm, but the highest peak on the spectrum was 5,36 µm (Diagram 12).

Picture 46 reveals the shape of inline-PCC particles after the incineration. The exact influence of incineration to PCC particle size and shape and how quickly mixing the ash to Millipore water would change vaterite to calcite could not be proven during this study. However, the obtained results appeared rational.

4 DISCUSSION

One of the main objectives of the study was to examine how inline-precipitated calcium carbonate would act compared to calcined kaolin as filler. When paperboards using said two different fillers with equal filler content are compared, calcium carbonate is better than calcined kaolin in most of the strength properties, but falls relatively far behind in optical properties. For attaining equal brightness to that of 5% calcined kaolin, a 7% or more calcium carbonate content is required. However, increasing the filler content from 5% to 8% deteriorates the strength properties by approximately 5-10%. Applying 3-5% starch with 2-3% carboxymethyl cellulose to the total filler content among the calcium hydroxide increases the strength properties to equal or higher levels compared to those of 5% calcined kaolin. The application of starch and CMC will however have a slightly negative effect on optical properties, therefore a calcium carbonate content of 7,5 to 8% would be recommended. Increasing the starch dosage from 5% to 10% (experimented with in trials 3 and 5) does not seem to have remarkable advantage in paper strength properties. Both dosages, when compared to plain inline-PCC of each trial, give approximately the same increase in strength properties. It seems that when CMC is left out the negative effect of starch to brightness and whiteness values of the paper is minimal. Other effects resulting from a lack of CMC in this experiment remain unsolved. When comparing inline-PCC to offline-PCC or other studied PCC application methods, the most obvious advantage of inline-

PCC is the easiness of controlling the system online and the eliminated need for external satellite plants. Other advantages consist of improved runnability of the machine due to the cleansing effect of inline-PCC and the reduced demand for retention aids. With inline-PCC technology, the filler particles attach firmly around the fiber fines, while with offline-PCC, the particles lay loosely between the fibers and fines. This is likely one of the reasons why inline-PCC overall has improved the elastic-modulus and tensile stiffness values.

With inline-PCC, the limited ability of affecting the crystal morphology, and managing of possible coagulations in the system, may be seen as disadvantages of the method compared to offline-PCC manufacturing

Inline-PCC was found to precipitate mostly into a spherical crystal form which was later proven to include major portions of vaterite. High vaterite content is believed to be caused by a high supersaturation level of calcium hydroxide in the reactor which expedites the spontaneous precipitation reaction. Promising results in affecting the morphology by altering the CO_2 supply and injector flow volume were however observed in trials 4 and 5.

An inadequate amount of CO_2 results in a high pH value that seems to be favorable for the aragonite form of PCC. Reducing the injector flow seems to increase the calcite content and to change the PCC particles from spherical into more cubical forms. According to the SEM images, the cubical forms also have a more constant particle size distribution. According to the laboratory tests, the sample with the higher calcite content has an improved light scattering coefficient and opacity which results in higher brightness against a brown background. Reducing the flow is believed to decrease the supersaturation level and therefore to provide more time for calcium hydroxide and carbon dioxide to react with each other. In addition, reducing the process water temperature causes more vaterite to form as calcium dissolving improves and the supersaturation level rises.

In the example the current use of calcined kaolin as filler is approximately 5500 tonnes annually. The price of calcined kaolin is roughly 5 times more than PCC. Even though it has been proven that a higher filler content of PCC is required for attaining equal properties with calcined kaolin, the savings in just filler costs alone would be significant. Additional savings in fiber consumption could be gained due to inline-PCC's improvement in e-modulus which enables reducing the grammage on the mid layer while the total stiffness of the multilayer board still remains at the same level. Certainly, there would be notable investments in installing a full scale

inline-PCC system and constructing a source of calcium hydroxide, but it would pay itself back in a very reasonable amount of time. Increased savings could be achieved if other paperboard machines at the Stora Enso Imatra mills were to be affiliated with the plan.

5 CONCLUSIONS

The main targets of the study were to develop a method for how inline-PCC equipment is used in the pilot scale environment, study how it would fare against calcined kaolin and offline-PCC as an alternative filler and find out the other properties it would offer for multilayer liquid packaging board.

The installation of the equipment and the procedure control for variables were successfully achieved in this study. The optimal inline-PCC content which fares very well against calcined kaolin and offline-PCC was found, the content being equal or better in all the paper technical properties. In addition, inline-PCC was found to offer properties which allow for replacing a portion of the fiber with filler without losing the key properties of multilayer board. As a summary of the study, it can be stated that Inline-PCC is a considerable option for calcined kaolin, while more research in the field is recommended in order to discover the whole potential that inline-PCC offers, and the ways said potential can be optimized for commercial use.

With regards to future research, experiments in morphology changes should be carried out by altering the proportional injection flow between the CO_2 line and the calcium hydroxide line and thereby affecting the supersaturation level. The mixture filler experiments in trial 3 and 5 supports a trial point where the amount of calcined kaolin content would be kept at 2% but the inline-PCC content would be increased to around 5,5%, thus providing a total filler content of 7,5%. Increased light scattering, and opacity levels would be expected. In addition, interesting results could be obtained using micro fibrillated cellulose (MFC) amongst the calcium hydroxide. For future research, a method for reliably determining the filler particle size distribution from the paper samples would be of great help when the different settings in the production are experimented with.

REFERENCES

Alen R, 2007, Papermaking Science and Technology, Book 4, Papermaking Chemistry, 2nd edition, Finnish papermaking engineer's association, Helsinki, Finland

Auranen J, Robertsen L, Tamminen T, 2006, Fiber wall loading, KCL note 131.

Cizer O, Van Balen K. Elsen J, Van Gemert D./ ACEME08, 2nd International Conference on Accelerated Carbonation for Environmental and
Materials Engineering, 1-3 October 2008, Rome, Italy

Gullichsen J, Paulapuro H, 2000, Papermaking science and technology, Book 18, Paper and board grades, Fapet Oy, Jyväskylä, Finland

Hagemayer R, 1984, Pigments for paper. Technical association of the pulp and paper industry. Technology park Atlanta, Tappi press, USA

Haggblom-Ahner U, Komulainen P, 2003, Kemiallinen metsäteollisuus 2, Paperin ja kartongin valmistus. 3rd edition, Gummerus kirjapaino Oy, Jyväskylä

Holik H, 2006, Handbook of paper and board, Wiley-VHC Verlag GmbH & Co. KGaA, Weinheim, Germany

Hansen, K.V, Pedersen, M, Process for production of PCC, 2008, WO Pat 2008/128545.

Hockman J, Sohara J, 1999, Lumen loading of mineral filler into cellulose fibers for papermaking, EP Pat. 0960236B1

Haslam J.H, Steele F.A 1936, The retention of pigments in paper. Technical association papers 19

Holmberg M, Krogerus B, 1992, KCL Keskuslaboratorio printout.

Imerys-Paper Technical guide, 2010. Fillers for uncoated woodfree papers. http://www.imerys-paper.com/ pdf/Technical_Guide_Fillers_for_ Uncoated_Wood_Free_A4.pdf. Website Accessed 13.9.2012

Imppola O, A method and apparatus to produce precipitated calcium carbonate, WO Pat. 2009/083633 A1

Imppola O, Kukkamäki E, Matula J, A method and reactor for in-line production of calcium carbonate into the production process of a fibrous web, WO Pat. 2011/110744 A2

Kumar P, Gautam S, Kumar V, Singh S, 2009, Peer Reviewed article Enhancement of optical properties of bagasse pulp by in-situ filler precipitation. Bio Resources 4(4), 1635-1646

Lappeenranta University of technology, fiber laboratory website, accessed 6.7.2012. http://www.lut.fi/en/mikkeli/fiberlaboratory/services/laboratory/mbf/Pages/Default.aspx

Lehtinen E, Gullichsen J, Paulapuro H, 2000, Papermaking Science and Technology, Book 11, Pigment coating and surface sizing of paper, Fapet Oy, Jyväskylä, Finland

Liukkonen L, 2012, Stora Enso Internal presentation, 18.4.2012

Maloney T, 2010, Fiber and paper physics 1, Papermaking fillers and pigments. Lecture material. https://noppa.aalto.fi/noppa/kurssi/puu-21.3050/luennot

Middleton S.R, Desmeules J, Scallan A.M, 2003, Lumen loading with calcium carbonate fillers, Journal of pulp and paper science, vol 29, no 7, July 2003

Mueller, K.; Pulp & Paper Chemicals Outlook, New Orleans, LA February 24-25, 2005 Topic: Overview of coated and uncoated calcium carbonate containing papers; current status and prognosis. http://www.specialtyminerals.com/fileadmin/user_upload/smi/Publications/S-PA-AT-PB-138.pdf

Murray H, 1984, Pigments for paper, Chapter 6, Technical association of the pulp and paper industry, Edited by R. Hagemayer, Technology park Atlanta, Tappi press, USA

Niskanen K, Gullichsen J, Paulapuro H, 1998, Papermaking science and technology, Book 16, Paper Physics, Fapet Oy, Jyväskylä, Finland.

Norström A, AEL Insko Seminar 2008 Kouvola, Paperinvalmistuksen märkäosan kemian aja ilmiöiden hallinta, AEL Helsinki, Finland

Pauler N, 2002. Paper Optics, AB Lorentzen & Wettre, Elanders tofters, Östervåla, Sweden

Peel, J.D, 1999, Paper science and paper manufacture, Angus Wilde Publications Inc. Vancouver, Canada

Roberts C.J, 1991. Paper Chemistry, 1st edition, Chapman & Hall, UK

Ruohoniemi N, 2012 method of using Handy Mottle v3 paper cloudiness measuring program. 2012

Specialty Minerals website 2012, Precipitated Calcium Carbonate (PCC) Chemical & Physical Properties. http://www.specialtyminerals.com/paper/pcc-pigments/features-of-pcc/pcc-morphology-comparison/. Accessed 10.8.2012

Stora Enso OYJ, Archives, Presentation slides of Imatra mills, accessed 11.5.2012 http://imatramills.imm.corp.storaenso.com/avoin/Esitysaineisto/IMT/Imatra_Mills.pdf

Stora Enso internal communication, Matti Väkeväinen – Isto Heiskanen 2012

Subramanian R, Fordsmand H, Paulapuro H, 2007, Peer Reviewed article, PCC cellulose composite fillers; Effect of PCC particle structure on the production and properties of uncoated fine paper. Bio Resources 2(1), 91-105

Teir S, Eloneva S, Zevenhoven R, 2005, Energy conversion and management 46, Production of precipitated calcium carbonate from calcium silicates and carbon dioxide, Elsevier Ltd

Thorn I, 2009, Applications of wet-end paper chemistry. 2nd edition, Springer Dordrecht, Heidelberg, London, New York

Ukrainczyk M, Kontrec J, Babic-Ivancic V, Brecevik L, Kralj D, Powder Technology 171, 2007, 192-199, Science Direct, Experimental design approach to calcium carbonate precipitation in semicontinuous process, Elsevier Ltd

Wetend Technologies LTD, website accessed 13.4.2012 http://www.wetend.com/media/TrumpJet_products.pdf

Yamada H, Hara N, 1985_a Formation process of colloidal calcium carbonate in the reaction of the system Ca $(OH)_2$-H_2O-CO_2, Gypsum & Lime, No 194

Yamada H, Hara N, 1985_b Synthesis of basic $CaCO_3$ from the reaction of the system $Ca(OH)_2$-H_2O-CO_2, Gypsum & Lime, No 196

Yamada H, Hara N, 1985_c Transformation of amorphous $CaCO_3$ from the reaction of the system $Ca(OH)_2$-H_2O-CO_2, Gypsum & Lime, No 203

Yeakey, Scott, 2009, Omya Inc. Papercon ’09 seminar, St Louis, Missouri

Zhao Y, Zeshan H, Ragauskas A, Yulin D, 2005, Improvement of paper properties using starch-modified precipitated calcium carbonate filler, Tappi Journal, Vol 4, No:2, 2005

APPENDICES

APPENDIX 1. Standards used in the Metso Paperlab testing system

Modules and Standards

Measurement	According to standard	Related to standard
Burst	SCAN-P 24:77, ISO 2758, TAPPI 403	BS 3137, JIS 8112, CPPA D.8, DIN 53141
Tear		TAPPI 414, SCAN-P11, CPPA D.9, ISO 1974, DIN 53128, BS 4468
Tensile	SCAN-P 38:80, ISO 1924/2, TAPPI 494	BS 4415, DIN 53112, CPPA D.34
Roughness/Smoothness		
1. PPS	ISO 8791-4	TAPPI 555, BS 6563
2. SHEFFIELD	TAPPI 538	ISO 8791-3, CPPA D.29
3. BEKK	TAPPI 479	JIS P8119, ISO 5627
4. OKEN	JAPAN TAPPI 5-74	
5. BENDTSEN	SCAN P21, ISO 8791-2	DIN 53108, BS 4420
Porosity		
1. BENDTSEN	SCAN-P60:87, TAPPI 460, ISO 5636-3	
2. GURLEY	SCAN-P19:78, TAPPI 460	CPPA D.14, BS 2925
3. SHEFFIELD	TAPPI 547	DIN 53120
4. OKEN	JAPAN TAPPI 5-74	ISO 5636/4
Optical		
1. Directional	No indefinite paper pile	TAPPI 452, TAPPI 519, TAPPI 524
2. UV-Directional		TAPPI 452, TAPPI 519, TAPPI 524
3. Diffuse (3", 6")		TAPPI 525, TAPPI 527, ISO 2469, ISO 2470, ISO 2471
4. UV-Diffuse (3")		TAPPI 525, TAPPI 527, ISO 2469, ISO 2470, ISO 2471
Gloss 75 °	TAPPI 480, DIN 54502, ISO 8254-1	
45 °	DIN 54502	
Caliper	SCAN-P7, ISO 534, TAPPI 411, JIS P8118	
Basis Weight	Note! Measuring principle is the same in all standards, only measuring area varies.	SCAN-P6, TAPPI 410, ISO 536, BS 3432, DIN 53104
Formation	No Standard	
Tensile Stiffness Orientation	No Standard	
Filler		TAPPI 413 om-93, CPPAG.11, APPITA P418s, ISO 2144

 4.2.2005 P8610.5_En

metso automation

APPENDIX 2. The effect of filler content to mottling and light scattering

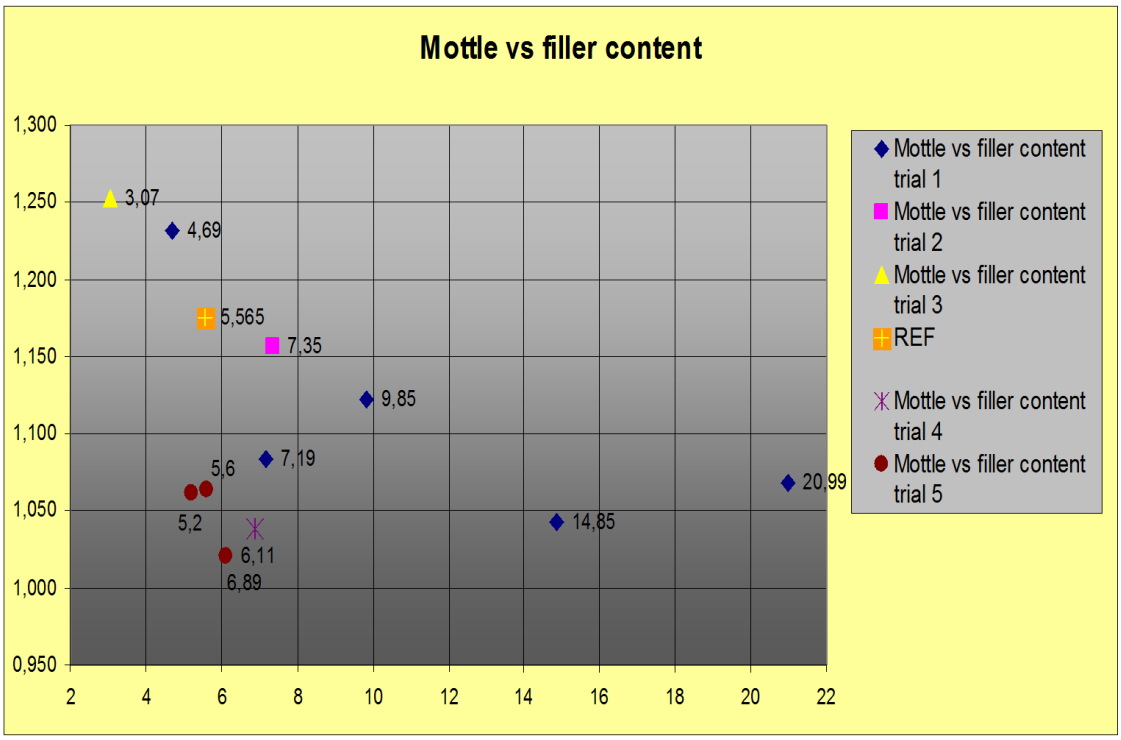

The effect of filler content to mottling

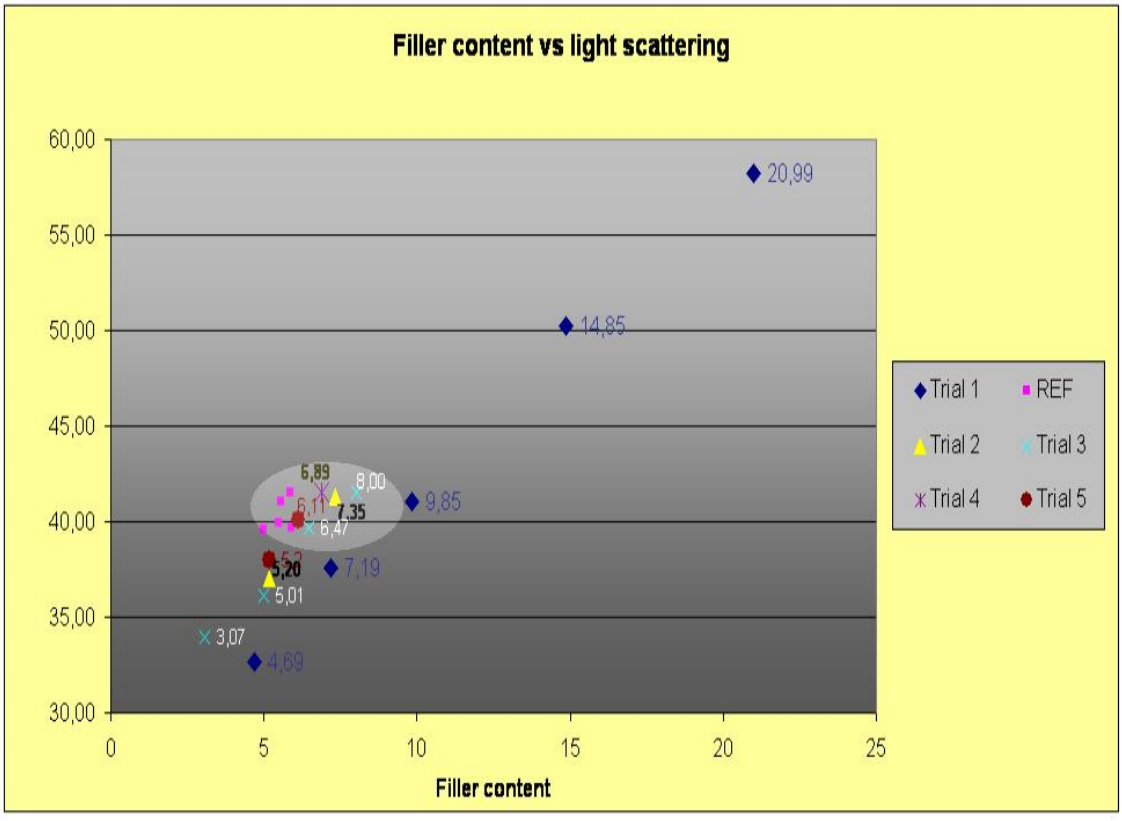

The effect of filler content to light scattering. Target area brightened.

APPENDIX 3. Trial 1 Paperlab results

Optical properties

Trial point		**1**	**2**	**3**	**4**	**5**	**6**	**7**	**8**
	Unit								
Grammage	g/m²	68,0	66,8	65,7	66,8	62,9	62,9	65,5	63,3
Thickness	µm	88	85	86	86	86	85	86	86
Density	kg/m³	773	786	764	777	731	740	762	736
Bulk	cm³/g	1,29	1,27	1,31	1,29	1,37	1,35	1,31	1,36
Air resistance Gurley	s/100 ml	33	21	15	13	10	9	18	11
Bendtsen-roughness, ts	ml/min	291	269	252	281	261	189	301	296
Bendtsen-roughness, bs	ml/min	360	307	299	283	313	196	337	344
PPS 0.5, ts	µm	5,98	6,00	6,01	5,96	5,91	5,75	6,02	6,04
PPS 0.5, bs	µm	6,23	6,18	6,24	6,16	6,15	5,97	6,24	6,31
PPS 1.0, ts	µm	5,72	5,74	5,74	5,68	5,59	5,38	5,74	5,75
PPS 1.0, bs	µm	6,02	5,96	6,03	5,91	5,88	5,63	6,01	6,07
PPS 2.0, ts	µm	5,41	5,44	5,42	5,36	5,23	4,99	5,44	5,44
PPS 2.0, bs	µm	5,25	5,17	5,26	5,11	5,07	4,79	5,22	5,28
Gloss, ts	%	6,6	6,7	6,4	6,4	5,7	5,6	6,3	6,2
Gloss, bs	%	7,3	7,4	6,8	6,7	5,9	6,0	6,5	6,4
Brightness D65/10° +UV, ts	%	83,9	79,8	80,8	81,8	83,1	84,3	80,6	81,4
Brightness D65/10° +UV, bs	%	84,8	80,2	81,6	82,5	84,0	85,4	81,2	82,1
Brightness C/2° +UV, ts	%	84,6	80,3	81,4	82,3	83,7	85,0	81,2	82,0
Brightness C/2° +UV, bs	%	84,6	80,2	81,5	82,3	83,8	85,1	81,1	81,9
Brightness C/2° -UV, ts	%	84,0	79,6	80,7	81,6	83,1	84,4	80,5	81,2
Brightness C/2° -UV, bs	%	84,0	80,1	81,2	81,9	83,3	84,4	80,9	81,6
CIE-whiteness C/2° +UV, ts	%	70,7	59,9	62,2	64,4	67,6	70,7	61,5	63,6
CIE-whiteness C/2° +UV, bs	%	67,4	59,4	61,3	63,1	65,3	67,5	60,6	62,3
CIE-whiteness D65/10° -UV, ts	%	70,3	60,5	62,6	64,4	67,5	70,2	62,2	63,8
CIE-whiteness D65/10° -UV, bs	%	70,7	60,8	63,0	65,0	68,2	70,6	62,5	64,3
CIE-whiteness C/2° -UV, ts	%	70,0	59,9	62,0	63,9	67,0	69,8	61,6	63,2
CIE-whiteness C/2° -UV, bs	%	70,1	60,3	62,4	64,4	67,5	69,9	62,0	63,7
CIE-whiteness D65/10° +UV, ts	%	67,3	59,0	60,6	62,3	64,6	67,0	59,8	61,7
CIE-whiteness D65/10° +UV, bs	%	70,4	62,1	63,8	65,7	67,8	70,1	63,0	64,8
Opacity C/2° +UV, ts	%	78,4	77,5	79,8	81,5	83,7	85,8	80,3	80,3
Opacity C/2° +UV, bs	%	78,1	77,3	79,3	81,1	83,2	85,4	80,1	79,7
Light absorption coefficient +UV, ts	m²/kg	0,22	0,32	0,32	0,31	0,32	0,31	0,33	0,32
Light absorption coefficient +UV, bs	m²/kg	0,20	0,29	0,28	0,28	0,28	0,27	0,30	0,29
Light scattering coefficient +UV, ts	m²/kg	35,89	32,64	37,62	41,01	50,21	58,26	38,65	40,57
Light scattering coefficient +UV, bs	m²/kg	35,89	32,71	37,56	40,87	49,96	58,03	38,82	40,09

Trial point		1	2	3	4	5	6	7	8
	Unit								
L* D65/10° +UV, ts		95,62	94,63	94,96	95,22	95,57	95,91	94,95	95,11
L* D65/10° +UV, bs		95,88	94,98	95,34	95,52	95,88	96,18	95,27	95,43
a* D65/10° +UV, ts		-0,32	-0,14	-0,12	-0,08	-0,14	-0,10	-0,14	-0,10
a* D65/10° +UV, bs		-0,47	-0,28	-0,24	-0,22	-0,26	-0,22	-0,27	-0,26
b* D65/10° +UV, ts		3,90	5,63	5,33	4,97	4,53	4,05	5,51	5,11
b* D65/10° +UV, bs		4,01	5,74	5,43	5,03	4,64	4,17	5,60	5,21
L* C/2° +UV, ts		95,58	94,58	94,92	95,19	95,55	95,90	94,92	95,08
L* C/2° +UV, bs		96,06	95,10	95,50	95,69	96,08	96,40	95,42	95,59
a* C/2° +UV, ts		-0,76	-0,79	-0,74	-0,70	-0,67	-0,59	-0,74	-0,71
a* C/2° +UV, bs		-0,94	-0,93	-0,89	-0,84	-0,81	-0,75	-0,89	-0,87
b* C/2° +UV, ts		4,06	5,87	5,56	5,24	4,74	4,28	5,71	5,36
b* C/2° +UV, bs		4,15	5,85	5,57	5,21	4,78	4,37	5,69	5,35
Dominant wavelength C/2° +UV, ts	nm	683,47	684,11	684,16	684,17	684,08	684,14	684,19	684,18
Dominant wavelength C/2° +UV, bs	nm	674,33	675,10	675,12	675,14	675,09	675,12	675,15	675,10
Spectral purity C/2° +UV, ts	%	5,40	7,62	7,24	6,85	6,24	5,68	7,42	6,99
Spectral purity C/2° +UV, bs	%	5,19	7,42	7,05	6,58	6,02	5,49	7,20	6,76

Optical properties against a brown background

Brightness R457 C/2° +UV, ts	%	71,8	68,1	70,7	72,7	75,0	77,5	71,3	71,3
Brightness R457 C/2° +UV, bs	%	71,8	67,8	70,5	72,6	74,9	77,0	70,9	71,1
Brightness R457 D65/10° +UV, ts	%	71,8	68,1	70,7	72,7	75,1	77,5	71,3	71,3
Brightness R457 D65/10° +UV, bs	%	71,8	67,9	70,5	72,6	74,9	77,0	71,0	71,1
CIE whiteness C/2° +UV, ts	%	66,95	58,12	61,87	64,81	68,30	71,57	62,81	63,64
CIE whiteness C/2° +UV, bs	%	66,90	57,82	61,67	64,68	68,19	71,31	62,66	63,59
CIE whiteness D65/10° +UV, ts	%	67,0	58,5	62,1	65,0	68,4	71,7	63,0	63,9
CIE whiteness D65/10° +UV, bs	%	67,0	58,2	61,9	64,9	68,3	71,4	62,9	63,9
L* C/2° +UV, ts		88,61	87,48	88,61	89,46	90,41	91,42	88,84	88,73
L* C/2° +UV, bs		88,57	87,35	88,51	89,40	90,33	91,18	88,66	88,63
L* D65/10° +UV, ts		88,56	87,40	88,55	89,41	90,37	91,39	88,79	88,67
L* D65/10° +UV, bs		88,52	87,28	88,45	89,34	90,29	91,14	88,60	88,58
a* C/2° +UV, ts		0,18	0,18	0,05	-0,05	-0,14	-0,23	-0,04	0,06
a* C/2° +UV, bs		0,18	0,21	0,06	-0,04	-0,12	-0,17	0,00	0,09
a* D65/10° +UV, ts		0,27	0,40	0,25	0,13	0,03	-0,08	0,16	0,23
a* D65/10° +UV, bs		0,28	0,43	0,27	0,14	0,04	-0,03	0,18	0,26
b* C/2° +UV, ts		1,31	2,60	2,35	2,13	1,85	1,65	2,26	2,04
b* C/2° +UV, bs		1,30	2,60	2,34	2,13	1,84	1,59	2,21	2,00
b* D65/10° +UV, ts		1,29	2,54	2,31	2,10	1,83	1,64	2,23	2,00
b* D65/10° +UV, bs		1,28	2,55	2,30	2,10	1,81	1,58	2,18	1,96
White top mottle		1,419	1,231	1,083	1,123	1,043	1,068	1,230	1,243

Mechanical properties

Trial point		**1**	**2**	**3**	**4**	**5**	**6**	**7**	**8**
	Unit								
Tensile strength, md	kN/m	5,27	4,81	4,46	3,91	2,81	1,86	4,12	3,89
Tensile strength, cd	kN/m	2,71	2,89	2,38	2,10	1,42	1,03	2,22	2,14
Stretch, md	%	1,9	2,0	1,9	1,7	1,6	1,3	1,7	1,6
Stretch, cd	%	5,9	5,9	5,3	5,2	4,2	3,7	5,0	5,1
Tensile index, md	Nm/g	77,5	72,0	67,9	58,5	44,7	29,6	62,9	61,5
Tensile index, cd	Nm/g	39,9	43,3	36,2	31,4	22,6	16,4	33,9	33,8
Tensile stiffness, md	kN/m	683,0	619,0	631,0	602,0	461,0	379,0	607,0	583,0
Tensile stiffness, cd	kN/m	289,0	270,0	275,0	250,0	204,4	129,0	276,0	235,0
Tensile stiffness index, md	MNm/kg	10,04	9,27	9,60	9,01	7,33	6,03	9,27	9,21
Tensile stiffness index, cd	MNm/kg	4,25	4,04	4,19	3,74	3,25	2,05	4,21	3,71
E-modulus, md	MPa	7761	7282	7337	7000	5360	4459	7058	6779
E-modulus, cd	MPa	3284	3176	3198	2907	2376	1518	3209	2733
Tensile energy absorption, md	J/m²	70,7	70,1	62,0	51,5	38,4	24,4	53,3	47,5
Tensile energy absorption, cd	J/m²	119,6	123,7	96,4	84,7	49,0	30,0	85,2	82,5
Tensile energy absorption index, md	kJ/kg	1,0	1,0	0,9	0,8	0,6	0,4	0,8	0,8
Tensile energy absorption index, cd	kJ/kg	1,8	1,9	1,5	1,3	0,8	0,5	1,3	1,3
Tear strength, md	mN	527	522	480	467	387	314	479	466
Tear strength, cd	mN	458	463	424	409	336	269	412	403
Tear index, md	mNm²/g	7,8	7,8	7,3	7,0	6,2	5,0	7,3	7,4
Tear index, cd	mNm²/g	6,7	6,9	6,5	6,1	5,3	4,3	6,3	6,4
Bursting strength	kPa	230	231	198	172	120	79	183	176
Burst index	kPam²/g	3,38	3,46	3,01	2,57	1,91	1,26	2,79	2,78

Measured ash content

Trial point	P1	P2	P3	P4	P5	P6	P7	P8
%	5,00 %	4,69 %	7,19 %	9,85 %	14,85 %	20,99 %	7,55 %	7,79 %

APPENDIX 4. Trial 2 Paperlab results

Optical properties

Trial point		**1**	**2**	**3**	**4**	**5**	**6**
	Unit						
Grammage	g/m²	64,9	66,8	66,6	65,7	64,2	64,6
Thickness	µm	89	92	88	88	86	86
Density	kg/m³	729	726	757	747	747	751
Bulk	cm³/g	1,37	1,38	1,32	1,34	1,34	1,33
Air resistance Gurley	s/100 ml	10	11	12	11	12	15
Bendtsen-roughness, ts	ml/min	263	257	257	256	214	214
Bendtsen-roughness, bs	ml/min	309	297	292	295	231	233
PPS 0.5, ts	µm	6,02	5,94	5,97	5,99	5,93	5,97
PPS 0.5, bs	µm	6,28	6,27	6,27	6,24	6,24	6,22
PPS 1.0, ts	µm	5,74	5,65	5,69	5,71	5,65	5,69
PPS 1.0, bs	µm	6,07	6,05	6,06	6,02	6,01	6,00
PPS 2.0, ts	µm	5,43	5,31	5,37	5,38	5,33	5,39
PPS 2.0, bs	µm	5,32	5,29	5,32	5,25	5,26	5,25
Gloss, ts	%	6,8	6,9	6,6	6,0	6,4	6,7
Gloss, bs	%	6,9	7,0	6,5	6,3	6,4	6,9
Brightness D65/10° +UV, ts	%	85,0	84,4	83,8	84,7	84,2	84,2
Brightness D65/10° +UV, bs	%	86,2	85,6	85,0	86,0	85,5	85,3
Brightness C/2° +UV, ts	%	85,7	85,1	84,4	85,3	84,8	84,8
Brightness C/2° +UV, bs	%	85,7	85,1	84,6	85,6	85,1	85,0
Brightness C/2° -UV, ts	%	85,2	84,5	83,8	84,8	84,2	84,1
Brightness C/2° -UV, bs	%	84,9	84,3	83,9	84,8	84,4	84,3
CIE-whiteness C/2° +UV, ts	%	73,2	71,5	69,7	71,8	71,1	70,8
CIE-whiteness C/2° +UV, bs	%	69,9	68,7	67,5	68,7	68,2	67,8
CIE-whiteness D65/10° -UV, ts	%	72,3	70,8	69,2	71,1	70,4	69,9
CIE-whiteness D65/10° -UV, bs	%	72,8	71,2	69,8	72,0	71,2	70,8
CIE-whiteness C/2° -UV, ts	%	72,2	70,5	68,9	70,9	70,2	69,7
CIE-whiteness C/2° -UV, bs	%	72,3	70,7	69,3	71,4	70,6	70,2
CIE-whiteness D65/10° +UV, ts	%	69,2	68,0	66,4	68,1	67,7	67,5
CIE-whiteness D65/10° +UV, bs	%	73,3	71,8	70,5	71,5	71,1	70,6
Opacity C/2° +UV, ts	%	79,1	78,2	78,4	80,1	79,0	78,5
Opacity C/2° +UV, bs	%	78,5	78,7	77,9	79,5	78,3	77,6
Light absorption coefficient +UV, ts	m²/kg	0,21	0,21	0,22	0,22	0,23	0,22
Light absorption coefficient +UV, bs	m²/kg	0,19	0,20	0,20	0,19	0,20	0,19
Light scattering coefficient +UV, ts	m²/kg	39,90	36,79	37,02	41,26	39,53	38,39
Light scattering coefficient +UV, bs	m²/kg	39,01	37,99	36,62	41,05	39,19	37,52

Trial point		1	2	3	4	5	6
	Unit						
L* D65/10° +UV, ts		39,90	36,79	37,02	41,26	39,53	39,90
L* D65/10° +UV, bs		39,01	37,99	36,62	41,05	39,19	39,01
a* D65/10° +UV, ts		95,93	95,81	95,72	95,93	95,74	95,93
a* D65/10° +UV, bs		96,11	96,03	95,97	96,23	96,09	96,11
b* D65/10° +UV, ts		-0,40	-0,34	-0,32	-0,31	-0,36	-0,40
b* D65/10° +UV, bs		-0,63	-0,58	-0,55	-0,52	-0,53	-0,63
L* C/2° +UV, ts		3,54	3,80	4,14	3,81	3,84	3,54
L* C/2° +UV, bs		3,42	3,73	4,03	3,87	3,92	3,42
a* C/2° +UV, ts		95,91	95,78	95,69	95,91	95,70	95,91
a* C/2° +UV, bs		96,29	96,20	96,14	96,44	96,28	96,29
b* C/2° +UV, ts		-0,82	-0,80	-0,82	-0,77	-0,80	-0,82
b* C/2° +UV, bs		-1,04	-1,02	-1,03	-0,97	-0,99	-1,04
Dominant wavelength C/2° +UV, ts	nm	3,71	4,01	4,36	4,01	4,05	3,71
Dominant wavelength C/2° +UV, bs	nm	3,67	3,99	4,27	4,05	4,12	3,67
Spectral purity C/2° +UV, ts	%	4,96	5,32	5,74	5,33	5,38	5,48
Spectral purity C/2° +UV, bs	%	4,54	4,95	5,32	5,03	5,12	5,23

Optical properties against a brown background

Brightness R457 C/2° +UV, ts	%	72,2	71,5	70,6	73,0	71,5	71,3
Brightness R457 C/2° +UV, bs	%	71,9	71,2	70,8	73,2	71,5	71,1
Brightness R457 D65/10° +UV, ts	%	72,1	71,5	70,6	73,1	71,5	71,4
Brightness R457 D65/10° +UV, bs	%	71,9	71,3	70,9	73,2	71,5	71,2
CIE whiteness C/2° +UV, ts	%	67,73	65,35	64,01	67,58	65,20	64,98
CIE whiteness C/2° +UV, bs	%	67,44	65,05	64,35	67,70	65,19	64,77
CIE whiteness D65/10° +UV, ts	%	67,8	65,6	64,3	67,8	65,5	65,3
CIE whiteness D65/10° +UV, bs	%	67,6	65,3	64,6	68,0	65,5	65,1
L* C/2° +UV, ts		88,69	88,64	88,22	89,28	88,64	88,58
L* C/2° +UV, bs		88,58	88,51	88,35	89,33	88,63	88,49
L* D65/10° +UV, ts		88,65	88,59	88,17	89,24	88,59	88,53
L* D65/10° +UV, bs		88,54	88,46	88,30	89,29	88,58	88,44
a* C/2° +UV, ts		0,22	0,23	0,26	0,15	0,23	0,23
a* C/2° +UV, bs		0,24	0,25	0,25	0,13	0,24	0,25
a* D65/10° +UV, ts		0,30	0,37	0,41	0,26	0,37	0,38
a* D65/10° +UV, bs		0,33	0,39	0,39	0,25	0,38	0,39
b* C/2° +UV, ts		1,18	1,65	1,74	1,48	1,68	1,70
b* C/2° +UV, bs		1,20	1,65	1,72	1,48	1,68	1,70
b* D65/10° +UV, ts		1,17	1,61	1,68	1,44	1,63	1,64
b* D65/10° +UV, bs		1,17	1,61	1,67	1,43	1,63	1,65
White top mottle		1,20	1,20	1,18	1,16	1,15	1,07

Mechanical properties

Trial point		**1**	**2**	**3**	**4**	**5**	**6**
	Unit						
Tensile strength, md	kN/m	4,57	4,72	4,67	4,05	4,11	4,52
Tensile strength, cd	kN/m	2,41	2,50	2,47	2,25	2,26	2,54
Stretch, md	%	1,8	1,8	1,9	1,8	1,8	1,9
Stretch, cd	%	5,1	5,1	5,3	5,2	5,2	5,7
Tensile index, md	Nm/g	70,4	70,7	70,1	61,6	64,0	70,0
Tensile index, cd	Nm/g	37,2	37,4	37,1	34,2	35,2	39,3
Tensile stiffness, md	kN/m	582,0	564,0	628,0	557,0	545,0	552,0
Tensile stiffness, cd	kN/m	243,7	246,2	233,0	216,0	199,0	230,0
Tensile stiffness index, md	MNm/kg	8,97	8,44	9,43	8,48	8,49	8,54
Tensile stiffness index, cd	MNm/kg	3,75	3,69	3,50	3,29	3,10	3,56
E-modulus, md	MPa	6539	6130	7136	6330	6337	6419
E-modulus, cd	MPa	2738	2676	2648	2455	2314	2674
Tensile energy absorption, md	J/m²	61,2	61,8	63,0	54,3	55,6	63,5
Tensile energy absorption, cd	J/m²	95,0	92,5	100,3	88,7	89,0	111,0
Tensile energy absorption index, md	kJ/kg	0,9	0,9	0,9	0,8	0,9	1,0
Tensile energy absorption index, cd	kJ/kg	1,5	1,4	1,5	1,4	1,4	1,7
Tear strength, md	mN	484	535	514	483	479	512
Tear strength, cd	mN	451	507	501	478	462	474
Tear index, md	mNm²/g	7,5	8,0	7,7	7,4	7,5	7,9
Tear index, cd	mNm²/g	7,0	7,6	7,5	7,3	7,2	7,3
Bursting strength	kPa	189	205	199	173	191	212
Burst index	kPam²/g	2,91	3,07	2,99	2,63	2,98	3,28

Measured ash content

Trial point	P1	P2	P3	P4	P5	P6
%	5,49 %	5,02 %	5,20 %	7,35 %	7,75 %	7,09 %

APPENDIX 5. Trial 3 Paperlab results

Optical properties

Trial point		**1**	**2**	**3**	**4**	**5**	**6**	**7**	**8**
	Unit								
Grammage	g/m²	65,7	64,8	63,6	64,4	65,1	65,0	64,3	64,9
Thickness	µm	85	87	85	86	88	86	87	85
Density	kg/m³	773	745	748	749	740	756	739	764
Bulk	cm³/g	1,29	1,34	1,34	1,34	1,35	1,32	1,35	1,31
Air resistance Gurley	s/100 ml	14	13	12	11	12	13	13	18
Bendtsen-roughness, ts	ml/min	170	253	238	221	252	261	255	257
Bendtsen-roughness, bs	ml/min	200	285	275	275	272	299	294	284
PPS 0.5, ts	µm	5,71	5,89	5,87	5,86	5,83	5,90	5,95	5,94
PPS 0.5, bs	µm	5,96	6,12	6,14	6,15	6,13	6,15	6,18	6,15
PPS 1.0, ts	µm	5,35	5,59	5,55	5,54	5,51	5,60	5,63	5,63
PPS 1.0, bs	µm	5,68	5,90	5,89	5,90	5,88	5,91	5,92	5,92
PPS 2.0, ts	µm	4,96	5,24	5,20	5,19	5,16	5,28	5,28	5,29
PPS 2.0, bs	µm	4,89	5,12	5,11	5,13	5,09	5,13	5,15	5,15
Gloss, ts	%	6,6	6,9	6,3	6,1	6,2	6,2	6,3	6,7
Gloss, bs	%	6,7	7,0	6,4	6,2	6,4	6,4	6,4	7,1
Brightness D65/10° +UV, ts	%	84,2	80,0	80,7	81,2	81,7	80,9	81,7	80,4
Brightness D65/10° +UV, bs	%	85,2	80,5	81,4	81,9	82,5	81,6	82,4	80,9
Brightness C/2° +UV, ts	%	84,8	80,5	81,3	81,8	82,3	81,4	82,2	80,9
Brightness C/2° +UV, bs	%	84,9	80,5	81,3	81,8	82,4	81,5	82,3	80,9
Brightness C/2° -UV, ts	%	84,2	79,8	80,6	81,2	81,5	80,6	81,4	80,1
Brightness C/2° -UV, bs	%	84,3	80,4	81,1	81,5	82,0	81,3	81,9	80,7
CIE-whiteness C/2° +UV, ts	%	71,3	59,8	61,8	62,8	64,2	62,0	64,4	61,6
CIE-whiteness C/2° +UV, bs	%	68,0	59,8	61,2	62,0	62,7	61,2	62,9	60,8
CIE-whiteness D65/10° -UV, ts	%	70,5	60,4	62,4	63,4	64,3	62,1	64,3	61,7
CIE-whiteness D65/10° -UV, bs	%	71,6	61,7	63,4	64,3	65,3	63,2	65,3	62,7
CIE-whiteness C/2° -UV, ts	%	70,2	59,9	61,9	62,9	63,8	61,6	63,9	61,2
CIE-whiteness C/2° -UV, bs	%	71,0	61,2	62,9	63,8	64,7	62,7	64,8	62,2
CIE-whiteness D65/10° +UV, ts	%	68,1	58,6	59,9	60,5	62,2	60,5	62,5	60,6
CIE-whiteness D65/10° +UV, bs	%	71,1	62,4	63,9	64,5	65,2	63,6	65,6	63,7
Opacity C/2° +UV, ts	%	79,7	77,4	78,2	80,2	81,3	79,7	80,8	76,7
Opacity C/2° +UV, bs	%	79,6	76,9	78,1	80,0	81,4	79,5	80,7	76,7
Light absorption coefficient +UV, ts	m²/kg	0,24	0,31	0,30	0,31	0,31	0,31	0,32	0,30
Light absorption coefficient +UV, bs	m²/kg	0,22	0,29	0,29	0,29	0,29	0,28	0,29	0,28
Light scattering coefficient +UV, ts	m²/kg	39,66	33,94	36,14	39,67	41,55	37,98	40,89	32,67
Light scattering coefficient +UVt, bs	m²/kg	40,24	33,49	36,52	39,69	42,56	38,44	41,41	33,11

Trial point		1	2	3	4	5	6	7	8
	Unit								
L* D65/10° +UV, ts		95,69	94,79	94,97	95,14	95,20	95,03	95,13	94,75
L* D65/10° +UV, bs		95,97	95,06	95,25	95,38	95,55	95,38	95,47	95,09
a* D65/10° +UV, ts		-0,33	-0,24	-0,28	-0,25	-0,23	-0,19	-0,20	-0,23
a* D65/10° +UV, bs		-0,54	-0,47	-0,47	-0,43	-0,40	-0,40	-0,39	-0,45
b* D65/10° +UV, ts		3,74	5,79	5,49	5,41	5,01	5,37	4,91	5,28
b* D65/10° +UV, bs		3,89	5,69	5,40	5,27	5,16	5,49	5,04	5,40
L* C/2° +UV, ts		95,65	94,74	94,93	95,11	95,16	94,99	95,09	94,69
L* C/2° +UV, bs		96,15	95,19	95,39	95,53	95,72	95,53	95,63	95,21
a* C/2° +UV, ts		-0,78	-0,90	-0,89	-0,84	-0,83	-0,85	-0,80	-0,87
a* C/2° +UV, bs		-0,96	-1,07	-1,04	-0,99	-0,96	-0,99	-0,95	-1,04
b* C/2° +UV, ts		3,97	6,00	5,67	5,56	5,26	5,66	5,18	5,57
b* C/2° +UV, bs		4,01	5,75	5,46	5,35	5,25	5,58	5,15	5,49
Dominant wavelength C/2° +UV, ts	nm	683,34	683,91	683,81	683,89	683,83	683,92	683,87	683,82
Dominant wavelength C/2° +UV, bs	nm	674,19	674,70	674,66	674,75	674,81	674,84	674,80	674,69
Spectral purity C/2° +UV, ts	%	5,29	7,74	7,33	7,20	6,85	7,32	6,75	7,23
Spectral purity C/2° +UV, bs	%	5,00	7,25	6,88	6,73	6,60	7,03	6,48	6,93

Optical properties against a brown background

Trial point		1	2	3	4	5	6	7	8
Brightness R457 C/2° +UV, ts	%	72,7	67,7	69,1	70,7	72,4	70,4	71,8	67,3
Brightness R457 C/2° +UV, bs	%	72,7	67,9	69,2	70,8	72,5	70,5	71,9	67,7
Brightness R457 D65/10° +UV, ts	%	72,8	67,7	69,1	70,7	72,5	70,5	71,8	67,4
Brightness R457 D65/10° +UV, bs	%	72,8	68,0	69,3	70,9	72,6	70,6	71,9	67,7
CIE whiteness C/2° +UV, ts	%	67,23	57,08	59,46	61,73	63,98	60,95	63,66	56,88
CIE whiteness C/2° +UV, bs	%	67,25	57,45	59,69	61,90	64,08	61,11	63,80	57,31
CIE whiteness D65/10° +UV, ts	%	67,3	57,5	59,8	62,0	64,2	61,2	63,8	57,3
CIE whiteness D65/10° +UV, bs	%	67,4	57,8	60,0	62,1	64,3	61,3	63,9	57,7
L* C/2° +UV, ts		89,14	87,36	87,93	88,66	89,44	88,58	89,08	87,17
L* C/2° +UV, bs		89,13	87,48	88,01	88,71	89,46	88,65	89,11	87,36
L* D65/10° +UV, ts		89,10	87,29	87,87	88,60	89,38	88,52	89,03	87,10
L* D65/10° +UV, bs		89,09	87,41	87,94	88,65	89,41	88,58	89,06	87,28
a* C/2° +UV, ts		0,24	0,34	0,28	0,15	0,04	0,14	0,08	0,38
a* C/2° +UV, bs		0,25	0,33	0,27	0,15	0,04	0,14	0,08	0,35
a* D65/10° +UV, ts		0,32	0,55	0,47	0,34	0,22	0,34	0,25	0,59
a* D65/10° +UV, bs		0,33	0,54	0,46	0,34	0,22	0,33	0,24	0,56
b* C/2° +UV, ts		1,49	2,76	2,53	2,40	2,29	2,52	2,19	2,72
b* C/2° +UV, bs		1,48	2,74	2,52	2,38	2,28	2,52	2,18	2,71
b* D65/10° +UV, ts		1,48	2,70	2,49	2,36	2,27	2,48	2,18	2,66
b* D65/10° +UV, bs		1,47	2,68	2,47	2,35	2,25	2,49	2,16	2,65
White top mottle		1,056	1,252	1,214	1,122	1,135	1,129	1,065	1,271

Mechanical properties

Trial point		1	2	3	4	5	6	7	8
	Unit								
Tensile strength, md	kN/m	4,13	4,46	4,03	3,76	3,33	3,88	3,86	4,57
Tensile strength, cd	kN/m	2,33	2,59	2,30	2,12	2,13	2,41	2,22	2,84
Stretch, md	%	2,0	2,0	1,9	1,9	1,7	1,9	1,8	2,1
Stretch, cd	%	5,7	5,6	5,5	5,2	5,4	5,8	5,3	6,1
Tensile index, md	Nm/g	62,9	68,8	63,4	58,4	51,1	59,7	60,0	70,5
Tensile index, cd	Nm/g	35,5	40,0	36,2	32,9	32,7	37,1	34,5	43,8
Tensile stiffness, md	kN/m	527,0	522,0	511,0	513,0	511,0	530,0	539,0	525,0
Tensile stiffness, cd	kN/m	220,0	206,0	222,0	216,0	237,0	220,0	240,0	248,0
Tensile stiffness index, md	MNm/kg	8,02	8,06	8,03	7,97	7,85	8,15	8,38	8,09
Tensile stiffness index, cd	MNm/kg	3,35	3,18	3,49	3,35	3,64	3,38	3,73	3,82
E-modulus, md	MPa	6200	6000	6012	5965	5807	6163	6195	6176
E-modulus, cd	MPa	2588	2368	2612	2512	2693	2558	2759	2918
Tensile energy absorption, md	J/m²	61,8	65,9	60,3	55,5	47,5	56,0	53,9	69,4
Tensile energy absorption, cd	J/m²	99,8	106,3	95,9	84,3	89,4	104,3	89,1	126,1
Tensile energy absorption index, md	kJ/kg	0,9	1,0	0,9	0,9	0,7	0,9	0,8	1,1
Tensile energy absorption index, cd	kJ/kg	1,5	1,6	1,5	1,3	1,4	1,6	1,4	1,9
Tear strength, md	mN	498	521	492	475	481	507	482	539
Tear strength, cd	mN	477	501	463	448	455	445	445	530
Tear index, md	mNm²/g	7,6	8,0	7,7	7,4	7,4	7,8	7,5	8,3
Tear index, cd	mNm²/g	7,3	7,7	7,3	7,0	7,0	6,8	6,9	8,2
Bursting strength	kPa	194	219	193	180	174	202	182	227
Burst index	kPam²/g	2,95	3,38	3,03	2,80	2,67	3,11	2,83	3,50

Measured ash content

Trial point	P1	P2	P3	P4	P5	P6	P7	P8
%	5,90	3,07	5,01	6,47	8,00	6,84	6,63	2,74

APPENDIX 6. Trial 4 Paperlab results

Optical properties

Trial point		**1**	**2**	**3**	**4**	**5**	**6**	**7**
	Unit							
Grammage	g/m²	64,1	65,3	65,6	65,1	67,8	65,6	65,0
Thickness	µm	87	87	87	86	88	89	88
Density	kg/m³	737	751	754	757	770	737	739
Bulk	cm³/g	1,36	1,33	1,33	1,32	1,30	1,36	1,35
Air resistance Gurley	s/100 ml	11	12	10	10	11	12	10
Bendtsen-roughness, ts	ml/min	212	206	207	189	818	220	221
Bendtsen-roughness, bs	ml/min	239	224	222	209	258	254	263
PPS 0.5, ts	µm	5,75	5,84	5,78	5,77	5,88	5,91	5,86
PPS 0.5, bs	µm	6,05	6,11	6,09	5,97	6,13	6,14	6,12
PPS 1.0, ts	µm	5,39	5,50	5,42	5,41	5,55	5,57	5,51
PPS 1.0, bs	µm	5,75	5,85	5,80	5,66	5,88	5,87	5,85
PPS 2.0, ts	µm	5,00	5,13	5,04	5,03	5,19	5,21	5,14
PPS 2.0, bs	µm	4,94	5,06	5,00	4,87	5,11	5,07	5,07
Gloss, ts	%	6,3	6,2	6,1	6,2	5,9	5,9	6,2
Gloss, bs	%	6,7	6,5	6,2	6,6	6,1	6,1	6,4
Brightness D65/10° +UV, ts	%	84,0	80,4	81,3	81,2	80,8	81,3	81,1
Brightness D65/10° +UV, bs	%	84,8	80,9	81,8	81,8	81,6	82,0	81,6
Brightness C/2° +UV, ts	%	84,6	80,9	81,8	81,7	81,2	81,8	81,6
Brightness C/2° +UV, bs	%	84,7	80,9	81,8	81,6	81,5	81,9	81,5
Brightness C/2° -UV, ts	%	84,0	80,2	81,1	80,9	80,4	81,0	80,8
Brightness C/2° -UV, bs	%	84,1	80,8	81,5	81,4	81,2	81,6	81,2
CIE-whiteness C/2° +UV, ts	%	70,7	61,1	63,1	63,0	61,9	63,4	62,7
CIE-whiteness C/2° +UV, bs	%	67,4	60,2	61,7	61,9	61,7	62,1	61,6
CIE-whiteness D65/10° -UV, ts	%	70,1	61,6	63,3	63,0	62,2	63,3	62,6
CIE-whiteness D65/10° -UV, bs	%	71,4	62,6	64,3	64,0	63,7	64,5	63,7
CIE-whiteness C/2° -UV, ts	%	69,8	61,0	62,8	62,5	61,6	62,7	62,0
CIE-whiteness C/2° -UV, bs	%	70,8	62,0	63,8	63,4	63,2	64,0	63,1
CIE-whiteness D65/10° +UV, ts	%	67,4	59,7	61,2	61,5	60,6	61,8	61,4
CIE-whiteness D65/10° +UV, bs	%	70,5	62,7	64,3	64,6	64,3	64,7	64,2
Opacity C/2° +UV, ts	%	80,2	81,9	81,7	81,2	81,2	81,5	81,8
Opacity C/2° +UV, bs	%	80,0	81,8	81,2	81,2	81,4	81,3	81,3
Light absorption coefficient +UV, ts	m²/kg	0,25	0,37	0,33	0,33	0,33	0,33	0,34
Light absorption coefficient +UV, bs	m²/kg	0,24	0,34	0,30	0,31	0,31	0,30	0,32
Light scattering coefficient +UV, ts	m²/kg	41,54	41,51	41,58	40,69	38,85	41,08	42,00
Light scattering coefficient +UVt, bs	m²/kg	41,56	41,85	41,13	41,35	39,80	41,43	41,51

Trial point		1	2	3	4	5	6	7
	Unit							
L* D65/10° +UV, ts		95,65	94,86	95,11	95,04	94,93	95,05	95,03
L* D65/10° +UV, bs		95,87	95,19	95,38	95,33	95,28	95,40	95,29
a* D65/10° +UV, ts		-0,39	-0,20	-0,22	-0,21	-0,22	-0,18	-0,13
a* D65/10° +UV, bs		-0,60	-0,39	-0,41	-0,40	-0,42	-0,42	-0,37
b* D65/10° +UV, ts		3,88	5,53	5,22	5,14	5,34	5,05	5,15
b* D65/10° +UV, bs		3,99	5,65	5,34	5,25	5,29	5,24	5,32
L* C/2° +UV, ts		95,61	94,81	95,06	94,99	94,87	95,01	94,98
L* C/2° +UV, bs		96,04	95,33	95,52	95,47	95,41	95,55	95,43
a* C/2° +UV, ts		-0,85	-0,83	-0,81	-0,81	-0,84	-0,81	-0,79
a* C/2° +UV, bs		-0,99	-0,96	-0,96	-0,97	-0,99	-0,97	-0,95
b* C/2° +UV, ts		4,09	5,76	5,46	5,43	5,60	5,36	5,50
b* C/2° +UV, bs		4,05	5,67	5,37	5,36	5,39	5,31	5,42
Dominant wavelength C/2° +UV, ts	nm	683,18	683,98	683,93	683,94	683,92	683,91	684,01
Dominant wavelength C/2° +UV, bs	nm	674,09	674,95	674,86	674,81	674,79	674,79	674,89
Spectral purity C/2° +UV, ts	%	5,41	7,46	7,09	7,06	7,26	6,98	7,14
Spectral purity C/2° +UV, bs	%	5,05	7,17	6,77	6,76	6,79	6,69	6,84

Optical properties against a brown background

Trial point		1	2	3	4	5	6	7
Brightness R457 C/2° +UV, ts	%	72,7	72,2	71,9	71,9	71,4	71,5	71,9
Brightness R457 C/2° +UV, bs	%	72,8	72,0	71,9	71,8	71,8	71,7	71,6
Brightness R457 D65/10° +UV, ts	%	72,7	72,2	71,9	71,9	71,5	71,6	72,0
Brightness R457 D65/10° +UV, bs	%	72,8	72,1	72,0	71,9	71,9	71,7	71,6
CIE whiteness C/2° +UV, ts	%	67,07	63,08	63,00	63,36	62,47	62,72	62,86
CIE whiteness C/2° +UV, bs	%	67,12	63,11	63,08	63,52	62,94	62,97	62,62
CIE whiteness D65/10° +UV, ts	%	67,2	63,3	63,2	63,6	62,7	62,9	63,1
CIE whiteness D65/10° +UV, bs	%	67,3	63,3	63,3	63,7	63,2	63,2	62,9
L* C/2° +UV, ts		89,14	89,40	89,24	89,16	89,02	89,05	89,27
L* C/2° +UV, bs		89,17	89,30	89,23	89,10	89,20	89,11	89,08
L* D65/10° +UV, ts		89,10	89,34	89,18	89,11	88,96	88,99	89,21
L* D65/10° +UV, bs		89,13	89,24	89,17	89,05	89,15	89,05	89,02
a* C/2° +UV, ts		0,20	-0,05	0,03	0,03	0,06	0,07	0,01
a* C/2° +UV, bs		0,20	-0,01	0,04	0,05	0,04	0,07	0,06
a* D65/10° +UV, ts		0,30	0,15	0,22	0,21	0,25	0,25	0,21
a* D65/10° +UV, bs		0,30	0,17	0,23	0,22	0,23	0,25	0,25
b* C/2° +UV, ts		1,52	2,46	2,40	2,29	2,41	2,37	2,44
b* C/2° +UV, bs		1,52	2,41	2,38	2,23	2,40	2,35	2,41
b* D65/10° +UV, ts		1,51	2,43	2,38	2,26	2,37	2,34	2,40
b* D65/10° +UV, bs		1,50	2,38	2,35	2,20	2,37	2,32	2,37
White top mottle		1,026	1,039	1,071	1,042	1,049	1,028	1,083

Mechanical properties

Trial point		1	2	3	4	5	6	7
	Unit							
Tensile strength, md	kN/m	3,89	3,61	3,61	3,44	3,67	3,83	3,76
Tensile strength, cd	kN/m	2,33	2,09	2,04	1,94	1,91	2,10	2,22
Stretch, md	%	1,8	1,7	1,8	1,8	1,8	1,8	1,8
Stretch, cd	%	5,5	5,1	5,2	5,0	4,5	4,7	5,3
Tensile index, md	Nm/g	60,7	55,3	55,0	52,8	54,1	58,4	57,8
Tensile index, cd	Nm/g	36,3	32,0	31,1	29,8	28,2	32,0	34,2
Tensile stiffness, md	kN/m	366,0	497,0	396,0	478,0	439,0	513,0	424,0
Tensile stiffness, cd	kN/m	155,0	178,0	191,0	208,0	182,0	215,0	176,0
Tensile stiffness index, md	MNm/kg	5,71	7,61	6,04	7,34	6,47	7,82	6,52
Tensile stiffness index, cd	MNm/kg	2,42	2,73	2,91	3,20	2,68	3,28	2,71
E-modulus, md	MPa	4207	5713	4552	5558	4989	5764	4818
E-modulus, cd	MPa	1782	2046	2195	2419	2068	2416	2000
Tensile energy absorption, md	J/m²	54,4	49,0	49,4	50,1	51,0	53,4	51,1
Tensile energy absorption, cd	J/m²	92,5	79,9	78,7	73,8	67,3	73,6	86,4
Tensile energy absorption index, md	kJ/kg	0,8	0,8	0,8	0,8	0,8	0,8	0,8
Tensile energy absorption index, cd	kJ/kg	1,4	1,2	1,2	1,1	1,0	1,1	1,3
Tear strength, md	mN	476	473	473	460	482	487	476
Tear strength, cd	mN	439	494	443	433	485	504	485
Tear index, md	mNm²/g	7,4	7,2	7,2	7,1	7,1	7,4	7,3
Tear index, cd	mNm²/g	6,9	7,6	6,8	6,7	7,2	7,7	7,5
Bursting strength	kPa	186	157	162	159	172	169	171
Burst index	kPam²/g	2,90	2,40	2,47	2,44	2,54	2,58	2,63

Measured ash content

Trial point	P1	P2	P3	P4	P5	P6	P7
%	5,87	6,89	6,85	6,80	6,28	6,37	6,60

APPENDIX 7. Trial 5 Paperlab results

Optical properties

Trial point		**1**	**2**	**3**	**4**	**5**	**6**	**7**
	Unit							
Grammage	g/m²	63,2	65,2	64,7	67,5	65,7	64,7	66,4
Thickness	µm	85	86	85	88	82	85	87
Density	kg/m³	744	758	761	767	801	761	763
Bulk	cm³/g	1,34	1,32	1,31	1,30	1,25	1,31	1,31
Air resistance Gurley	s/100 ml	10	12	11	10	20	15	15
Bendtsen-roughness, ts	ml/min	193	188	175	200	192	197	194
Bendtsen-roughness, bs	ml/min	223	203	192	196	205	205	236
PPS 0.5, ts	µm	5,75	5,72	5,69	5,62	5,77	5,70	5,78
PPS 0.5, bs	µm	6,03	5,96	5,90	5,90	6,06	5,97	6,02
PPS 1.0, ts	µm	5,42	5,40	5,36	5,25	5,45	5,37	5,45
PPS 1.0, bs	µm	5,75	5,68	5,58	5,59	5,82	5,70	5,76
PPS 2.0, ts	µm	5,04	5,04	4,99	4,88	5,12	5,02	5,10
PPS 2.0, bs	µm	4,98	4,94	4,83	4,83	5,10	4,97	5,01
Gloss, ts	%	6,6	6,9	7,0	6,7	6,3	6,9	6,8
Gloss, bs	%	6,7	7,2	7,1	6,3	6,2	7,0	6,9
Brightness D65/10° +UV, ts	%	83,4	80,6	80,5	81,1	80,3	80,5	81,0
Brightness D65/10° +UV, bs	%	84,5	81,4	81,1	81,9	81,1	81,2	81,7
Brightness C/2° +UV, ts	%	84,0	81,1	81,0	81,6	80,9	81,0	81,6
Brightness C/2° +UV, bs	%	84,2	81,3	81,0	81,8	81,0	81,1	81,6
Brightness C/2° -UV, ts	%	83,4	80,3	80,2	80,8	80,2	80,3	80,8
Brightness C/2° -UV, bs	%	83,6	81,0	80,7	81,5	80,8	80,8	81,2
CIE-whiteness C/2° +UV, ts	%	70,9	62,6	62,1	63,2	63,2	61,6	63,9
CIE-whiteness C/2° +UV, bs	%	68,2	62,2	61,6	62,4	62,7	61,2	63,0
CIE-whiteness D65/10° -UV, ts	%	70,1	62,8	62,3	63,4	63,7	62,2	64,1
CIE-whiteness D65/10° -UV, bs	%	71,1	63,9	63,2	64,6	64,3	62,7	64,7
CIE-whiteness C/2° -UV, ts	%	69,9	62,3	61,7	62,8	63,2	61,7	63,7
CIE-whiteness C/2° -UV, bs	%	70,6	63,4	62,7	64,0	63,8	62,2	64,2
CIE-whiteness D65/10° +UV, ts	%	68,2	61,4	61,0	61,6	61,9	60,0	62,3
CIE-whiteness D65/10° +UV, bs	%	72,1	65,4	64,7	65,2	66,3	64,0	66,3
Opacity C/2° +UV, ts	%	80,3	80,2	80,5	81,8	78,1	79,4	79,3
Opacity C/2° +UV, bs	%	80,1	79,7	80,5	81,8	78,0	79,1	78,9
Light absorption coefficient +UV, ts	m²/kg	0,30	0,36	0,36	0,34	0,35	0,33	0,33
Light absorption coefficient +UV, bs	m²/kg	0,28	0,32	0,34	0,31	0,32	0,31	0,30
Light scattering coefficient +UV, ts	m²/kg	41,08	37,95	38,62	40,12	33,69	37,05	35,97
Light scattering coefficient +UVt, bs	m²/kg	41,11	37,66	39,29	40,91	34,04	37,24	35,76

Trial point		1	2	3	4	5	6	7
	Unit							
L* D65/10° +UV, ts		95,30	94,74	94,73	94,97	94,52	94,84	94,82
L* D65/10° +UV, bs		95,57	95,08	95,04	95,30	94,87	95,17	95,11
a* D65/10° +UV, ts		-0,42	-0,31	-0,27	-0,26	-0,32	-0,31	-0,41
a* D65/10° +UV, bs		-0,57	-0,42	-0,40	-0,39	-0,37	-0,37	-0,46
b* D65/10° +UV, ts		3,60	5,08	5,18	5,10	4,90	5,43	4,90
b* D65/10° +UV, bs		3,54	4,99	5,14	5,08	4,71	5,35	4,77
L* C/2° +UV, ts		95,22	94,66	94,66	94,91	94,43	94,78	94,75
L* C/2° +UV, bs		95,69	95,19	95,15	95,44	94,95	95,30	95,22
a* C/2° +UV, ts		-0,86	-0,89	-0,87	-0,85	-0,85	-0,89	-0,92
a* C/2° +UV, bs		-1,00	-0,99	-0,99	-0,96	-0,93	-0,98	-1,01
b* C/2° +UV, ts		3,81	5,32	5,44	5,34	5,06	5,61	5,08
b* C/2° +UV, bs		3,76	5,15	5,29	5,20	4,90	5,50	4,95
Dominant wavelength C/2° +UV, ts	nm	682,98	683,68	683,78	683,80	683,69	683,80	683,51
Dominant wavelength C/2° +UV, bs	nm	673,83	674,67	674,75	674,79	674,74	674,84	674,53
Spectral purity C/2° +UV, ts	%	5,10	6,93	7,07	6,95	6,64	7,27	6,63
Spectral purity C/2° +UV, bs	%	4,69	6,50	6,69	6,56	6,21	6,94	6,24

Optical properties against a brown background

Trial point		1	2	3	4	5	6	7
Brightness R457 C/2° +UV, ts	%	72,7	70,0	70,5	71,9	68,7	69,6	69,6
Brightness R457 C/2° +UV, bs	%	72,7	70,0	70,5	71,8	68,5	69,6	69,9
Brightness R457 D65/10° +UV, ts	%	72,7	70,1	70,5	72,0	68,8	69,7	69,6
Brightness R457 D65/10° +UV, bs	%	72,7	70,1	70,6	71,9	68,6	69,6	70,0
CIE whiteness C/2° +UV, ts	%	67,06	60,69	60,96	63,05	59,50	59,62	60,77
CIE whiteness C/2° +UV, bs	%	67,13	60,79	61,05	62,96	59,29	59,59	61,16
CIE whiteness D65/10° +UV, ts	%	67,2	61,1	61,3	63,4	59,9	60,0	61,1
CIE whiteness D65/10° +UV, bs	%	67,3	61,2	61,4	63,3	59,7	60,0	61,5
L* C/2° +UV, ts		89,11	88,36	88,62	89,25	87,68	88,25	88,08
L* C/2° +UV, bs		89,13	88,38	88,66	89,21	87,61	88,24	88,25
L* D65/10° +UV, ts		89,07	88,29	88,56	89,20	87,62	88,18	88,01
L* D65/10° +UV, bs		89,09	88,32	88,60	89,15	87,55	88,17	88,20
a* C/2° +UV, ts		0,21	0,20	0,12	0,03	0,34	0,20	0,27
a* C/2° +UV, bs		0,20	0,20	0,13	0,05	0,36	0,20	0,23
a* D65/10° +UV, ts		0,31	0,40	0,34	0,23	0,54	0,42	0,45
a* D65/10° +UV, bs		0,31	0,40	0,34	0,25	0,56	0,43	0,42
b* C/2° +UV, ts		1,51	2,47	2,54	2,40	2,41	2,64	2,33
b* C/2° +UV, bs		1,50	2,46	2,54	2,39	2,42	2,64	2,33
b* D65/10° +UV, ts		1,49	2,41	2,48	2,35	2,34	2,57	2,27
b* D65/10° +UV, bs		1,48	2,40	2,48	2,35	2,35	2,58	2,27
White top mottle		1,064	1,061	1,064	1,020	0,995	1,090	1,071

Mechanical properties

Trial point		1	2	3	4	5	6	7
	Unit							
Tensile strength, md	kN/m	3,88	4,42	4,22	4,03	4,94	4,79	4,78
Tensile strength, cd	kN/m	2,08	2,26	2,12	2,05	2,43	2,47	2,64
Stretch, md	%	1,9	1,8	1,8	1,7	2,0	2,0	2,1
Stretch, cd	%	5,1	5,8	5,4	5,0	6,8	5,7	5,9
Tensile index, md	Nm/g	61,4	67,8	65,2	59,7	75,2	74,0	72,0
Tensile index, cd	Nm/g	32,9	34,7	32,8	30,4	37,0	38,2	39,8
Tensile stiffness, md	kN/m	440,0	612,0	588,0	580,0	628,0	617,0	563,0
Tensile stiffness, cd	kN/m	202,0	249,0	236,0	226,0	234,0	239,0	256,0
Tensile stiffness index, md	MNm/kg	6,96	9,39	9,09	8,59	9,56	9,54	8,48
Tensile stiffness index, cd	MNm/kg	3,20	3,82	3,65	3,35	3,56	3,69	3,86
E-modulus, md	MPa	5176	7116	6918	6591	7659	7259	6471
E-modulus, cd	MPa	2376	2895	2776	2568	2854	2812	2943
Tensile energy absorption, md	J/m²	56,0	60,4	55,5	51,3	73,8	67,9	73,9
Tensile energy absorption, cd	J/m²	79,8	101,3	88,8	80,4	131,5	107,1	115,8
Tensile energy absorption index, md	kJ/kg	0,9	0,9	0,9	0,8	1,1	1,0	1,1
Tensile energy absorption index, cd	kJ/kg	1,3	1,6	1,4	1,2	2,0	1,7	1,7
Tear strength, md	mN	483	506	501	484	564	512	514
Tear strength, cd	mN	442	474	464	500	525	496	508
Tear index, md	mNm²/g	7,6	7,8	7,7	7,2	8,6	7,9	7,7
Tear index, cd	mNm²/g	7,0	7,3	7,2	7,4	8,0	7,7	7,6
Bursting strength	kPa	189	203	188	179	228	229	234
Burst index	kPam²/g	2,99	3,11	2,91	2,65	3,47	3,54	3,52

Measured ash content

Trial point	P1	P2	P3	P4	P5	P6	P7
%	5,79	5,20	5,60	6,11	5,29	5,41	4,35

APPENDIX 8. XRD measurement report

STUDY REPORT

Subject:	Polymorphy study of $CaCO_3$ filler in paper samples
Method(s):	XRD measurements
No. of samples:	6
Customer:	Stora Enso
Ref:	Matti Väkeväinen
Researcher:	Jorma Roine

Laboratory of Industrial Physics
Department of Physics and Astronomy
University of Turku
FI-20014 TURKU

Measurements:

XRD	6

Objectives

The purpose of the present study was to investigate the polymorphism of calcium carbonate ($CaCO_3$) filler substance in the supplied paper samples (6).

Materials

Six (6) sample paper sheets with following batch numbers:

- P23 KP-2
- P23 KP-3
- P23 KP-4
- P23 KP-5
- P23 KP-6
- P23 KP-7

Abbreviations KP-2, KP-3, etc. will be used throughout the report when referring to the samples. The samples were expected by the supplier to contain approximately 6.5 % of $CaCO_3$ in two different crystal forms – calcite and vaterite. The samples were stored at ambient conditions, away from direct sunlight.

Methods

The Philips X'Pert Pro MPD X-ray powder diffractometer was used in the XRD measurements. The diffractometer was operated in Bragg-Brentano diffraction mode, and the Cu-K_α radiation was generated with a voltage of 40 kV and a current of 50 mA. The primary X-ray beam was collimated with a fixed 1.00° divergence slit and a fixed 20 mm mask. Before entering the proportional counter, the diffracted beam was monochromatized and limited by a 1.00° fixed anti-scatter slit and a programmable receiving slit set at 0.40 mm. In order to determine the instrumental function of the instrument a silicon standard was measured.

The measured 2θ angle range was 5.0° - 55.0°, with a step size of 0.04° and measurement time of 2.0 s per step. Each sample consisted of a stack of 10 parallel paper sheets, with an exposed surface area of 20 x 20 mm^2. The stacks were clamped tightly onto plastic sample holders. The measurements were done during August 21-22, 2012.

The measured diffractograms were analyzed using Philips X'Pert HighScore and MAUD (http://www.ing.unitn.it/~maud/) programs. HighScore was used for peak identification and phase analysis by comparing the peak relative intensities, and MAUD was used for the Rietveld refinement analysis. The PDF-2 and ICSD databases were used as sources of reference [1-2]. The crystal structure references of the $CaCO_3$ polymorphs - calcite (ground $CaCO_3$, GCC), vaterite and aragonite (precipitated $CaCO_3$, PCC) - were taken from the PDF-2 database [3-5], and the corresponding crystal information (.cif) files for the Rietveld refinement analysis were retrieved from the ICSD database [6-8].

Results and discussion

The measured diffractograms are shown in full side by side in Figure 1, and cropped to the diffraction angle area of the observed $CaCO_3$ diffraction peaks in Figure 2. The zoomed diffractograms are shown overlapping in Figure 3. For samples KP-3, KP-4, KP-5, KP-6 and KP-7, $CaCO_3$ diffraction peaks were detected from the calcite and vaterite polymorphs of $CaCO_3$, as expected. For sample KP-2, calcite and aragonite crystal forms were found instead.

Seven diffraction peaks caused by calcite were observed for samples KP-3, KP-5, KP-6 and KP-7, with the following diffraction angles 2θ and Miller indices (*hkl*): 29.4° (104), 36.0° (110), 39.4° (113), 43.2° (202), 47.2° (024), 47.5° (018) and 48.6° (116). For sample KP-2, the (024) peak was too weak to be separable from the adjacent (018) peak, and the (116) peak was overlapped by the (041) and (202) peaks from aragonite. For sample KP-4, due to low calcite content only the (104) peak was observed (see Appendix for peak data).

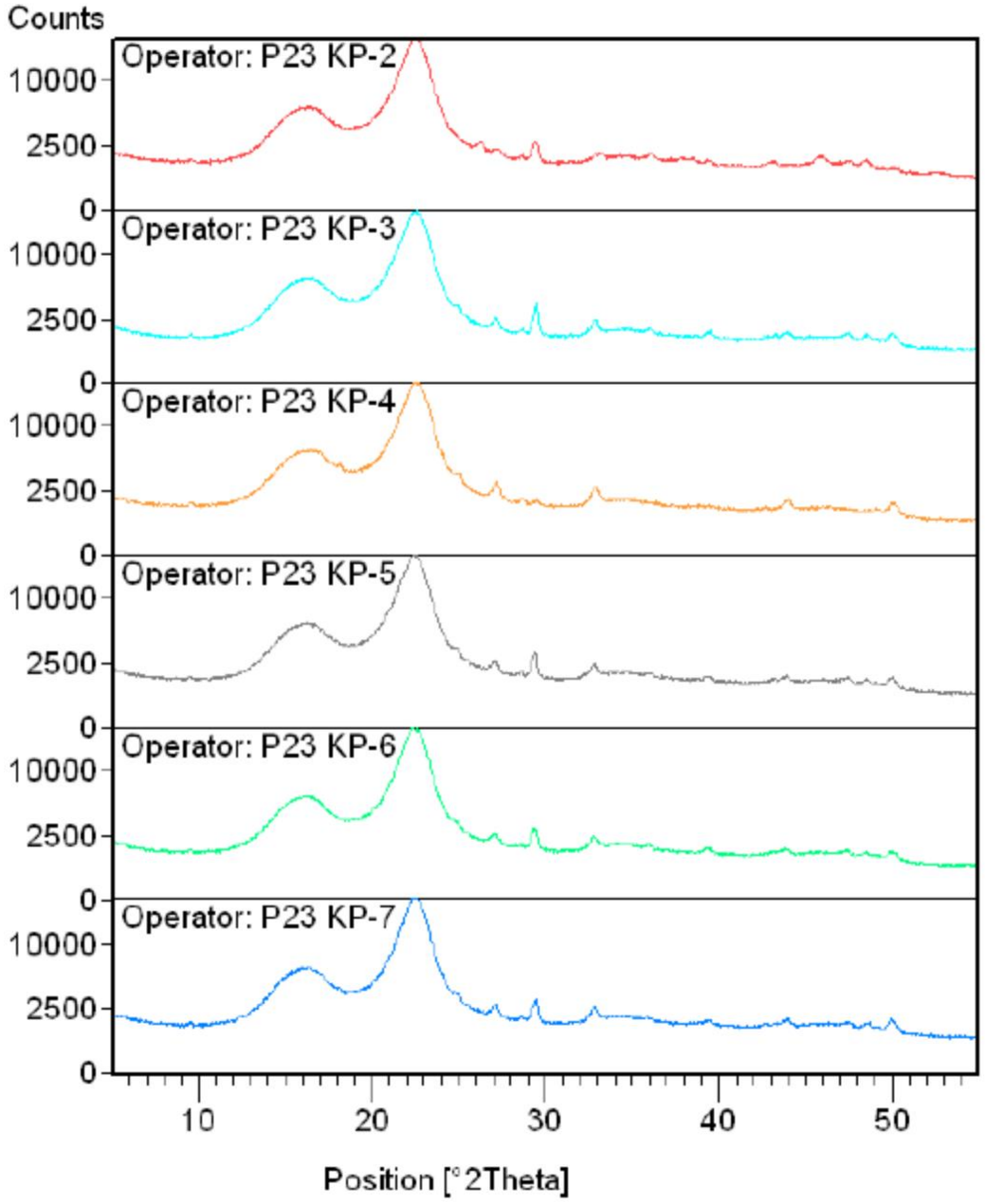

Figure 1. The complete measured diffractograms. The difference in calcite content can be easily seen by observing the difference in the calcite (104) peak intensity at 2θ = 29.4°. The two wide peaks at 2θ = 16.4° and 2θ = 22.5° are caused by the base paper fibers.

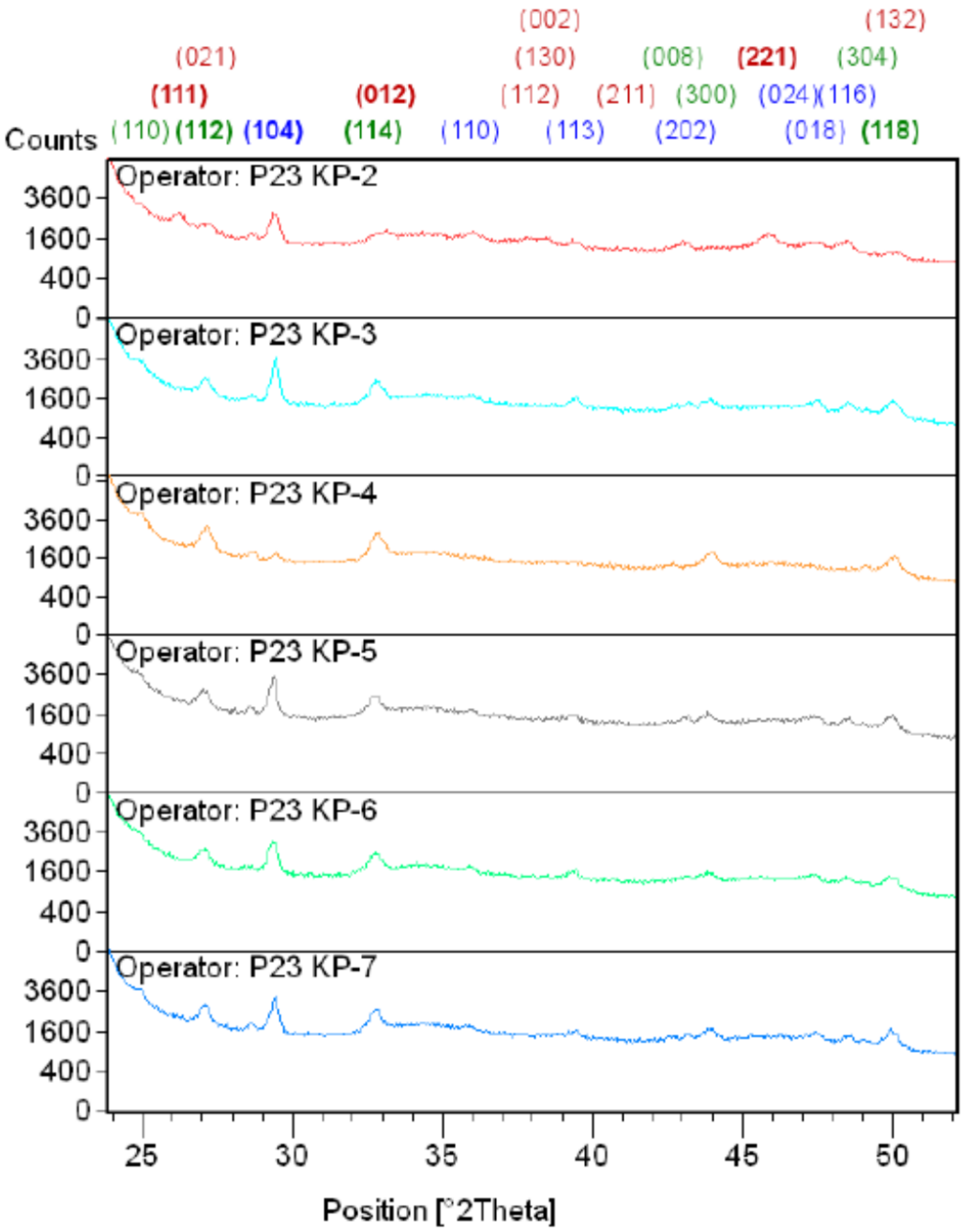

Figure 2. Zoomed portion of the measured diffractograms. The locations and Miller indices (*hkl*) of the detected calcite (blue), vaterite (green) and aragonite (red) diffraction peaks are shown. All the samples contain calcite, while sample KP-2 also contains aragonite and samples KP-3 thru KP-7 contain vaterite.

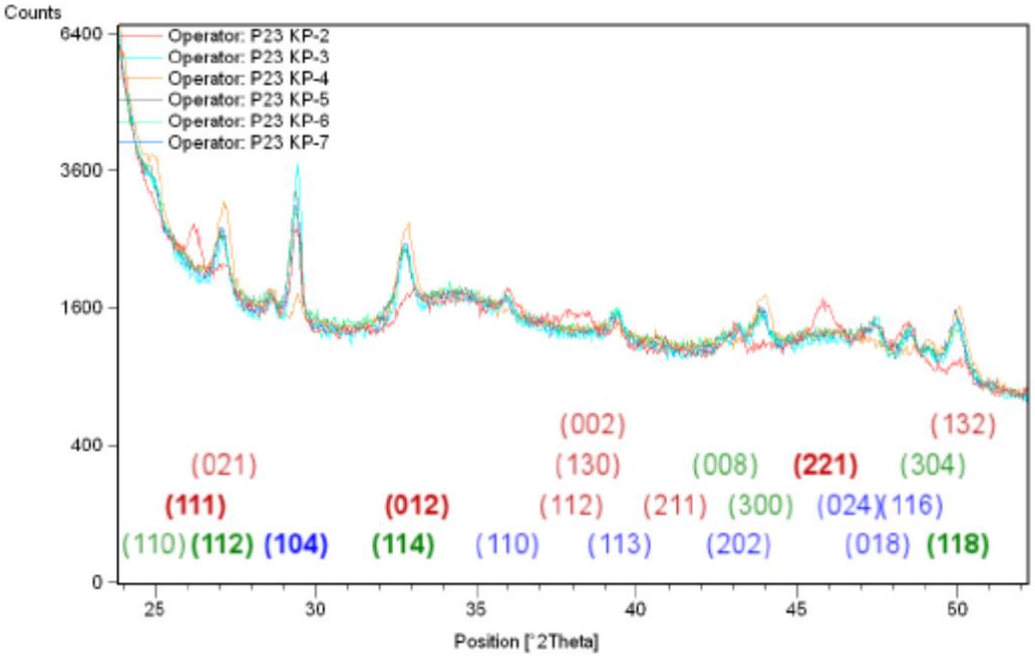

Figure 3. Zoomed portion of the measured diffractograms, overlapped. The locations and Miller indices (*hkl*) of the detected calcite (blue), vaterite (green) and aragonite (red) diffraction peaks are shown. All the samples contain calcite. It can be seen particularly well from the vaterite (300) peak at 43.9° and aragonite (221) peak at 45.9° that sample KP-2 additionally contains aragonite, while the rest of the samples contain vaterite.

Seven diffraction peaks from vaterite were observed for samples KP-3, KP-4, KP-5 and KP-7, with the following diffraction angles 2θ and Miller indices (*hkl*): 24.9° (110), 27.1° (112), 32.8° (114), 42.8° (008), 43.9° (300), 49.1° (304) and 50.1° (118). For sample KP-2, no vaterite was detected. For sample KP-6, the (008) peak was not separable from the adjacent (300) peak due to low intensity (see Appendix for peak data).

For sample KP-2, nine diffraction peaks from the aragonite crystal form of $CaCO_3$ was observed. Seven of the observed peaks were separable as single Miller reflections. No aragonite was detected in any other sample (see Appendix for peak data).

In addition to the $CaCO_3$ diffraction peaks, two very wide and intense diffraction maxima located at $2\theta = 16.4°$ and $2\theta = 22.5°$ stand out in the measured diffractograms. It has been confirmed in earlier XRD measurements of paper that these two peaks are caused by the base paper fibers [9]. Finally, three weak diffraction peaks of unknown origin were detected at $2\theta = 9.5°$, $2\theta = 18.1°$ and $2\theta = 28.6°$.

Generally, the detection limit of this kind of X-ray powder diffraction measurement is limited to roughly 5 percent. The measured intensity of $CaCO_3$ diffraction peaks was low in these measurements due to the very small $CaCO_3$ content of the samples (ca. 6,5 %). But since many peaks were observed, the amount of data was abundant for reliable $CaCO_3$ phase analysis. However, it must be stressed that due to the detection threshold of the used method, it is possible that the samples may contain additional, proportionally very small $CaCO_3$ polymorph phases (a few percent or less) that cannot be detected by the used method. Phase proportions of the detected phases are presented in the results.

The crystalline $CaCO_3$ contents of the samples were analyzed by the peak relative intensity method and Rietveld refinement method. The Rietveld refinement plots for the samples are shown in Figures 4-9. The difference in texture (crystal preferred orientation) between samples was neglected for the purpose of phase analysis. While it is good to bear in mind that difference in texture between samples may have a small effect on the obtained phase content results, the effect is most likely not significant since the results from the two used methods agree well with each other. However, due to the possibility of some texture differences and due to the small $CaCO_3$ contents in the samples, there is naturally some uncertainty in the results.

The sample $CaCO_3$ phase analysis results and error limits are summarized in Table 1, and visualized as a stacked column graph in Figure 10.

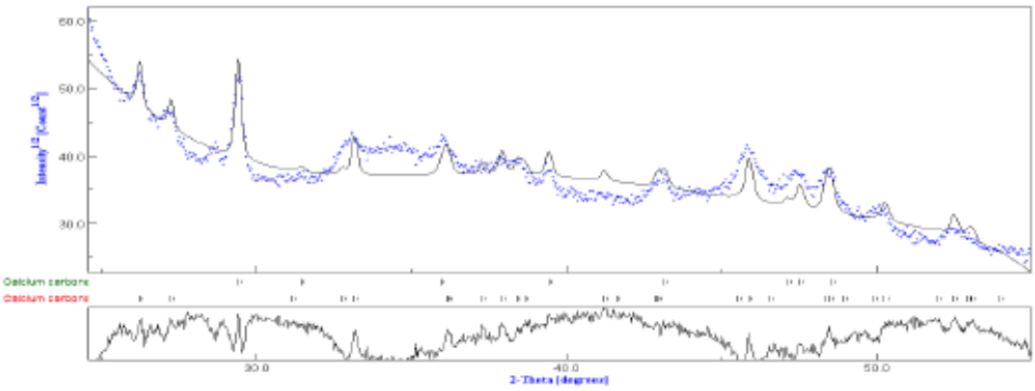

Figure 4. The Rietveld refinement of sample KP-2, with calcite (green) and aragonite (red) peaks shown.

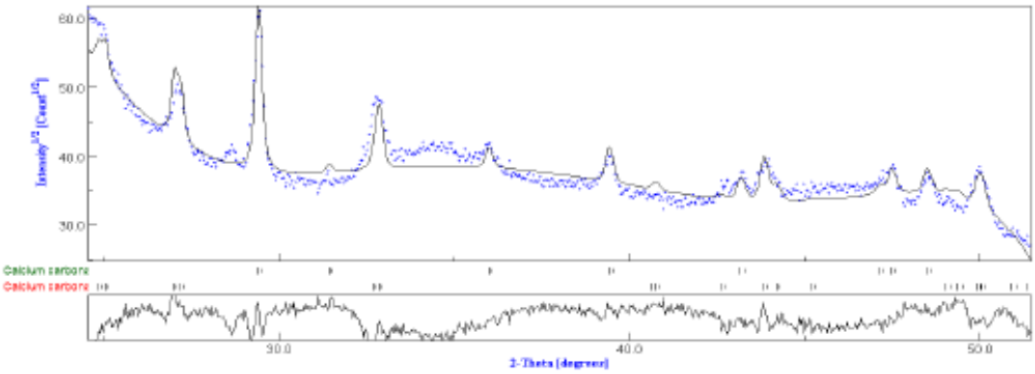

Figure 5. The Rietveld refinement of sample KP-3, with calcite (green) and vaterite (red) peaks shown.

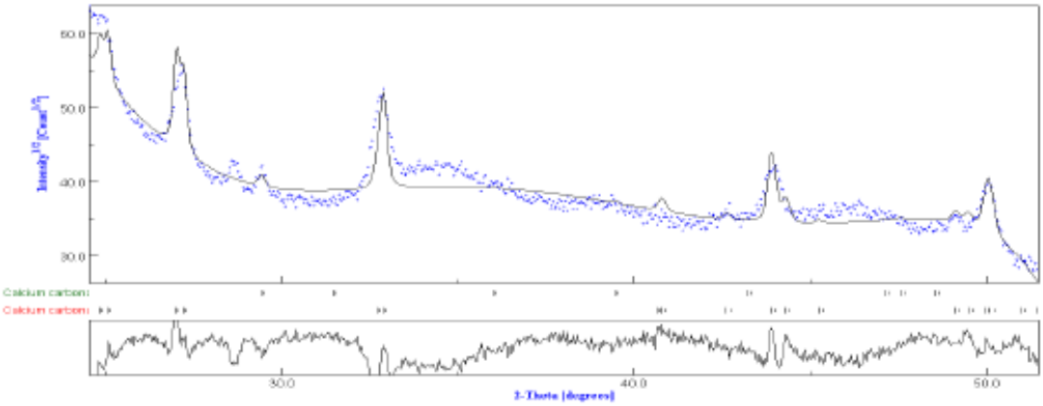

Figure 6. The Rietveld refinement of sample KP-4, with calcite (green) and vaterite (red) peaks shown.

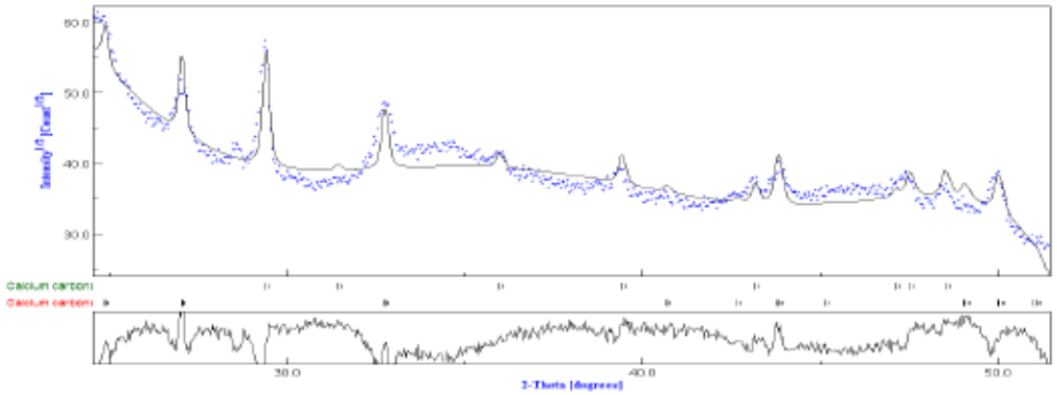

Figure 7. The Rietveld refinement of sample KP-5, with calcite (green) and vaterite (red) peaks shown.

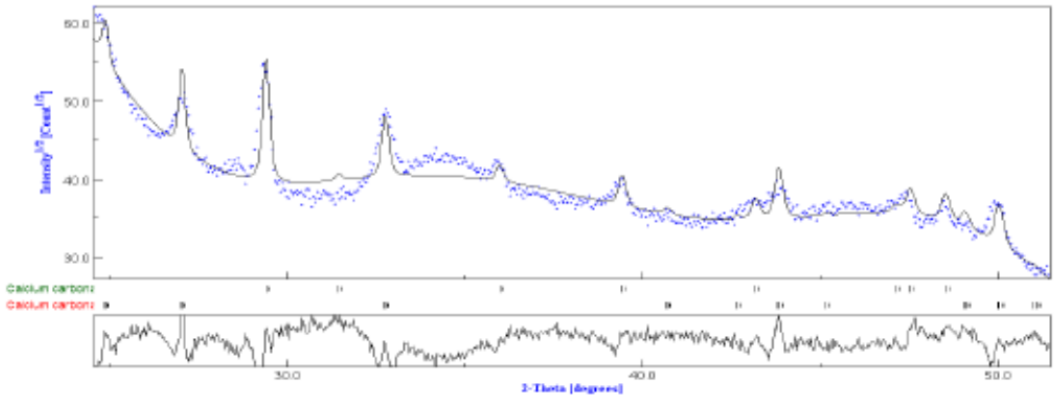

Figure 8. The Rietveld refinement of sample KP-6, with calcite (green) and vaterite (red) peaks shown.

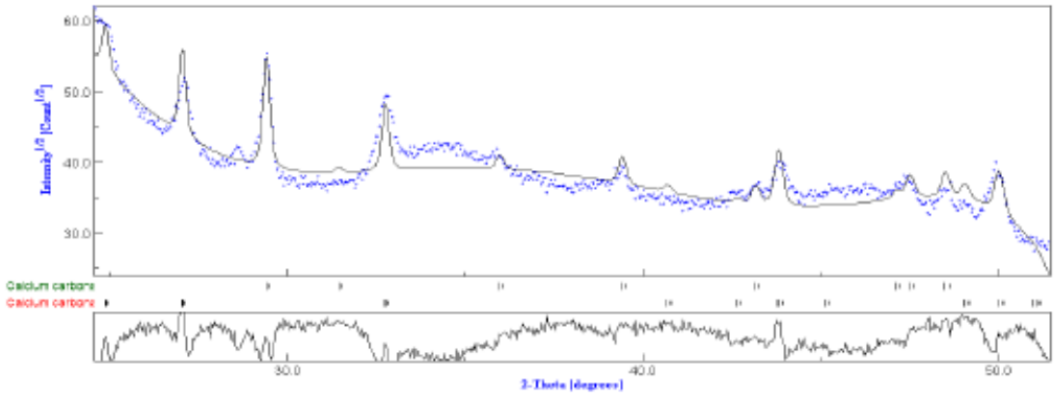

Figure 9. The Rietveld refinement of sample KP-7, with calcite (green) and vaterite (red) peaks shown.

Table 1. The $CaCO_3$ polymorph phase analysis results from samples P23 KP-2 thru KP-7. Proportional $CaCO_3$ phase contents and error limits for the detected phases are given in mass-%.

	$CaCO_3$ polymorph phase proportions [m-%]		
Sample	Calcite (GCC)	Vaterite	Aragonite (PCC)
P23 KP-2	38.6 ± 3.9		61.4 ± 3.9
P23 KP-3	49.6 ± 2.7	50.4 ± 2.7	
P23 KP-4	4.2 ± 2.5	95.8 ± 2.5	
P23 KP-5	42.8 ± 3.1	57.2 ± 3.1	
P23 KP-6	43.7 ± 2.7	56.3 ± 2.7	
P23 KP-7	40.5 ± 4.5	59.5 ± 4.5	

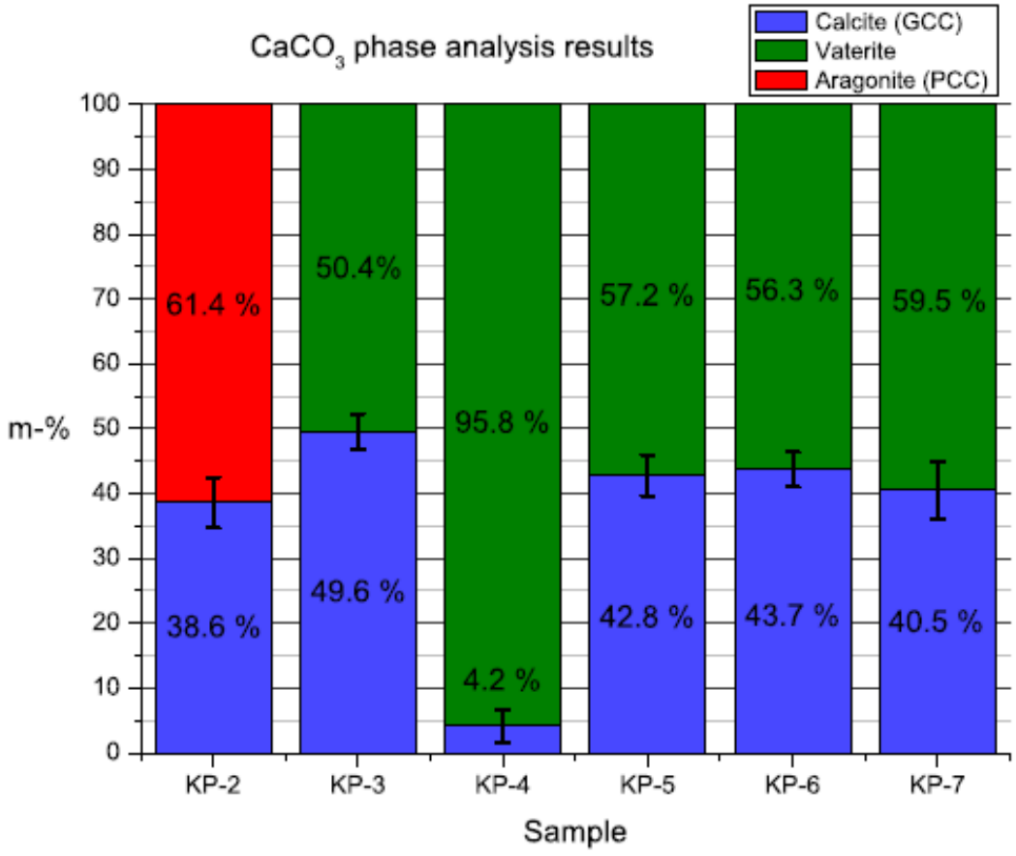

Figure 10. The $CaCO_3$ polymorph phase analysis results shown as a stacked column graph. Proportional $CaCO_3$ phase contents for the detected phases are given in mass-% and error limits are shown.

References

[1] *Powder Diffraction File 2 (PDF-2)*, sets 1-46, 1996 release, International Centre for Diffraction Data (ICDD).

[2] *Inorganic Crystal Structure Database (ICSD)*, version 2.1.0, *http://www.fiz-karlsruhe.de/icsd.html*, April 2012, Fiz Karlsruhe.

[3] Swanson, Fuyat., Natl. Bur. Stand. (U.S.), Circ. 539, **II**, 51, (1953).

[4] Rouse, R., Dept. of Geological Sciences, Univ. of Michigan, Ann Arbor, MI, USA., Private Communication, (1980).

[5] Keller, L., Rask, J., Buseck, P., Arizona State Univ., Tempe, AZ, USA., ICDD Grant-in-Aid, (1989).

[6] Effenberger, H., Mereiter, K., Zemann, J., Z. Kristallogr. 156 (1981), 233-243.

[7] Le Bail, A., Ouhenia, S., Chateigner, D., Powder Diffr. 26 (2011), 16-21.

[8] Pilati, T., Demartin, F., Gramaccioli, C.M., J. Solid State Chem. 146 (1999), 73-78.

[9] Roine J., Tenho M., Murtomaa M., Lehto V.-P., Kansanaho R., *X-ray texture analysis of paper coating pigments and the correlation with chemical composition analysis*, J. Appl. Phys. 102, 083530 (2007).

APPENDIX. Measured and separable $CaCO_3$ peak parameters with reference data.

Sample P23 KP-2 (measured data)					Reference pattern data [1, 3-5]					
Peak no.	Position [°2θ]	d-spacing [Å]	Height [cts/s]	Relat. int. [%]	Polymorph	PDF-no.	hkl	Position [°2θ]	d-spacing [Å]	Relat. int.[1] [%]
A1	26.23	3.398	260.0	40.6	Aragonite	41-1475	(111)	26,233	3,3970	100,0
A2	27.23	3.275	171.7	26.8	Aragonite	41-1475	(021)	27,237	3,2740	50,0
C1	29.42	3.036	640.5	100.0	Calcite	05-0586	(104)	29,429	3,0350	100,0
A3	33.10	2.707	150.4	23.5	Aragonite	41-1475	(012)	33,154	2,7020	60,0
C2	36.05	2.491	127.2	19.9	Calcite	05-0586	(110)	35,995	2,4950	14,0
A4	37.86	2.376	85.0	13.3	Aragonite	41-1475	(112)	37,914	2,3730	45,0
A5	38.46	2.341	85.0	13.3	Aragonite	41-1475	(130)/(022)	38,538[2]	2,3360[2]	50,0[3]
C3	39.42	2.286	98.0	15.3	Calcite	05-0586	(113)	39,433	2,2850	18,0
A6	41.13	2.195	25.0	3.9	Aragonite	41-1475	(211)	41,220	2,1900	12,0
C4	43.12	2.098	100.3	15.7	Calcite	05-0586	(202)	43,181	2,0950	18,0
A7	45.89	1.978	184.1	28.7	Aragonite	41-1475	(221)	45,890	1,9774	55,0
C6	47.44	1.916	105.0	16.4	Calcite	05-0586	(018)	47,529	1,9130	17,0
A8	50.09	1.821	90.0	14.1	Aragonite	41-1475	(212)/(132)	50,208[2]	1,8170[2]	24,0[3]
A9	52.61	1.738	60.0	9.4	Aragonite	41-1475	(113)	52,499	1,7430	25,0

[1]Relative intensity as compared to peaks of the same phase.
[2]Weighed average of adjacent peaks.
[3]Sum of adjacent peaks.

Sample P23 KP-3 (measured data)					Reference pattern data [1, 3-5]					
Peak no.	Position [°2θ]	d-spacing [Å]	Height [cts/s]	Relat. int. [%]	Polymorph	PDF-no.	hkl	Position [°2θ]	d-spacing [Å]	Relat. int.[1] [%]
V1	24.97	3.566	195.7	17.1	Vaterite	33-0268	(110)	24.920	3.5730	60.0
V2	27.06	3.295	337.0	29.4	Vaterite	33-0268	(112)	27.069	3.2940	100.0
C1	29.46	3.032	1147.5	100.0	Calcite	05-0586	(104)	29.429	3.0350	100.0
V3	32.88	2.724	374.1	32.6	Vaterite	33-0268	(114)	32.804	2.7300	90.0
C2	35.97	2.497	126.7	11.0	Calcite	05-0586	(110)	35.995	2.4950	14.0
C3	39.44	2.285	159.2	13.9	Calcite	05-0586	(113)	39.433	2.2850	18.0
V4	42.71	2.117	80.0	7.0	Vaterite	33-0268	(008)	42.794	2.1130	20.0
C4	43.21	2.094	84.9	7.4	Calcite	05-0586	(202)	43.181	2.0950	18.0
V5	43.90	2.062	133.2	11.6	Vaterite	33-0268	(300)	43.885	2.0630	60.0
C5	47.22	1.925	110.0	9.6	Calcite	05-0586	(024)	47.162	1.9270	5.0
C6	47.54	1.913	147.3	12.8	Calcite	05-0586	(018)	47.529	1.9130	17.0
C7	48.57	1.874	124.6	10.9	Calcite	05-0586	(116)	48.553	1.8750	17.0
V6	49.10	1.855	37.5	3.3	Vaterite	33-0268	(304)	49.139	1.8540	30.0
V7	50.00	1.823	237.9	20.7	Vaterite	33-0268	(118)	50.120	1.8200	70.0

[1]Relative intensity as compared to peaks of the same phase.

Sample P23 KP-4 (measured data)					Reference pattern data [1, 3-5]					
Peak no.	Position [°2θ]	d-spacing [Å]	Height [cts/s]	Relat. int. [%]	Polymorph	PDF-no.	hkl	Position [°2θ]	d-spacing [Å]	Relat. int.[1] [%]
V1	25.01	3.560	305.0	53.5	Vaterite	33-0268	(110)	24.920	3.5730	60.0
V2	27.17	3.282	569.9	100.0	Vaterite	33-0268	(112)	27.069	3.2940	100.0
C1	29.46	3.032	150.0	26.3	Calcite	05-0586	(104)	29.429	3.0350	100.0
V3	32.84	2.727	535.9	94.0	Vaterite	33-0268	(114)	32.804	2.7300	90.0
V4	42.71	2.117	65.0	11.4	Vaterite	33-0268	(008)	42.794	2.1130	20.0
V5	43.93	2.061	222.9	39.1	Vaterite	33-0268	(300)	43.885	2.0630	60.0
V6	49.01	1.859	49.1	8.6	Vaterite	33-0268	(304)	49.139	1.8540	30.0
V7	50.06	1.821	280.0	49.1	Vaterite	33-0268	(118)	50.120	1.8200	70.0

[1]Relative intensity as compared to peaks of the same phase.

Sample P23 KP-5 (measured data)					Reference pattern data [1, 3-5]					
Peak no.	Position [°2θ]	d-spacing [Å]	Height [cts/s]	Relat. int. [%]	Polymorph	PDF-no.	hkl	Position [°2θ]	d-spacing [Å]	Relat. int.[1] [%]
V1	24.85	3.584	210.0	28.3	Vaterite	33-0268	(110)	24.920	3.5730	60.0
V2	27.07	3.294	338.3	45.6	Vaterite	33-0268	(112)	27.069	3.2940	100.0
C1	29.34	3.044	741.4	100.0	Calcite	05-0586	(104)	29.429	3.0350	100.0
V3	32.76	2.734	336.5	45.4	Vaterite	33-0268	(114)	32.804	2.7300	90.0
C2	35.95	2.498	66.2	8.9	Calcite	05-0586	(110)	35.995	2.4950	14.0
C3	39.34	2.291	98.0	13.2	Calcite	05-0586	(113)	39.433	2.2850	18.0
V4	42.58	2.123	10.0	1.4	Vaterite	33-0268	(008)	42.794	2.1130	20.0
C4	43.13	2.097	85.0	11.5	Calcite	05-0586	(202)	43.181	2.0950	18.0
V5	43.88	2.063	143.1	19.3	Vaterite	33-0268	(300)	43.885	2.0630	60.0
C5	47.11	1.929	42.5	5.7	Calcite	05-0586	(024)	47.162	1.9270	5.0
C6	47.46	1.916	100.9	13.6	Calcite	05-0586	(018)	47.529	1.9130	17.0
C7	48.46	1.879	82.8	11.2	Calcite	05-0586	(116)	48.553	1.8750	17.0
V6	49.02	1.858	50.0	6.7	Vaterite	33-0268	(304)	49.139	1.8540	30.0
V7	49.97	1.824	223.0	30.1	Vaterite	33-0268	(118)	50.120	1.8200	70.0

[1]Relative intensity as compared to peaks of the same phase.

Sample P23 KP-6 (measured data)					Reference pattern data [1, 3-5]					
Peak no.	Position [°2θ]	d-spacing [Å]	Height [cts/s]	Relat. int. [%]	Polymorph	PDF-no.	hkl	Position [°2θ]	d-spacing [Å]	Relat. int.[1] [%]
V1	24.89	3.577	162.0	23.0	Vaterite	33-0268	(110)	24.920	3.5730	60.0
V2	27.09	3.292	333.1	47.2	Vaterite	33-0268	(112)	27.069	3.2940	100.0
C1	29.37	3.041	706.0	100.0	Calcite	05-0586	(104)	29.429	3.0350	100.0
V3	32.75	2.735	396.0	56.1	Vaterite	33-0268	(114)	32.804	2.7300	90.0
C2	35.91	2.501	114.0	16.1	Calcite	05-0586	(110)	35.995	2.4950	14.0
C3	39.35	2.290	136.2	19.3	Calcite	05-0586	(113)	39.433	2.2850	18.0
C4	43.14	2.097	65.0	9.2	Calcite	05-0586	(202)	43.181	2.0950	18.0
V5	43.91	2.062	114.4	16.2	Vaterite	33-0268	(300)	43.885	2.0630	60.0
C5	47.00	1.933	60.0	8.5	Calcite	05-0586	(024)	47.162	1.9270	5.0
C6	47.40	1.918	118.5	16.8	Calcite	05-0586	(018)	47.529	1.9130	17.0
C7	48.43	1.880	89.9	12.7	Calcite	05-0586	(116)	48.553	1.8750	17.0
V6	49.09	1.856	40.0	5.7	Vaterite	33-0268	(304)	49.139	1.8540	30.0
V7	50.00	1.824	186.4	26.4	Vaterite	33-0268	(118)	50.120	1.8200	70.0

[1]Relative intensity as compared to peaks of the same phase.

Sample P23 KP-7 (measured data)					Reference pattern data [1, 3-5]					
Peak no.	Position [°2θ]	d-spacing [Å]	Height [cts/s]	Relat. int. [%]	Polymorph	PDF-no.	hkl	Position [°2θ]	d-spacing [Å]	Relat. int.[1] [%]
V1	24.95	3.569	212.5	27.4	Vaterite	33-0268	(110)	24.920	3.5730	60.0
V2	27.10	3.291	429.7	55.5	Vaterite	33-0268	(112)	27.069	3.2940	100.0
C1	29.42	3.037	774.8	100.0	Calcite	05-0586	(104)	29.429	3.0350	100.0
V3	32.78	2.732	462.3	59.7	Vaterite	33-0268	(114)	32.804	2.7300	90.0
C2	35.90	2.502	89.0	11.5	Calcite	05-0586	(110)	35.995	2.4950	14.0
C3	39.37	2.289	97.6	12.6	Calcite	05-0586	(113)	39.433	2.2850	18.0
V4	42.64	2.120	35.0	4.5	Vaterite	33-0268	(008)	42.794	2.1130	20.0
C4	43.20	2.094	60.0	7.7	Calcite	05-0586	(202)	43.181	2.0950	18.0
V5	43.89	2.063	165.6	21.4	Vaterite	33-0268	(300)	43.885	2.0630	60.0
C5	47.17	1.927	60.0	7.7	Calcite	05-0586	(024)	47.162	1.9270	5.0
C6	47.49	1.915	130.0	16.8	Calcite	05-0586	(018)	47.529	1.9130	17.0
C7	48.55	1.875	85.6	11.1	Calcite	05-0586	(116)	48.553	1.8750	17.0
V6	49.08	1.856	42.5	5.5	Vaterite	33-0268	(304)	49.139	1.8540	30.0
V7	49.99	1.823	272.2	35.1	Vaterite	33-0268	(118)	50.120	1.8200	70.0

[1]Relative intensity as compared to peaks of the same phase.

APPENDIX 9. pH adjustment by the amount of CO_2

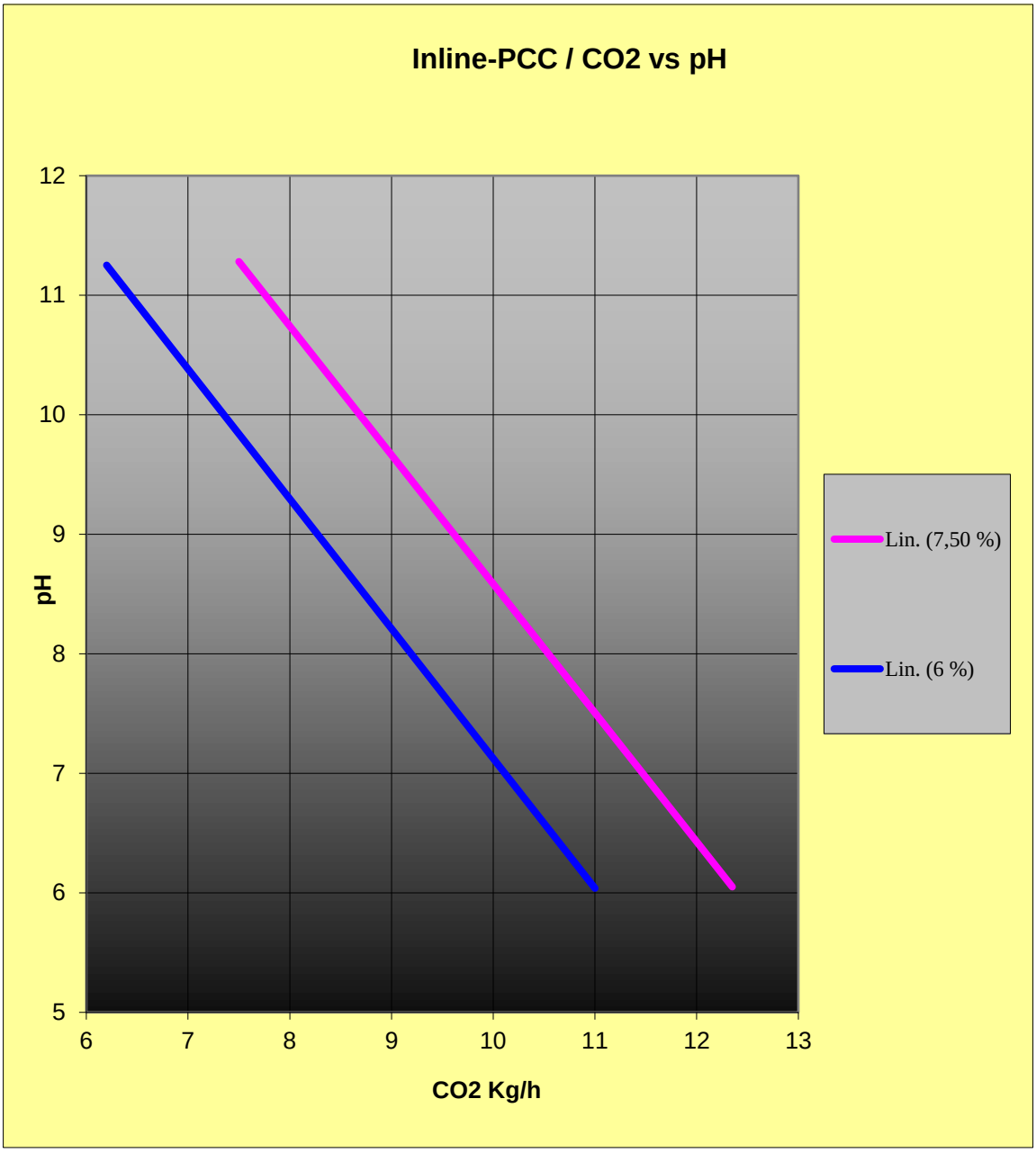

6% and 7,5% Inline-PCC content pH adjustment chart

APPENDIX 10, table of all trial points and their targets

Trial point no	**Trial 1**	Target
1	Pilot machine standard recipe with 5% calcined kaolin	Reference
2	5% filler content with inline-PCC	Runnability & Paper quality
3	7,5% filler content with inline-PCC	Runnability & Paper quality
4	10% filler content with inline-PCC	Runnability & Paper quality
5	15% filler content with inline-PCC	Runnability & Paper quality
6	20% filler content with inline-PCC	Runnability & Paper quality
7	7,5% filler content with inline-PCC,-5% carbon dioxide from calculatory stoichiometric value	pH level check
8	7,5%filler content with inline-PCC, +5% carbon dioxide from calculatory stoichiometric value	pH level check
	Trial 2	
1	Pilot machine standard recipe with 5% calcined kaolin	Reference
2	5% filler content with offline-PCC	5% Offline-PCC reference
3	5% filler content with inline-PCC	5% Inline-PCC reference
4	7,5% filler content with inline-PCC	7,5% Inline-PCC reference
5	7,5% filler content with inline-PCC, + 3% + 1% cationic starch among calcium hydroxide + 1% carboxymethyl cellulose (from total filler volume)	Strength improvement
6	7,5% filler content with inline-PCC, + 3% cationic starch among calcium hydroxide + 3% carboxymethyl cellulose (from total filler volume)	Strength improvement

	Trial 3	
1	Pilot machine standard recipe with 5% calcined kaolin	Reference
2	3% filler content with inline-PCC	3% Offline-PCC reference
3	5% filler content with inline-PCC	5% Inline-PCC reference
4	6% filler content with inline-PCC	6% Inline-PCC reference
5	7,5% filler content with inline-PCC	7,5% Inline-PCC reference
6	6% filler content with inline-PCC, + 5%cationic starch among calcium hydroxide + 2,5% carboxymethyl cellulose (from total filler volume)	Strength improvement
7	7. 5% total filler content including 3% inline-PCC and 2% calcined kaolin	Mixture filler, Paper quality
8	8. 3% filler content with inline-PCC	Rerun of tp2
	Trial 4	
1	Pilot machine standard recipe with 5% calcined kaolin	Reference
2	Elongated trial point of 6% filler content with inline-PCC	Elongated stabilizing period
3	6% filler content with inline-PCC using filtered calcium hydroxide using minimum process water temperature	Highly homogenous raw material
4	6% filler content with inline-PCC using minimum process water temperature	Crystal structure changes
5	6% filler content with inline-PCC + 100g/t Cloisite Na+ bentonite	Precipitation seeding
6	6% filler content with inline-PCC, process water treated with calcium chloride and sodium sulphate	paper machine process water simulation
7	6% filler content with inline-PCC, increased carbon dioxide pressure	CO2 flow stability
	Trial 5	
1	Pilot machine standard recipe with 5% calcined kaolin	Reference
2	6% filler content with inline-PCC as reference point two	6% Inline-PCC reference
3	6% filler content with inline-PCC, increased Trumpjet® injection flow	Crystal structure changes
4	6% filler content with inline-PCC reduced Trumpjet® injection flow	Crystal structure changes
5	6% filler content with inline-PCC using undried birch pulp	Strength properties comparison
6	6% filler content with inline-PCC + 10% cationic starch among calcium hydroxide (from total filler volume)	Strength improvement
7	7.5% total filler content including 3% inline-PCC and 2% calcined kaolin + 4% cationic starch and 2% CMC among calcium hydroxide (from total filler volume)	Strength improvement